Multiple Light Source Optical Flow for Translations and Rotations in the Image Plane

by

Shingo Jason Takagi

Honours B.Sc., University of Toronto, 1998

A THESIS SUBMITTED IN PARTIAL FULFILLMENT OF

THE REQUIREMENTS FOR THE DEGREE OF

Master of Science

in

THE FACULTY OF GRADUATE STUDIES

(Department of Computer Science)

We accept this thesis as conforming
to the required standard

The University of British Columbia

October 2000

Department of Computer Science

The University of British Columbia
Vancouver, Canada

Date October, 23 2000.

Abstract

The classic optical flow constraint equation is accurate under conditions of translation and distant light sources, but becomes inaccurate under conditions where the object may rotate or deform. The inaccuracies are generally a result of the changing intensities at points under rotation or deformation. The changing intensities of these points are associated with the changing surface gradients. We investigate a novel approach to multiple light source optical flow under known reflectance properties. This novel approach is specialized for translation and for rotation around axes which are parallel to the optical axis. The assumption that the object is moving under translation, rotation, or a combination of translation and rotation in the image plane allows us to introduce a physical surface area constraint. Even with this additional constraint, however, the problem still remains locally underdetermined.

At each time frame, our multiple light source optical flow approach assumes that three images are acquired from the same viewpoint, but under three different illumination conditions. Photometric stereo determines many of the coefficients in our underdetermined system, which has six equations in seven unknowns at each pixel in the image. Two of the unknowns are the optical flow components. Another three of the unknowns are the total derivatives of the three intensities with respect to time. The last two are the total derivatives of the surface gradients with respect to time. A variety of local regularization methods were investigated to select optical flow estimates which best matched the known motion fields. All the experimental results for this approach were obtained from synthetic data, in which the motion fields were known.

Contents

Abstract ii

Contents iii

List of Tables v

List of Figures xi

Acknowledgements xviii

1 Optical Flow 1

1.1 Introduction 1

2 Multiple Light Source Optical Flow 4

2.1 Introduction 4

3 Physical Surface Area Based Approach 7

3.1 Introduction 7

3.2 Photometric Surface Constraint 10

3.3 The Physical Surface Area Constraint For Rotations 13

3.4 Degenerate Cases 16

4 Implementation 20

4.1 Hardware and Software Setup 20

4.2 Local Regularization 25

5 Synthetic Image Data 35

5.1 Calibration sphere 35

5.2 Translation of a Sphere 38

5.3 Curving Sheet 40

5.4 Curved Translating Sheet 47

5.5 Rotation of a Surface With Negative Gaussian Curvature 48

5.6 Translation of a Surface With Negative Gaussian Curvature 50

5.7 Rotation and Translation of a Surface With Negative Gaussian Curvature 52
5.8 Rotation of a Surface With Positive Gaussian Curvature 54
5.9 Translation of a Surface With Positive Gaussian Curvature 56
5.10 Rotation and Translation of a Surface With Positive Gaussian Curvature ... 58

6 Results 60

6.1 Optical Flow Estimation Techniques Tested 60
6.2 Optical Flow Estimation Quality Measures 63
6.3 Translation of the Calibration Sphere 70
6.4 Curving Sheet 80
6.5 Curved Translating Sheet 89
6.6 Rotation of a Surface With Negative Gaussian Curvature 98
6.7 Translation of a Surface With Negative Gaussian Curvature 108
6.8 Rotation and Translation of a Surface with Negative Gaussian Curvature 118
6.9 Rotation of a Surface With Positive Gaussian Curvature 128
6.10 Translation of a Surface With Positive Gaussian Curvature 138
6.11 Rotation and Translation of a Surface with Positive Gaussian Curvature .. 148

7 Conclusions and Future Work 158

Bibliography 162

List of Tables

Table 6.1.1: The different optical flow estimation algorithms implemented and tested.. 62
Table 6.3.1: The averages and standard deviations of measures associated with the known motion field. The units for all measures are pixels. 70
Table 6.3.2: The averages and standard deviations of measures associated with the type 1 optical flow estimation. The measure r is unitless. The measure $\angle$ is in radians. All other measures are in pixels. 71
Table 6.3.3: The averages and standard deviations of measures associated with the type 2A Min. A optical flow estimation. The measure r is unitless. The measure $\angle$ is in radians. All other measures are in pixels. 72
Table 6.3.4: The averages and standard deviations of measures associated with the type 2A Min. B optical flow estimation. The measure r is unitless. The measure $\angle$ is in radians. All other measures are in pixels. 73
Table 6.3.5: The averages and standard deviations of measures associated with the type 2A Min. C optical flow estimation. The measure r is unitless. The measure $\angle$ is in radians. All other measures are in pixels. 74
Table 6.3.6: The averages and standard deviations of measures associated with the type 2A Min. D optical flow estimation. The measure r is unitless. The measure $\angle$ is in radians. All other measures are in pixels. 75
Table 6.3.7: The averages and standard deviations of measures associated with the type 2B, 2B′, and 2B″ Min. A optical flow estimation. The measure r is unitless. The measure $\angle$ is in radians. All other measures are in pixels. 76
Table 6.3.8: The averages and standard deviations of measures associated with the type 2B, 2B′, and 2B″ Min. B optical flow estimation. The measure r is unitless. The measure $\angle$ is in radians. All other measures are in pixels. 77
Table 6.3.9: The averages and standard deviations of measures associated with the type 2B, 2B′, and 2B″ Min. C optical flow estimation. The measure r is unitless. The measure $\angle$ is in radians. All other measures are in pixels. 78
Table 6.3.10: The averages and standard deviations of measures associated with the type 2B, 2B′, and 2B″ Min. D optical flow estimation. The measure r is unitless. The measure $\angle$ is in radians. All other measures are in pixels. 79
Table 6.4.1: The averages and standard deviations of measures associated with the known motion field. The measure r is unitless. All measures are in pixels. 80
Table 6.4.2: The averages and standard deviations of measures associated with the type 2A Min. A optical flow estimation. The measure r is unitless. The measure $\angle$ is in radians. All other measures are in pixels. 81
Table 6.4.3: The averages and standard deviations of measures associated with the type 2A Min. B optical flow estimation. The measure r is unitless. The measure $\angle$ is in radians. All other measures are in pixels. 82
Table 6.4.4: The averages and standard deviations of measures associated with the type 2A Min. C optical flow estimation. The measure r is unitless. The measure $\angle$ is in radians. All other measures are in pixels. 83

Table 6.4.5: The averages and standard deviations of measures associated with the type 2A Min. D optical flow estimation. The measure r is unitless. The measure $\angle$ is in radians. All other measures are in pixels. 84
Table 6.4.6: The averages and standard deviations of measures associated with the type 2B, 2B′, and 2B″ Min. A optical flow estimation. The measure r is unitless. The measure $\angle$ is in radians. All other measures are in pixels. 85
Table 6.4.7: The averages and standard deviations of measures associated with the type 2B, 2B′, and 2B″ Min. B optical flow estimation. The measure r is unitless. The measure $\angle$ is in radians. All other measures are in pixels. 86
Table 6.4.8: The averages and standard deviations of measures associated with the type 2B, 2B′, and 2B″ Min. C optical flow estimation. The measure r is unitless. The measure $\angle$ is in radians. All other measures are in pixels. 87
Table 6.4.9: The averages and standard deviations of measures associated with the type 2B, 2B′, and 2B″ Min. D optical flow estimation. The measure r is unitless. The measure $\angle$ is in radians. All other measures are in pixels. 88
Table 6.5.1: The averages and standard deviations of measures associated with the known motion field. All measures are in pixels. 89
Table 6.5.2: The averages and standard deviations of measures associated with the type 2A Min. A optical flow estimation. The measure r is unitless. The measure $\angle$ is in radians. All other measures are in pixels. 90
Table 6.5.3: The averages and standard deviations of measures associated with the type 2A Min. B optical flow estimation. The measure r is unitless. The measure $\angle$ is in radians. All other measures are in pixels. 91
Table 6.5.4: The averages and standard deviations of measures associated with the type 2A Min. C optical flow estimation. The measure r is unitless. The measure $\angle$ is in radians. All other measures are in pixels. 92
Table 6.5.5: The averages and standard deviations of measures associated with the type 2A Min. D optical flow estimation. The measure r is unitless. The measure $\angle$ is in radians. All other measures are in pixels. 93
Table 6.5.6: The averages and standard deviations of measures associated with the type 2B, 2B′, and 2B″ Min. A optical flow estimation. The measure r is unitless. The measure $\angle$ is in radians. All other measures are in pixels. 94
Table 6.5.7: The averages and standard deviations of measures associated with the type 2B, 2B′, and 2B″ Min. B optical flow estimation. The measure r is unitless. The measure $\angle$ is in radians. All other measures are in pixels. 95
Table 6.5.8: The averages and standard deviations of measures associated with the type 2B, 2B′, and 2B″ Min. C optical flow estimation. The measure r is unitless. The measure $\angle$ is in radians. All other measures are in pixels. 96
Table 6.5.9: The averages and standard deviations of measures associated with the type 2B, 2B′, and 2B″ Min. D optical flow estimation. The measure r is unitless. The measure $\angle$ is in radians. All other measures are in pixels. 97
Table 6.6.1: The averages and standard deviations of measures associated with the known motion field. The measure r is unitless. The measure $\angle$ is in radians. All other measures are in pixels. 98

Table 6.6.2: The averages and standard deviations of measures associated with the type 1 optical flow estimation. The measure r is unitless. The measure $\angle$ is in radians. All other measures are in pixels. 99
Table 6.6.3: The averages and standard deviations of measures associated with the type 2A Min. A optical flow estimation. The measure r is unitless. The measure $\angle$ is in radians. All other measures are in pixels. 100
Table 6.6.4: The averages and standard deviations of measures associated with the type 2A Min. B optical flow estimation. The measure r is unitless. The measure $\angle$ is in radians. All other measures are in pixels. 101
Table 6.6.5: The averages and standard deviations of measures associated with the type 2A Min. C optical flow estimation. The measure r is unitless. The measure $\angle$ is in radians. All other measures are in pixels. 102
Table 6.6.6: The averages and standard deviations of measures associated with the type 2A Min. D optical flow estimation. The measure r is unitless. The measure $\angle$ is in radians. All other measures are in pixels. 103
Table 6.6.7: The averages and standard deviations of measures associated with the type 2B, 2B′, and 2B″ Min. A optical flow estimation. The measure r is unitless. The measure $\angle$ is in radians. All other measures are in pixels. 104
Table 6.6.8: The averages and standard deviations of measures associated with the type 2B, 2B′, and 2B″ Min. B optical flow estimation. The measure r is unitless. The measure $\angle$ is in radians. All other measures are in pixels. 105
Table 6.6.9: The averages and standard deviations of measures associated with the type 2B, 2B′, and 2B″ Min. C optical flow estimation. The measure r is unitless. The measure $\angle$ is in radians. All other measures are in pixels. 106
Table 6.6.10: The averages and standard deviations of measures associated with the type 2B, 2B′, and 2B″ Min. D optical flow estimation. The measure r is unitless. The measure $\angle$ is in radians. All other measures are in pixels. 107
Table 6.7.1: The averages and standard deviations of measures associated with the known motion field. The measure r is unitless. The measure $\angle$ is in radians. All other measures are in pixels. 108
Table 6.7.2: The averages and standard deviations of measures associated with the type 1 optical flow estimation. The measure r is unitless. The measure $\angle$ is in radians. All other measures are in pixels. 109
Table 6.7.3: The averages and standard deviations of measures associated with the type 2A Min. A optical flow estimation. The measure r is unitless. The measure $\angle$ is in radians. All other measures are in pixels. 110
Table 6.7.4: The averages and standard deviations of measures associated with the type 2A Min. B optical flow estimation. The measure r is unitless. The measure $\angle$ is in radians. All other measures are in pixels. 111
Table 6.7.5: The averages and standard deviations of measures associated with the type 2A Min. C optical flow estimation. The measure r is unitless. The measure $\angle$ is in radians. All other measures are in pixels. 112
Table 6.7.6: The averages and standard deviations of measures associated with the type 2A Min. D optical flow estimation. The measure r is unitless. The measure $\angle$ is in radians. All other measures are in pixels. 113

Table 6.7.7: The averages and standard deviations of measures associated with the type 2B, 2B′, and 2B″ Min. A optical flow estimation. The measure r is unitless. The measure $\angle$ is in radians. All other measures are in pixels. 114
Table 6.7.8: The averages and standard deviations of measures associated with the type 2B, 2B′, and 2B″ Min. B optical flow estimation. The measure r is unitless. The measure $\angle$ is in radians. All other measures are in pixels. 115
Table 6.7.9: The averages and standard deviations of measures associated with the type 2B, 2B′, and 2B″ Min. C optical flow estimation. The measure r is unitless. The measure $\angle$ is in radians. All other measures are in pixels. 116
Table 6.7.10: The averages and standard deviations of measures associated with the type 2B, 2B′, and 2B″ Min. D optical flow estimation. The measure r is unitless. The measure $\angle$ is in radians. All other measures are in pixels. 117
Table 6.8.1: The averages and standard deviations of measures associated with the known motion field. All measures are in pixels. 118
Table 6.8.2: The averages and standard deviations of measures associated with the type 1 optical flow estimation. The measure r is unitless. The measure $\angle$ is in radians. All other measures are in pixels. 119
Table 6.8.3: The averages and standard deviations of measures associated with the type 2A Min. A optical flow estimation. The measure r is unitless. The measure $\angle$ is in radians. All other measures are in pixels. 120
Table 6.8.4: The averages and standard deviations of measures associated with the type 2A Min. B optical flow estimation. The measure r is unitless. The measure $\angle$ is in radians. All other measures are in pixels. 121
Table 6.8.5: The averages and standard deviations of measures associated with the type 2A Min. C optical flow estimation. The measure r is unitless. The measure $\angle$ is in radians. All other measures are in pixels. 122
Table 6.8.6: The averages and standard deviations of measures associated with the type 2A Min. D optical flow estimation. The measure r is unitless. The measure $\angle$ is in radians. All other measures are in pixels. 123
Table 6.8.7: The averages and standard deviations of measures associated with the type 2B, 2B′, and 2B″ Min. A optical flow estimation. The measure r is unitless. The measure $\angle$ is in radians. All other measures are in pixels. 124
Table 6.8.8: The averages and standard deviations of measures associated with the type 2B, 2B′, and 2B″ Min. B optical flow estimation. The measure r is unitless. The measure $\angle$ is in radians. All other measures are in pixels. 125
Table 6.8.9: The averages and standard deviations of measures associated with the type 2B, 2B′, and 2B″ Min. C optical flow estimation. The measure r is unitless. The measure $\angle$ is in radians. All other measures are in pixels. 126
Table 6.8.10: The averages and standard deviations of measures associated with the type 2B, 2B′, and 2B″ Min. D optical flow estimation. The measure r is unitless. The measure $\angle$ is in radians. All other measures are in pixels. 127
Table 6.9.1: The averages and standard deviations of measures associated with the known motion field. All measures are in pixels. 128

Table 6.9.2: The averages and standard deviations of measures associated with the type 1 optical flow estimation. The measure r is unitless. The measure $\angle$ is in radians. All other measures are in pixels. 129
Table 6.9.3: The averages and standard deviations of measures associated with the type 2A Min. A optical flow estimation. The measure r is unitless. The measure $\angle$ is in radians. All other measures are in pixels. 130
Table 6.9.4: The averages and standard deviations of measures associated with the type 2A Min. B optical flow estimation. The measure r is unitless. The measure $\angle$ is in radians. All other measures are in pixels. 131
Table 6.9.5: The averages and standard deviations of measures associated with the type 2A Min. C optical flow estimation. The measure r is unitless. The measure $\angle$ is in radians. All other measures are in pixels. 132
Table 6.9.6: The averages and standard deviations of measures associated with the type 2A Min. D optical flow estimation. The measure r is unitless. The measure $\angle$ is in radians. All other measures are in pixels. 133
Table 6.9.7: The averages and standard deviations of measures associated with the type 2B, 2B′, and 2B″ Min. A optical flow estimation. The measure r is unitless. The measure $\angle$ is in radians. All other measures are in pixels. 134
Table 6.9.8: The averages and standard deviations of measures associated with the type 2B, 2B′, and 2B″ Min. B optical flow estimation. The measure r is unitless. The measure $\angle$ is in radians. All other measures are in pixels. 135
Table 6.9.9: The averages and standard deviations of measures associated with the type 2B, 2B′, and 2B″ Min. C optical flow estimation. The measure r is unitless. The measure $\angle$ is in radians. All other measures are in pixels. 136
Table 6.9.10: The averages and standard deviations of measures associated with the type 2B, 2B′, and 2B″ Min. D optical flow estimation. The measure r is unitless. The measure $\angle$ is in radians. All other measures are in pixels 137
Table 6.10.1: The averages and standard deviations of measures associated with the known motion field. All measures are in pixels. 138
Table 6.10.2: The averages and standard deviations of measures associated with the type 1 optical flow estimation. The measure r is unitless. The measure $\angle$ is in radians. All other measures are in pixels. 139
Table 6.10.3: The averages and standard deviations of measures associated with the type 2A Min. A optical flow estimation. The measure r is unitless. The measure $\angle$ is in radians. All other measures are in pixels. 140
Table 6.10.4: The averages and standard deviations of measures associated with the type 2A Min. B optical flow estimation. The measure r is unitless. The measure $\angle$ is in radians. All other measures are in pixels. 141
Table 6.10.5: The averages and standard deviations of measures associated with the type 2A Min. C optical flow estimation. The measure r is unitless. The measure $\angle$ is in radians. All other measures are in pixels. 142
Table 6.10.6: The averages and standard deviations of measures associated with the type 2A Min. D optical flow estimation. The measure r is unitless. The measure $\angle$ is in radians. All other measures are in pixels. 143

Table 6.10.7: The averages and standard deviations of measures associated with the type 2B, 2B′, and 2B″ Min. A optical flow estimation. The measure r is unitless. The measure $\angle$ is in radians. All other measures are in pixels. 144
Table 6.10.8: The averages and standard deviations of measures associated with the type 2B, 2B′, and 2B″ Min. B optical flow estimation. The measure r is unitless. The measure $\angle$ is in radians. All other measures are in pixels. 145
Table 6.10.9: The averages and standard deviations of measures associated with the type 2B, 2B′, and 2B″ Min. C optical flow estimation. The measure r is unitless. The measure $\angle$ is in radians. All other measures are in pixels. 146
Table 6.10.10: The averages and standard deviations of measures associated with the type 2B, 2B′, and 2B″ Min. D optical flow estimation. The measure r is unitless. The measure $\angle$ is in radians. All other measures are in pixels. 147
Table 6.11.1: The averages and standard deviations of measures associated with the known motion field. All measures are in pixels. 148
Table 6.11.2: The averages and standard deviations of measures associated with the type 1 optical flow estimation. The measure r is unitless. The measure $\angle$ is in radians. All other measures are in pixels. 149
Table 6.11.3: The averages and standard deviations of measures associated with the type 2A Min. A optical flow estimation. The measure r is unitless. The measure $\angle$ is in radians. All other measures are in pixels. 150
Table 6.11.4: The averages and standard deviations of measures associated with the type 2A Min. B optical flow estimation. The measure r is unitless. The measure $\angle$ is in radians. All other measures are in pixels. 151
Table 6.11.5: The averages and standard deviations of measures associated with the type 2A Min. C optical flow estimation. The measure r is unitless. The measure $\angle$ is in radians. All other measures are in pixels. 152
Table 6.11.6: The averages and standard deviations of measures associated with the type 2A Min. D optical flow estimation. The measure r is unitless. The measure $\angle$ is in radians. All other measures are in pixels. 153
Table 6.11.7: The averages and standard deviations of measures associated with the type 2B, 2B′, and 2B″ Min. A optical flow estimation. The measure r is unitless. The measure $\angle$ is in radians. All other measures are in pixels. 154
Table 6.11.8: The averages and standard deviations of measures associated with the type 2B, 2B′, and 2B″ Min. B optical flow estimation. The measure r is unitless. The measure $\angle$ is in radians. All other measures are in pixels. 155
Table 6.11.9: The averages and standard deviations of measures associated with the type 2B, 2B′, and 2B″ Min. C optical flow estimation. The measure r is unitless. The measure $\angle$ is in radians. All other measures are in pixels. 156
Table 6.11.10: The averages and standard deviations of measures associated with the type 2B, 2B′, and 2B″ Min. D optical flow estimation. The measure r is unitless. The measure $\angle$ is in radians. All other measures are in pixels. 157

List of Figures

Figure 1.1.1: Imaging axis under orthographic projection. 1
Figure 5.1.1: The calibration sphere under the red illumination. 37
Figure 5.1.2: The calibration sphere under the green illumination. 37
Figure 5.1.3: The calibration sphere under the blue illumination. 38
Figure 5.2.1: The first of 11 images in the translating calibration sphere sequence. The red, green, and blue illuminations have been superimposed. 39
Figure 5.2.2: The last of 11 images in the translating calibration sphere sequence. The red, green, and blue illuminations have been superimposed. 39
Figure 5.3.1: Diagram depicting the parameterization of curving surface. 40
Figure 5.3.2: A wire mesh visualization of the curved sheet, at the end of its deformation. Units are in pixels. 44
Figure 5.3.3: The first of 11 images in the curving sheet sequence. The red, green, and blue illuminations have been superimposed. 45
Figure 5.3.4: The last of 11 images in the curving sheet sequence. The red, green, and blue illuminations have been superimposed. 45
Figure 5.4.1: The first of 11 images in the curved translating sheet sequence. The red, green, and blue illuminations have been superimposed. 47
Figure 5.4.2: The last of 11 images in the curved translating sheet sequence. The red, green, and blue illuminations have been superimposed. 48
Figure 5.5.1: A wire mesh visualization of the surface with negative Gaussian curvature. Units are in pixels. 49
Figure 5.5.2: The first of 11 images in the sequence of a rotating surface with negative Gaussian curvature. The red, green, and blue illuminations have been superimposed. 49
Figure 5.5.3: The last of 11 images in the sequence of a rotating surface with negative Gaussian curvature. The red, green, and blue illuminations have been superimposed. 50
Figure 5.6.1: The first of 11 images in the sequence of a translating surface with negative Gaussian curvature. The red, green, and blue illuminations have been superimposed. 51
Figure 5.6.2: The last of 11 images in the sequence of a translating surface with negative Gaussian curvature. The red, green, and blue illuminations have been superimposed. 52
Figure 5.7.1: The first of 11 images in the sequence of a rotating and translating surface with negative Gaussian curvature. The red, green, and blue illuminations have been superimposed. 53
Figure 5.7.2: The last of 11 images in the sequence of a rotating and translating surface with negative Gaussian curvature. The red, green, and blue illuminations have been superimposed. 53
Figure 5.8.1: A wire mesh visualization of the surface with positive Gaussian curvature. Units are in pixels. 54
Figure 5.8.2: The first of 11 images in the sequence of a rotating surface with positive Gaussian curvature. The red, green, and blue illuminations have been superimposed. 55

Figure 5.8.3: The last of 11 images in the sequence of a rotating surface with positive Gaussian curvature. The red, green, and blue illuminations have been superimposed. 56
Figure 5.9.1: The first of 11 images in the sequence of a translating surface with positive Gaussian curvature. The red, green, and blue illuminations have been superimposed. 57
Figure 5.9.2: The last of 11 images in the sequence of a translating surface with positive Gaussian curvature. The red, green, and blue illuminations have been superimposed. 58
Figure 5.10.1: The first of 11 images in the sequence of a rotating and translating surface with positive Gaussian curvature. The red, green, and blue illuminations have been superimposed. 59
Figure 5.10.2: The last of 11 images in the sequence of a rotating and translating surface with positive Gaussian curvature. The red, green, and blue illuminations have been superimposed. 59
Figure 6.2.1 The 5 by 5 neighborhood of the pixel P. All cells labelled "N" are in the 5 by 5 neighborhood. 63
Figure 6.3.1: The known motion field for the translating calibration sphere. Vectors are magnified 10 times and sampled every 20 pixels. 70
Figure 6.3.2: The type 1 optical flow estimation for the translating calibration sphere. Vectors are magnified 10 times and sampled every 20 pixels. 71
Figure 6.3.3: The type 2A Min. A optical flow estimation for the translating calibration sphere. Vectors are magnified 10 times and sampled every 20 pixels. 72
Figure 6.3.4: The type 2A Min. B optical flow estimation for the translating calibration sphere. Vectors are magnified 10 times and sampled every 20 pixels. 73
Figure 6.3.5: The type 2A Min. C optical flow estimation for the translating calibration sphere. Vectors are magnified 10 times and sampled every 20 pixels. 74
Figure 6.3.6: The type 2A Min. D optical flow estimation for the translating calibration sphere. Vectors are magnified 10 times and sampled every 20 pixels. 75
Figure 6.3.7: The type 2B Min. A optical flow estimation for the translating calibration sphere. Vectors are magnified 10 times and sampled every 20 pixels. 76
Figure 6.3.8: The type 2B Min. B optical flow estimation for the translating calibration sphere. Vectors are magnified 10 times and sampled every 20 pixels. 77
Figure 6.3.9: The type 2B Min. C optical flow estimation for the translating calibration sphere. Vectors are magnified 10 times and sampled every 20 pixels. 78
Figure 6.3.10: The type 2B Min. D optical flow estimation for the translating calibration sphere. Vectors are magnified 10 times and sampled every 20 pixels. 79
Figure 6.4.1: The known motion field for the curving sheet. Vectors are magnified 35 times and sampled every 20 pixels. 80
Figure 6.4.2: The type 2A Min. A optical flow estimation for the curving sheet. Vectors are magnified 0.000000000000004 times and sampled every 20 pixels. 81
Figure 6.4.3: The type 2A Min. B optical flow estimation for the curving sheet. Vectors are magnified 2 times and sampled every 20 pixels. 82
Figure 6.4.4: The type 2A Min. C optical flow estimation for the curving sheet. Vectors are magnified 2 times and sampled every 20 pixels. 83

Figure 6.4.5: The type 2A Min. D optical flow estimation for the curving sheet. Vectors are magnified 0.000000000000004 times and sampled every 20 pixels. 84
Figure 6.4.6: The type 2B Min. A optical flow estimation for the curving sheet. Vectors are magnified 2 times and sampled every 20 pixels. 85
Figure 6.4.7: The type 2B Min. B optical flow estimation for the curving sheet. Vectors are magnified 2 times and sampled every 20 pixels. 86
Figure 6.4.8: The type 2B Min. C optical flow estimation for the curving sheet. Vectors are magnified 2 times and sampled every 20 pixels. 87
Figure 6.4.9: The type 2B Min. D optical flow estimation for the curving sheet. Vectors are magnified 2 times and sampled every 20 pixels. 88
Figure 6.5.1: The known motion field for the translating curved sheet. Vectors are magnified 10 times and sampled every 20 pixels. 89
Figure 6.5.2: The type 2A Min. A optical flow estimation for the translating curved sheet. Vectors are magnified 0.00000000000001 times and sampled every 20 pixels. 90
Figure 6.5.3: The type 2A Min. B optical flow estimation for the translating curved sheet. Vectors are magnified 10 times and sampled every 20 pixels. 91
Figure 6.5.4: The type 2A Min. C optical flow estimation for the translating curved sheet. Vectors are magnified 10 times and sampled every 20 pixels. 92
Figure 6.5.5: The type 2A Min. D optical flow estimation for the translating curved sheet. Vectors are magnified 0.00000000000001 times and sampled every 20 pixels. 93
Figure 6.5.6: The type 2B Min. A optical flow estimation for the translating curved sheet. Vectors are magnified 10 times and sampled every 20 pixels. 94
Figure 6.5.7: The type 2B Min. B optical flow estimation for the translating curved sheet. Vectors are magnified 10 times and sampled every 20 pixels. 95
Figure 6.5.8: The type 2B Min. C optical flow estimation for the translating curved sheet. Vectors are magnified 10 times and sampled every 20 pixels. 96
Figure 6.5.9: The type 2B Min. D optical flow estimation for the translating curved sheet. Vectors are magnified 10 times and sampled every 20 pixels. 97
Figure 6.6.1: The known motion field for the rotating surface with negative Gaussian curvature. Vectors are magnified 10 times and sampled every 20 pixels. 98
Figure 6.6.2: The type 1 optical flow estimation for the rotating surface with negative Gaussian curvature. Vectors are magnified 10 times and sampled every 20 pixels. 99
Figure 6.6.3: The type 2A Min. A optical flow estimation for the rotating surface with negative Gaussian curvature. Vectors are magnified 10 times and sampled every 20 pixels. 100
Figure 6.6.4: The type 2A Min. B optical flow estimation for the rotating surface with negative Gaussian curvature. Vectors are magnified 10 times and sampled every 20 pixels. 101
Figure 6.6.5: The type 2A Min. C optical flow estimation for the rotating surface with negative Gaussian curvature. Vectors are magnified 10 times and sampled every 20 pixels. 102
Figure 6.6.6: The type 2A Min. D optical flow estimation for the rotating surface with negative Gaussian curvature. Vectors are magnified 10 times and sampled every 20 pixels. 103

Figure 6.6.7: The type 2B Min. A optical flow estimation for the rotating surface with negative Gaussian curvature. Vectors are magnified 10 times and sampled every 20 pixels. 104
Figure 6.6.8: The type 2B Min. B optical flow estimation for the rotating surface with negative Gaussian curvature. Vectors are magnified 10 times and sampled every 20 pixels. 105
Figure 6.6.9: The type 2B Min. C optical flow estimation for the rotating surface with negative Gaussian curvature. Vectors are magnified 10 times and sampled every 20 pixels. 106
Figure 6.6.10: The type 2B Min. D optical flow estimation for the rotating surface with negative Gaussian curvature. Vectors are magnified 10 times and sampled every 20 pixels. 107
Figure 6.7.1: The known motion field for the translating surface with negative Gaussian curvature. Vectors are magnified 10 times and sampled every 20 pixels. 108
Figure 6.7.2: The type 1optical flow estimation for the translating surface with negative Gaussian curvature. Vectors are magnified 10 times and sampled every 20 pixels. 109
Figure 6.7.3: The type 2A Min. A optical flow estimation for the translating surface with negative Gaussian curvature. Vectors are magnified 10 times and sampled every 20 pixels. 110
Figure 6.7.4: The type 2A Min. B optical flow estimation for the translating surface with negative Gaussian curvature. Vectors are magnified 10 times and sampled every 20 pixels. 111
Figure 6.7.5: The type 2A Min. C optical flow estimation for the translating surface with negative Gaussian curvature. Vectors are magnified 10 times and sampled every 20 pixels. 112
Figure 6.7.6: The type 2A Min. D optical flow estimation for the translating surface with negative Gaussian curvature. Vectors are magnified 10 times and sampled every 20 pixels. 113
Figure 6.7.7: The type 2B Min. A optical flow estimation for the translating surface with negative Gaussian curvature. Vectors are magnified 10 times and sampled every 20 pixels. 114
Figure 6.7.8: The type 2B Min. B optical flow estimation for the translating surface with negative Gaussian curvature. Vectors are magnified 10 times and sampled every 20 pixels. 115
Figure 6.7.9: The type 2B Min. C optical flow estimation for the translating surface with negative Gaussian curvature. Vectors are magnified 10 times and sampled every 20 pixels. 116
Figure 6.7.10: The type 2B Min. D optical flow estimation for the translating surface with negative Gaussian curvature. Vectors are magnified 10 times and sampled every 20 pixels. 117
Figure 6.8.1: The known motion field for the rotating and translating surface with negative Gaussian curvature. Vectors are magnified 10 times and sampled every 20 pixels. 118

Figure 6.8.2: The type 1 optical flow estimation for the rotating and translating surface with negative Gaussian curvature. Vectors are magnified 10 times and sampled every 20 pixels. 119
Figure 6.8.3: The type 2A Min. A optical flow estimation for the rotating and translating surface with negative Gaussian curvature. Vectors are magnified 10 times and sampled every 20 pixels..... 120
Figure 6.8.4: The type 2A Min. B optical flow estimation for the rotating and translating surface with negative Gaussian curvature. Vectors are magnified 10 times and sampled every 20 pixels..... 121
Figure 6.8.5: The type 2A Min. C optical flow estimation for the rotating and translating surface with negative Gaussian curvature. Vectors are magnified 10 times and sampled every 20 pixels..... 122
Figure 6.8.6: The type 2A Min. D optical flow estimation for the rotating and translating surface with negative Gaussian curvature. Vectors are magnified 10 times and sampled every 20 pixels..... 123
Figure 6.8.7: The type 2B Min. A optical flow estimation for the rotating and translating surface with negative Gaussian curvature. Vectors are magnified 10 times and sampled every 20 pixels..... 124
Figure 6.8.8: The type 2B Min. B optical flow estimation for the rotating and translating surface with negative Gaussian curvature. Vectors are magnified 10 times and sampled every 20 pixels..... 125
Figure 6.8.9: The type 2B Min. C optical flow estimation for the rotating and translating surface with negative Gaussian curvature. Vectors are magnified 10 times and sampled every 20 pixels..... 126
Figure 6.8.10: The type 2B Min. D optical flow estimation for the rotating and translating surface with negative Gaussian curvature. Vectors are magnified 10 times and sampled every 20 pixels..... 127
Figure 6.9.1: The known motion field for the rotating surface with positive Gaussian curvature. Vectors are magnified 10 times and sampled every 20 pixels. 128
Figure 6.9.2: The type 1 optical flow estimation for the rotating surface with positive Gaussian curvature. Vectors are magnified 20 times and sampled every 20 pixels. 129
Figure 6.9.3: The type 2A Min. A optical flow estimation for the rotating surface with positive Gaussian curvature. Vectors are magnified 20 times and sampled every 20 pixels..... 130
Figure 6.9.4: The type 2A Min. B optical flow estimation for the rotating surface with positive Gaussian curvature. Vectors are magnified 20 times and sampled every 20 pixels..... 131
Figure 6.9.5: The type 2A Min. C optical flow estimation for the rotating surface with positive Gaussian curvature. Vectors are magnified 20 times and sampled every 20 pixels..... 132
Figure 6.9.6: The type 2A Min. D optical flow estimation for the rotating surface with positive Gaussian curvature. Vectors are magnified 20 times and sampled every 20 pixels..... 133

Figure 6.9.7: The type 2B Min. A optical flow estimation for the rotating surface with positive Gaussian curvature. Vectors are magnified 20 times and sampled every 20 pixels. 134
Figure 6.9.8: The type 2B Min. B optical flow estimation for the rotating surface with positive Gaussian curvature. Vectors are magnified 20 times and sampled every 20 pixels. 135
Figure 6.9.9: The type 2B Min. C optical flow estimation for the rotating surface with positive Gaussian curvature. Vectors are magnified 20 times and sampled every 20 pixels. 136
Figure 6.9.10: The type 2B Min. D optical flow estimation for the rotating surface with positive Gaussian curvature. Vectors are magnified 20 times and sampled every 20 pixels. 137
Figure 6.10.1: The known motion field for the translating surface with positive Gaussian curvature. Vectors are magnified 10 times and sampled every 20 pixels. 138
Figure 6.10.2: The type 1 optical flow estimation for the translating surface with positive Gaussian curvature. Vectors are magnified 10 times and sampled every 20 pixels. 139
Figure 6.10.3: The type 2A Min. A optical flow estimation for the translating surface with positive Gaussian curvature. Vectors are magnified 10 times and sampled every 20 pixels. 140
Figure 6.10.4: The type 2A Min. B optical flow estimation for the translating surface with positive Gaussian curvature. Vectors are magnified 10 times and sampled every 20 pixels. 141
Figure 6.10.5: The type 2A Min. C optical flow estimation for the translating surface with positive Gaussian curvature. Vectors are magnified 10 times and sampled every 20 pixels. 142
Figure 6.10.6: The type 2A Min. D optical flow estimation for the translating surface with positive Gaussian curvature. Vectors are magnified 10 times and sampled every 20 pixels. 143
Figure 6.10.7: The type 2B Min. A optical flow estimation for the translating surface with positive Gaussian curvature. Vectors are magnified 10 times and sampled every 20 pixels. 144
Figure 6.10.8: The type 2B Min. B optical flow estimation for the translating surface with positive Gaussian curvature. Vectors are magnified 10 times and sampled every 20 pixels. 145
Figure 6.10.9: The type 2B Min. C optical flow estimation for the translating surface with positive Gaussian curvature. Vectors are magnified 10 times and sampled every 20 pixels. 146
Figure 6.10.10: The type 2B Min. D optical flow estimation for the translating surface with positive Gaussian curvature. Vectors are magnified 10 times and sampled every 20 pixels. 147
Figure 6.11.1: The known motion field for the rotating and translating surface with positive Gaussian curvature. Vectors are magnified 10 times and sampled every 20 pixels. 148

Figure 6.11.2: The type 1 optical flow estimation for the rotating and translating surface with positive Gaussian curvature. Vectors are magnified 10 times and sampled every 20 pixels. 149
Figure 6.11.3: The type 2A Min. A optical flow estimation for the rotating and translating surface with positive Gaussian curvature. Vectors are magnified 10 times and sampled every 20 pixels. 150
Figure 6.11.4: The type 2A Min. B optical flow estimation for the rotating and translating surface with positive Gaussian curvature. Vectors are magnified 10 times and sampled every 20 pixels. 151
Figure 6.11.5: The type 2A Min. C optical flow estimation for the rotating and translating surface with positive Gaussian curvature. Vectors are magnified 10 times and sampled every 20 pixels. 152
Figure 6.11.6: The type 2A Min. D optical flow estimation for the rotating and translating surface with positive Gaussian curvature. Vectors are magnified 10 times and sampled every 20 pixels. 153
Figure 6.11.7: The type 2B Min. A optical flow estimation for the rotating and translating surface with positive Gaussian curvature. Vectors are magnified 10 times and sampled every 20 pixels. 154
Figure 6.11.8: The type 2B Min. B optical flow estimation for the rotating and translating surface with positive Gaussian curvature. Vectors are magnified 10 times and sampled every 20 pixels. 155
Figure 6.11.9: The type 2B Min. C optical flow estimation for the rotating and translating surface with positive Gaussian curvature. Vectors are magnified 10 times and sampled every 20 pixels. 156
Figure 6.11.10: The type 2B Min. D optical flow estimation for the rotating and translating surface with positive Gaussian curvature. Vectors are magnified 10 times and sampled every 20 pixels. 157

Acknowledgements

I would like to thank my supervisor Dr. Robert J. Woodham for his guidance, support and insightful comments on all aspects of this thesis, Dr. James Little, for being my second reader, and providing valuable feedback on this thesis, and the technical and support staff in the Computer Science department, who helped solve some of my major computer problems.

The Laboratory for Computational Intelligence (LCI), the Active Measurement Facility (ACME), and the entire Computer Science department has been a fun and exciting place to work. Last but not least, I would like to thank all my family and friends. They have all helped me to complete this thesis, in one way or another.

Shingo Jason Takagi

The Univesity of British Columbia

October 2000

Chapter One

1 Optical Flow

1.1 Introduction

In this thesis we mainly investigate multiple light source optical flow [18] for objects which are translating or rotating around an axis parallel to the optical axis. The optical axis is the axis which passes through the image center and the optical center. In Figure 1.1.1, the imaging axis is the z-axis.

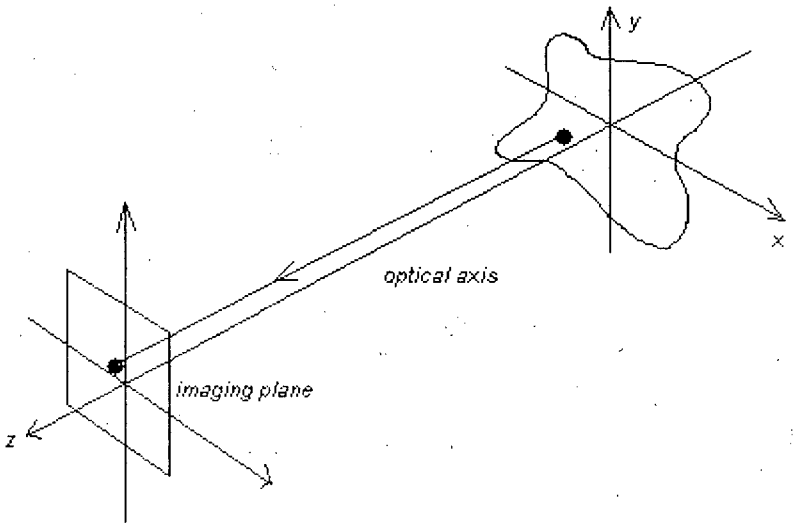

Figure 1.1.1: Imaging axis under orthographic projection.

Optical flow [7,9] is the apparent motion of the image intensity pattern. Often the optical flow will correspond with the actual motion field in the scene, but there are many cases in which this is not true. The classic example is that of a sphere that is rotating. In the absence of distinct surface markings, the image sequence of a sphere that is rotating will

be constant since there are no changes in the image intensity pattern. Hence the optical flow will be zero at points on the sphere. However the actual motion field is a rotation of the sphere.

Often in the calculation of the optical flow, it is assumed that the radiance of a point $E(x,y,t)$ does not change over time. This can be stated mathematically as

$$\frac{dE(x,y,t)}{dt} = \frac{\partial E}{\partial x}u + \frac{\partial E}{\partial y}v + \frac{\partial E}{\partial t} = 0$$

Equation 1.1.1

where u, and v are dx/dt, and dy/dt respectively. This assumption implies that no matter how the surface normal at that point changes over time its radiance is constant. This is true under translation under distant light sources, but in general this assumption is not correct. For example, under rotation, the radiance at a point changes with time as its surface normal changes with respect to the lights sources and the viewer.

It is enlightening to see that it is possible to solve Equation 1.1.1 for the normal velocity. The normal velocity is the component of (u,v) in the direction of the intensity gradient. If we let the normal velocity be v_n, then

$$v_n = \frac{-dE/dt}{\|\nabla E\|} \times \frac{\nabla E}{\|\nabla E\|}$$

Equation 1.1.2

However the velocity perpendicular to the normal velocity cannot be recovered, without additional information. Essentially the problem is that the system is under-determined.

Suppose we let a surface be represented by $z = f(x,y)$, under orthographic projection, where z points along the optical axis, and x and y form the image coordinates,

as in Figure 1.1.1. Letting the partial derivatives of f be represented by p and q, we have $p = \frac{\partial f}{\partial x}$, and $q = \frac{\partial f}{\partial y}$. The general image irradiance equation can be written as

$$E(x, y) = R(p, q)$$

Equation 1.1.3

where E is the image irradiance at the point (x,y) in the image and R is the scene radiance produced by a surface point with p and q as partial derivatives. Note that x and y are functions of time t, and p and q are functions of x, y and hence t.

Therefore compared to Equation 1.1.1, the general equation for dE/dt is

$$\frac{dE}{dt} = \frac{\partial E}{\partial x}u + \frac{\partial E}{\partial y}v + \frac{\partial E}{\partial t} = \frac{\partial R}{\partial p}\left[\frac{\partial p}{\partial x}u + \frac{\partial p}{\partial y}v + \frac{\partial p}{\partial t}\right] + \frac{\partial R}{\partial q}\left[\frac{\partial q}{\partial x}u + \frac{\partial q}{\partial y}v + \frac{\partial q}{\partial t}\right]$$

Equation 1.1.4

In Equation 1.1.1 and Equation 1.1.4, it is the u and v quantities that form the optical flow. Equation 1.1.1 is an equation in two unknowns, u and v, so it is not possible to solve for u and v uniquely, without regularization. Often, the minimum norm solution of (u,v) is chosen as an initial approximation for some global regularization method, in these cases.

Chapter Two

2 Multiple Light Source Optical Flow

2.1 Introduction

Photometric stereo is used in our optical flow estimation to help introduce more knowledge of the three dimensional world into our optical flow equations. Photometric stereo allows us to determine surface gradients at all points on an imaged object, and hence its curvature. It involves the use of multiple images of the same scene taken simultaneously from the same view point, but under different illumination conditions. This is typically accomplished by illuminating the scene with three light sources from different directions. The light sources are isolated in the red, green, and blue spectrums. A colour camera is then used to capture the scene. The red, green, and blue planes of the colour image records the scene under the red, green, and blue illuminations conditions, respectively.

In photometric stereo [17], the situation can be described with three image irradiance equations.

$$E_1(x,y) = R_1(p,q)$$
$$E_2(x,y) = R_2(p,q)$$
$$E_3(x,y) = R_3(p,q)$$

Equation 2.1.1

C. E. Siegerist's work [14,15] uses the classic optical flow constraint equation, and assumes that the image irradiance E is constant over time.

$$\frac{dE}{dt} = E_x \frac{dx}{dt} + E_y \frac{dy}{dt} + E_t = 0,$$

$$\text{where} \quad E_x = \frac{\partial E}{\partial x}, \quad E_y = \frac{\partial E}{\partial y}, \quad E_t = \frac{\partial E}{\partial t}$$

Equation 2.1.2

If three images are acquired, we end up with a system of three linear equations in two unknowns. The unknowns are dx/dt, and dy/dt, which form the optical flow. The equations are as follows.

$$\begin{aligned} E_{1x}u + E_{1y}v + E_{1t} &= 0 \\ E_{2x}u + E_{2y}v + E_{2t} &= 0 \\ E_{3x}u + E_{3y}v + E_{3t} &= 0 \end{aligned}$$

Equation 2.1.3

where, $u = \frac{dx}{dt}$, $v = \frac{dy}{dt}$. In general this is an over determined system, and the least squares solution for u and v can be found as

$$\begin{bmatrix} u \\ v \end{bmatrix} = (A^T A)^{-1} A^T \begin{bmatrix} -E_{1t} \\ -E_{2t} \\ -E_{3t} \end{bmatrix}$$

$$\text{where} \quad A = \begin{bmatrix} E_{1x} & E_{1y} \\ E_{2x} & E_{2y} \\ E_{3x} & E_{3y} \end{bmatrix}$$

Equation 2.1.4

However, under certain conditions, Equation 2.1.3 will not be over determined, and may be under determined. This will be discussed later in section 3.4 on degenerate cases.

C. E. Siegerist's work [14,15] on real time multiple light source optical flow shows that this method works quite well for translational motion. However the assumption that $dE/dt = 0$ is only correct under translation and infinitely distant light sources. In order to avoid making this assumption, Equation 1.1.4, the derivative of the full image irradiance equation with respect to time, was used. David Hsu's work [11] extends the classic optical flow constraint equation to an equation similar to Equation 1.1.4 for the three light sources. It tries to account for cases which are not just translational in nature by accounting for the changes in the intensity of a point due to surface normal changes at that point. This leads to an underdetermined system, and he was able to show that by tuning the regularization parameters, a minimal rotation, or a maximal rotation solution for the optical flow could be obtained. The minimal rotation solution favored a solution in which the surface normal did not change. This tends to yield the same results as if the optical flow constraint equation, Equation 1.1.1, had been used, and is accurate under conditions of translations. The maximal rotation solution favors a solution in which the surface normals change significantly. This yields results which are quite different from those had the optical flow constraint equation been used.

Chapter Three

3 Physical Surface Area Based Approach

3.1 Introduction

In our method, we also extend the optical flow constraint equations, and create an initial system of equations which are similar to that used by David Hsu [11], except that we have constructed the reflectance map, R, as a function of the surface gradient, p and q, instead of the unit surface normal, which can represented by three variables, and an additional constraint equation. We use the full image irradiance equation, Equation 1.1.4, for the three imaging conditions in multiple light source optical flow. The only unknowns in these equations are u and v. The other entities can be calculated from the image sequence or knowledge of the reflectance map.

$$E_{1x}u + E_{1y}v + E_{1t} = R_{1p}\frac{dp}{dt} + R_{1q}\frac{dq}{dt}$$

Equation 3.1.1

$$E_{2x}u + E_{2y}v + E_{2t} = R_{2p}\frac{dp}{dt} + R_{2q}\frac{dq}{dt}$$

Equation 3.1.2

$$E_{3x}u + E_{3y}v + E_{3t} = R_{3p}\frac{dp}{dt} + R_{3q}\frac{dq}{dt}$$

Equation 3.1.3

Note that

$$\frac{dp}{dt} = \frac{\partial p}{\partial x}u + \frac{\partial p}{\partial y}v + \frac{\partial p}{\partial t}$$

Equation 3.1.4

and

$$\frac{dq}{dt} = \frac{\partial q}{\partial x}u + \frac{\partial q}{\partial y}v + \frac{\partial q}{\partial t}$$

Equation 3.1.5

Note that

$$E_{1x} = R_{1p}\frac{\partial p}{\partial x} + R_{1q}\frac{\partial q}{\partial x}$$
$$E_{1y} = R_{1p}\frac{\partial p}{\partial y} + R_{1q}\frac{\partial q}{\partial y}$$
$$E_{1t} = R_{1p}\frac{\partial p}{\partial t} + R_{1q}\frac{\partial q}{\partial t}$$
$$E_{2x} = R_{2p}\frac{\partial p}{\partial x} + R_{2q}\frac{\partial q}{\partial x}$$
$$E_{2y} = R_{2p}\frac{\partial p}{\partial y} + R_{2q}\frac{\partial q}{\partial y}$$
$$E_{2t} = R_{2p}\frac{\partial p}{\partial t} + R_{2q}\frac{\partial q}{\partial t}$$
$$E_{3x} = R_{3p}\frac{\partial p}{\partial x} + R_{3q}\frac{\partial q}{\partial x}$$
$$E_{3y} = R_{3p}\frac{\partial p}{\partial y} + R_{3q}\frac{\partial q}{\partial y}$$
$$E_{3t} = R_{3p}\frac{\partial p}{\partial t} + R_{3q}\frac{\partial q}{\partial t}$$

Equation 3.1.6

The above equations can be rearranged as

$$E_{1x}u + E_{1y}v - \alpha_1 = -E_{1t}$$

Equation 3.1.7

$$E_{2x}u + E_{2y}v - \alpha_2 = -E_{2t}$$

Equation 3.1.8

$$E_{3x}u + E_{3y}v - \alpha_3 = -E_{3t}$$

Equation 3.1.9

$$p_x u + p_y v - a = -p_t$$

Equation 3.1.10

$$q_x u + q_y v - b = -q_t$$

Equation 3.1.11

And in matrix form the above can be represented as

$$\begin{bmatrix} E_{1x} & E_{1y} & -1 & 0 & 0 & 0 & 0 \\ E_{2x} & E_{2y} & 0 & -1 & 0 & 0 & 0 \\ E_{3x} & E_{3y} & 0 & 0 & -1 & 0 & 0 \\ p_x & p_y & 0 & 0 & 0 & -1 & 0 \\ q_x & q_y & 0 & 0 & 0 & 0 & -1 \end{bmatrix} \begin{bmatrix} u \\ v \\ \alpha_1 \\ \alpha_2 \\ \alpha_3 \\ a \\ b \end{bmatrix} = \begin{bmatrix} -E_{1t} \\ -E_{2t} \\ -E_{3t} \\ -p_t \\ -q_t \end{bmatrix}$$

Equation 3.1.12

where a, b, α_1, α_2, and α_3 are equal to the total derivatives of $\frac{dp}{dt}$, $\frac{dq}{dt}$ $\frac{dR_1}{dt}$, $\frac{dR_2}{dt}$, and $\frac{dR_3}{dt}$ respectively. The variables α_1, α_2, and α_3 are also equal to $\frac{dE_1}{dt}$, $\frac{dE_2}{dt}$, and $\frac{dE_3}{dt}$ respectively, because $\frac{dE_i}{dt} = \frac{dR_i}{dt}$, for i = 1, 2, and 3.

3.2 Photometric Surface Constraint

R. J. Woodham [17] introduced the notion that all the intensity triples from a lambertian surface, under photometric stereo conditions, lie on an ellipsoid in the space of intensity triples. Elli Angelopoulou and Lawrence B. Wolff [1,2,3] extended this to show that the intensity triples from a generalized diffuse surface lie on a closed convex surface in the space of intensity triples. This closed convex surface will be referred to as the photometric surface. At any given point in the image, its intensity triple will correspond to a point on this photometric surface. As time progresses, the surface normal (n_1, n_2, n_3) and the intensity triple at a point in the image will change and the respective point on the photometric surface will move to a new point on the photometric surface. Because the point is constrained to lie on this photometric surface, its velocity vector, $(\frac{dR_1}{dt}, \frac{dR_2}{dt}, \frac{dR_3}{dt})$, on the photometric surface will always be perpendicular to the surface normal of this photometric surface. From the notation used in Equation 3.1.7, Equation 3.1.8, and Equation 3.1.9, the velocity vector can be written as $(\alpha_1, \alpha_2, \alpha_3)$.

Let us define the photometric surface as

$$F(E_1, E_2, E_3) = 0$$

Equation 3.2.1

Then the normal (n_1, n_2, n_3) to this surface is

$$(n_1, n_2, n_3) = (\frac{dF}{dE_1}, \frac{dF}{dE_2}, \frac{dF}{dE_3})$$

Equation 3.2.2

Because of the relation in Equation 2.1.1, the surface normal can be equivalently expressed as a cross product of vector derivatives of the reflectance with respect to p and q.

$$\begin{aligned}(n_1, n_2, n_3) &= (R_{1p}, R_{2p}, R_{3p}) \times (R_{1q}, R_{2q}, R_{3q}) \\ &= (R_{2p}R_{3q} - R_{3p}R_{2q}, R_{3p}R_{1q} - R_{1p}R_{3q}, R_{1p}R_{2q} - R_{2p}R_{1q})\end{aligned}$$

Equation 3.2.3

Therefore the photometric constraint can be written as

$$(R_{2p}R_{3q} - R_{3p}R_{2q}, R_{3p}R_{1q} - R_{1p}R_{3q}, R_{1p}R_{2q} - R_{2p}R_{1q}) \bullet (\alpha_1, \alpha_2, \alpha_3) = 0$$

Equation 3.2.4

Hence it appears that knowledge of all the photometric surface normals will allow us to introduce an additional constraint on our optical flow equations. However this is not the case. In fact the photometric constraint is a consequence of Equation 3.1.7, Equation 3.1.8, Equation 3.1.9, Equation 3.1.10, and Equation 3.1.11. To see this, let us first convert Equation 3.1.7, Equation 3.1.8, and Equation 3.1.9 into equations using derivatives of the reflectance, using the identities in Equation 3.1.6. Equation 3.1.7, Equation 3.1.8, and Equation 3.1.9 become

$$(R_{1p}p_x + R_{1q}q_x)u + (R_{1p}p_y + R_{1q}q_y)v - \alpha_1 = -R_{1p}p_t - R_{1q}q_t$$

Equation 3.2.5

$$(R_{2p}p_x + R_{2q}q_x)u + (R_{2p}p_y + R_{2q}q_y)v - \alpha_2 = -R_{2p}p_t - R_{2q}q_t$$

Equation 3.2.6

$$(R_{3p}p_x + R_{3q}q_x)u + (R_{3p}p_y + R_{3q}q_y)v - \alpha_3 = -R_{3p}p_t - R_{3q}q_t$$

Equation 3.2.7

Now we can subtract Equation 3.1.10 multiplied by R_{1p} and Equation 3.1.11 multiplied by R_{1q}, from Equation 3.2.5 to get

$$-\alpha_1 + R_{1p}a + R_{1q}b = 0$$

Equation 3.2.8

Subtracting Equation 3.1.10 multiplied by R_{2p} and Equation 3.1.11 multiplied by R_{2q}, from Equation 3.2.6, we get

$$-\alpha_2 + R_{2p}a + R_{2q}b = 0$$

Equation 3.2.9

Subtracting Equation 3.1.10 multiplied by R_{3p} and Equation 3.1.11 multiplied by R_{3q}, from Equation 3.2.7, we get

$$-\alpha_3 + R_{3p}a + R_{3q}b = 0$$

Equation 3.2.10

Finally summing up Equation 3.2.8 multiplied by $-(R_{2p}R_{3q} - R_{3p}R_{2q})$, Equation 3.2.9 multiplied by $-(R_{3p}R_{1q} - R_{1p}R_{3q})$, and Equation 3.2.10 multiplied by $-(R_{1p}R_{2q} - R_{2p}R_{1q})$ yields

$$(R_{2p}R_{3q} - R_{3p}R_{2q})\alpha_1 + (R_{3p}R_{1q} - R_{1p}R_{3q})\alpha_2 + (R_{1p}R_{2q} - R_{2p}R_{1q})\alpha_3 = 0$$

Equation 3.2.11

which is just the photometric surface constraint, Equation 3.2.4. Hence the photometric surface constraint equation does not provide any additional constraint to our existing equations.

3.3 The Physical Surface Area Constraint For Rotations

Accounting for physical surface area in the scene however does provide an additional constraint on our optical flow equations. Let us represent a surface as $z = f(x, y)$, a function on x and y. Now let us consider trying to find the area of a patch Ω. Let us assume that we know the value of p and q at (x,y), where $p = \frac{\partial f}{\partial x}$, and $q = \frac{\partial f}{\partial y}$. The area S of the surface over a patch Ω in the x and y plane can be expressed as follows. Let n be the surface normal.

$$n = (1,0,p) \times (0,1,q) = (-p,-q,1)$$

Equation 3.3.1

$$S = \iint_{\Omega} |n| dxdy = \iint_{\Omega} \sqrt{p^2 + q^2 + 1} dxdy$$

Equation 3.3.2

Then a small area *ds*, at (x,y) can be expressed as

$$ds = \sqrt{1 + p^2 + q^2}\, dxdy$$

Equation 3.3.3

The surface gradients p and q are functions of x and y, and the x and y are themselves functions of the time, t. So the infinitesimal area, *ds*, will remain constant under conditions of translation. This is because the object is only translating and the surface gradients at a given (x,y), with respect to the viewer, are not changing. The infinitesimal area, *ds*, will also remain constant under conditions of rotation around an axis parallel to the optical axis, since, in this case, $(p^2 + q^2)$ is constant.

Therefore under conditions of translations and rotations around axes parallel to the optical axis, the area *ds* should not change as time moves along. This can be expressed as

$$\frac{d(ds)}{dt} = 0$$

Equation 3.3.4

Let us denote *ds* by A for convenience. Then we have.

$$\frac{dA(x, y, t)}{dt} = A_x u + A_y v + A_t$$

Equation 3.3.5

$$\frac{dA}{dx} = \frac{1}{2}(1 + p^2 + q^2)^{-\frac{1}{2}}(2pp_x + 2qq_x) = \frac{pp_x + qq_x}{\sqrt{1 + p^2 + q^2}}$$

Equation 3.3.6

$$\frac{dA}{dy} = \frac{pp_y + qq_x}{\sqrt{1 + p^2 + q^2}}$$

Equation 3.3.7

$$\frac{dA}{dt} = \frac{pp_t + qq_t}{\sqrt{1 + p^2 + q^2}}$$

Equation 3.3.8

So combining these equations, we get:

$$(pp_x + qq_x)u + (pp_y + qq_y)v + pp_t + qq_t = 0$$

Equation 3.3.9

Combining Equation 3.3.9 with Equation 3.1.7, Equation 3.1.8, Equation 3.1.9, Equation 3.1.10, and Equation 3.1.11, we get a system of 6 equations in 7 unknowns in the best case. This will be the system that we use in our approach to solve for optical flow.

$$\begin{bmatrix} E_{1x} & E_{1y} & -1 & 0 & 0 & 0 & 0 \\ E_{2x} & E_{2y} & 0 & -1 & 0 & 0 & 0 \\ E_{3x} & E_{3y} & 0 & 0 & -1 & 0 & 0 \\ p_x & p_y & 0 & 0 & 0 & -1 & 0 \\ q_x & q_y & 0 & 0 & 0 & 0 & -1 \\ pp_x + qq_x & pp_y + qq_y & 0 & 0 & 0 & 0 & 0 \end{bmatrix} \begin{bmatrix} u \\ v \\ \alpha_1 \\ \alpha_2 \\ \alpha_3 \\ a \\ b \end{bmatrix} = \begin{bmatrix} -E_{1t} \\ -E_{2t} \\ -E_{3t} \\ -p_t \\ -q_t \\ -pp_t - qq_t \end{bmatrix}$$

Equation 3.3.10

3.4 Degenerate Cases

In order to solve for the optical flow using Equation 2.1.3 or Equation 3.3.10, we generally need to calculate the matrix product $A^T A$. For solving Equation 2.1.3, we use $A^T A$ as described in Equation 2.1.4. For solving Equation 3.3.10, $A^T A$ is used in a local regularization process which is described in section 4.2 on local regularization. Hence knowledge of the rank of $A^T A$ is helpful in determining whether a solution can be found.

In Equation 2.1.3, u and v are over determined. There are, however, several cases in which this system of equations will degenerate, and it becomes impossible to solve for the optical flow using the method described after the definition of the systems of Equation 2.1.3. These degeneracies occur when the object's surface is planar or developable. When the surface being imaged is planar, the matrix A has no linearly independent rows. To see this we just need to note that if the surface is planar then

$$E_{ix} = E_{iy} = 0 \text{ for all i=1, 2, and 3}$$

Equation 3.4.1

as the image intensity is the same at all points on the planar surface. Hence $A^T A$, will have a rank of zero.

When the surface is developable, the matrix A has only one linearly independent row. The reason why the matrix A has one linearly independent row is due to the following property which occurs when the surface is developable [16].

$$\frac{E_{iy}}{E_{ix}} = \frac{E_{jy}}{E_{jx}} \text{ for } i=1, 2, 3, \text{ and } j=1, 2, 3$$

Equation 3.4.2

To see this we first note that

$$\begin{bmatrix} E_x \\ E_y \end{bmatrix} = H \begin{bmatrix} R_p \\ R_q \end{bmatrix} \text{ where } H = \begin{bmatrix} p_x & p_y \\ q_x & q_y \end{bmatrix}$$

Equation 3.4.3

H is known as the Hessian matrix, and for developable surfaces it can be shown that the determinant of the Hessian is zero. Because H is positive definite, it can be factored as

$$H = R^{-1} \begin{bmatrix} \lambda & 0 \\ 0 & 0 \end{bmatrix} R, \text{ where } R \text{ is a rotation matrix.}$$

Equation 3.4.4

Hence no matter what (R_p, R_q) is, it will be mapped to a point, (E_x, E_y), on a straight line. From this it can be shown that Equation 3.4.2 holds. Since A has one linearly independent row, the matrix product, $A^T A$, will have a rank less than or equal to one. This follows from the following inequality of matrix ranks [13].

$$rank(BC) < rank(B), \text{ and}$$

$$rank(BC) < rank(C)$$

Equation 3.4.5

Equation 3.3.10 also has similar degenerate cases. Before we delve into these degenerate cases, which can decrease the rank of $A^T A$, let us first prove another lemma concerning the number of independent rows of A and the rank of $A^T A$.

Lemma 1. If A is an m by p matrix with $m<p$ and has m independent rows, then $A^T A$ has full rank. (In other words, the rank of $A^T A$ is equal to m.)

Proof: This follows from Sylvester's inequality [10, page 13]

$$rank(B) + rank(C) - k \leq rank(BC) \leq \min(rank(B), rank(C)$$

Equation 3.4.6

where B is an m by k matrix with k independent columns, and C is an arbitrary k by n matrix. If we let B equal A^T, and C equal A, we get

$$m \leq rank(A^T A) \leq m$$

Equation 3.4.7

as k is equal to m, here. Hence the rank of $A^T A$ is m, if A is m by p with m independent rows.

Let us consider the Equation 3.3.10 as $Ax=b$. The maximum number of independent rows A can have is 6. In this case, from lemma 1, $A^T A$ will have full rank.

The minimium number of independent rows A can have is 5. In this case, from the inequalities in Equation 3.4.5, $A^T A$ will have a rank less than or equal to 5. A has a minimum of 5 independent rows because the first five rows has an element, -1, in a column where all other rows have zero. Hence these 5 rows are able to span a space with dimension 5, and are linearly independent. The matrix, A, will have 5 independent rows when $(pp_x + qq_x)$ and $(pp_y + qq_y)$ from the last row of Equation 3.3.10 are zero. If $(pp_x + qq_x)$ or $(pp_y + qq_y)$ are not equal to zero, the matrix A will have 6 independent rows.

There are many conditions which might cause $(pp_x + qq_x)$ and $(pp_y + qq_y)$ to be zero. An obvious case is when the surface is planar. In this case the p and q are constant and the partial derivatives of p and q are zero. It is interesting to note however that developable surfaces do not in general cause $(pp_x + qq_x)$ and $(pp_y + qq_y)$ to be zero, and hence do not in general decrease the rank of matrix A as they did when we were considering the matrix A from Equation 2.1.3, which uses the classic optical flow constraint equations.

Chapter Four

4 Implementation

4.1 Hardware and Software Setup

Optical flow calculations were carried out on a Pentium III 300 MHz computer. The programs were written in Visual C++ 6.0, and made use of CLAPACK (C Linear Algebra Package), and Microsoft's Vision Software Development Kit. One synthetic image was synthesized using Kinetic's 3D Studio Max, but most of the synthetic data was created by self made programs through a knowledge of surface gradients and reflectance maps.

In order to estimate the optical flow, the Equation 3.3.10 is solved through a local regularization at each pixel for the seven unknowns. All the elements in the 6 by 7 matrix, A, and the 6 by 1 matrix, b, can be calculated. The image gradients E_{1x}, E_{1y}, E_{1t}, E_{2x}, E_{2y}, E_{2t}, E_{3x}, E_{3y}, and E_{3t}, can be determined by taking partial derivatives in the image sequence. The surface gradients, p and q, can be determined from the photometric stereo lookup table. The derivatives of the surface gradients p_x, p_y, p_t, q_x, q_y, and q_t can be determined by taking discrete derivatives of p and q, but a method which is less sensitive to noise is used.

Before the image gradients are calculated, all the images are smoothed with a 5 by 5 discrete Gaussian filter, with $\sigma = 1$. The image gradients are calculated by using a kernel of size 5. The following are the exact values in this difference kernel.

diff_kernel[-2] = (float)-1.0/12.0

diff_kernel[-1] = (float)8.0/12.0

diff_kernel[0] = (float)0.0

diff_kernel[1] = (float)-8.0/12.0

diff_kernel[2] = (float)1.0/12.0

This kernel has element 0 as the center element, and is convolved with the smoothed images in the x, and y orientations, and also in time. The gradients in time are taken over 5 images, 2 before and after in the time sequence to the image of interest.

Photometric stereo [17] allows us to obtain surface gradient information from intensity triples. The photometric stereo lookup table is a table containing surface gradient doubles, (p,q), associated with intensity triples, and is indexed by these intensity triples. This photometric stereo lookup table yields important information about other potential imaged objects provided that they are made of the same material, have the same reflectance properties, and are imaged under the same imaging geometry. The imaging geometry refers to the camera, and the relative positions of the three light sources with respect to the camera. To build the photometric stereo lookup table, a real or synthetic image of a calibration sphere is used. The image is analysed and the associations between intensity triples and gradient doubles (p,q) are made. As in R. J. Woodham's work [17], we use the following equations to make the association between intensity triples and the gradient doubles (p,q). The sphere is represented as

$$x^2 + (\lambda y)^2 + z^2 = r^2$$

Equation 4.1.1

where λ takes the aspect ratio into account. The intensity triple at the point (x,y) in the image is associated with the gradient double (p,q), by the following equation.

$$p = -\frac{x}{z} \quad q = -\frac{\lambda^2 y}{z}$$

Equation 4.1.2

Hence if the imaging geometry or the material of interest changes, the photometric stereo lookup table must be recalibrated again in order to be useful.

Photometric stereo [17] utilizes spectral multiplexing. Spectral multiplexing involves the use of multiple images taken from the same viewpoint, but under different conditions of illuminations. As in R. J. Woodham's work [17], we use three images in our spectral multiplexing, under three illumination conditions. For real images, the three images are acquired simultaneously in a colour image, with a Sony DXC-950 3 CCD 24-bit colour camera with a Sony VCL-714BXEA zoom lens. The red, green, and blue fields of the colour image form the three images. The red, green, and blue fields of the colour image can capture a scene under three different illumination conditions, if the three light sources illuminate the scene from different directions, and are sufficiently isolated in the red, green, and blue parts of the visible spectrum. This photometric stereo setup for real images used three Newport MP-1000 Moire (white-light) projectors with associated Nikon lenses and spectral filters. The filters separted the white light into the red, blue, and green parts of the spectrum. The filters were manufactured by Corion. R.Woodham's work [17] showed that there was negligible overlap in the wavelengths of

the red, blue, and green filtered light sources. The light sources were placed so as to illuminate the camera's area of interest from different directions.

Spectral multiplexing was also artificially introduced into the synthetic images. This was accomplished by using different reflectance maps for the intensities in the red, green, and blue fields of the image. The different reflectance maps are specific to the different illumination directions of the red, green, and blue filtered light sources, and are derived from the calibration sphere used in the photometric stereo setup. This is done by inverting the association between and intensity triple (r,g,b), and its surface gradient (p,q). The red, green, and blue reflectance maps are tables which map the surface gradient (p,q) to the r, g, and b elements respectively of the intensity triple. Surface gradients (p,q) which are not explicitly in the table can be interpolated at run time from the recorded data.

In order to calculate the partial derivates of the surface gradient (p,q) in a manner which is less sensitive noise we make use the derivatives of the three reflectance maps for the three different illumination conditions, which in our case is the red, green, and blue illumination conditions. The derivatives of the reflectance maps R_{1p}, R_{1q}, R_{2p}, R_{2q}, R_{3p}, and R_{3q} are calculated at run time, as needed, from the reflectance maps. The derivatives of the surface gradient, p_x, p_y, p_t, q_x, q_y, and q_t are calculated as follows. The equations in Equation 3.1.6 in matrix form are

$$\begin{bmatrix} E_{1x} & E_{2x} & E_{3x} \\ E_{1y} & E_{2y} & E_{3y} \\ E_{1t} & E_{2t} & E_{3t} \end{bmatrix} = \begin{bmatrix} p_x & q_x \\ p_y & q_y \\ p_t & q_t \end{bmatrix} \begin{bmatrix} R_{1p} & R_{2p} & R_{3p} \\ R_{1q} & R_{2q} & R_{3q} \end{bmatrix}$$

Equation 4.1.3

Considering the above as

$$E = QM^T$$

Equation 4.1.4

we can solve for Q as

$$Q = EM(M^T M)^{-1}$$

Equation 4.1.5

The derivatives of the surface gradient, p_x, p_y, p_t, q_x, q_y, and q_t q_t can be extracted from Q.

Because tables used in gradient lookup are potentially very long, it became important to determine how many significant bits are in the images taken by our system. This was accomplished by looking at the least significant bits of the image and deciding whether there was a non-random pattern in the image. If there was a non-random pattern in the image, then it was likely that it reflected the underlying scene, and therefore contained significant information. We started by looking at the least significant bit, then the last two significant bits, etc. We found that the two least significant bits did not contain much information. Hence instead of indexing the tables with 8 bit intensity values, we use 6 bit intensity values. Hence instead of having 16,777,216 (2^8 * 2^8 * 2^8) entries in our tables, we have 262,144 (2^6 * 2^6 * 2^6) entries in our tables.

4.2 Local Regularization

Given that all the elements besides the unknowns can be estimated in Equation 3.3.10, local regularization can to be used. This local regularization does not consider information from any other points in the image, as in global regularization, or any other non-local regularization. Again, let us represent Equation 3.3.10 as

$$Ax = b$$

Equation 4.2.1

The regularization that is used is one which finds the x which minimizes

$$\lambda_0 \|Px\|^2 + \lambda_1 \|Ax - b\|$$

Equation 4.2.2

where $\lambda_1 \geq 0$ and $\lambda_2 \geq 0$ are regularization parameters chosen beforehand. P represents a stabilization function, and is also chosen in advance. Two types of regularization were implemented and tested. Both of which were studied by D. Hsu's work [11] on multiple light source optical flow. The regularizations make use of QR factorization and Singular Value Decomposition (SVD).

The standard QR factorization [13] of a real m by n matrix A is given by

$$A = Q \begin{pmatrix} R \\ 0 \end{pmatrix}$$

Equation 4.2.3

where R is an n by n upper triangular matrix , Q is an m by m orthogonal matrix, and $m \geq n$. If A has n linearly independent rows, then R is non-singular. Often the factorization is written as

$$A = (Q_1 Q_2) \begin{pmatrix} R \\ 0 \end{pmatrix}$$

Equation 4.2.4

which reduces to

$$A = Q_1 R$$

Equation 4.2.5

where Q_1 consists of the first n columns of Q, and Q_2 consists of the remaining columns.

The Singular Value Decomposition [13] of a real m by n matrix A is given by

$$A = U \Sigma V^T$$

Equation 4.2.6

Here, the U and V matrices are orthogonal, and Σ is an m by n diagonal matrix with real diagonal elements σ_i.

$$\sigma_1 \geq \sigma_2 \geq \ldots \geq \sigma_{\min(m,n)} \geq 0$$

Equation 4.2.7

These real diagonal elements σ_i are known as the singular values of A, and the first $\min(m,n)$ columns of U and V are known as the left and right singular vectors of A. The mathematical relation between singular values and singular vectors is described below.

$$Av_i = \sigma_i u_i \text{ and } A^T u_i = \sigma_i v_i$$

Equation 4.2.8

where u_i is the ith left singular vector, and v_i is the ith right singular vector.

Method 1

This method assumes that the measurements are exact. So $\|Ax - b\|$ is weighted heavily. In fact if we set $\lambda_1 = \infty$, and $\lambda_0 = 1$, the problem essentially becomes one of finding the x which minimizes $\|Px\|$, subject to $Ax = b$. This regularization problem has a unique solution up to the nullspace of P. The algorithm used is as follows.

First we use QR factorization on A^T to get $A^T = Q\begin{pmatrix} R \\ 0 \end{pmatrix} = (Q_1 Q_2)\begin{pmatrix} R \\ 0 \end{pmatrix}$. A^T is a 7 by 6 matrix, Q_1 is a 7 by 6 matrix, Q_2 is a 7 by 1 matrix, and R is a 6 by 6 upper triangular matrix. The matrix Q which is equal to $(Q_1 Q_2)$ is a 7 by 7 orthogonal matrix. Now

$$\begin{pmatrix} R \\ 0 \end{pmatrix}^T Q^T x = b$$

Equation 4.2.9

So if we let

$$z = Q^T x$$

Equation 4.2.10

we get

$$\begin{pmatrix} R \\ 0 \end{pmatrix}^T z = b$$

Equation 4.2.11

Now let $z = \begin{bmatrix} z_1 \\ z_2 \end{bmatrix}$, where z_1 is a vector of six elements, and z_2 is a scalar. Then

$$R^T z_1 = b$$

Equation 4.2.12

can be solved uniquely, because R, in general, will have a rank of 6. Note that z_2 can be any value and Equation 4.2.11 will still be satisfied. This means that z_2 can be adjusted so as to minimize $\|Px\|$.

Let

$$h(z_2) = \|Px\|^2$$

Equation 4.2.13

and $Q = [Q_1 : Q_2]$ where Q_1 is the first 6 columns of Q and Q_2 is the last column of Q. Substituting Equation 4.2.10 into Equation 4.2.13 we get

$$h(z_2) = \|PQz\|^2 = \|P(Q_1 z_1 + Q_2 z_2)\|^2$$

Equation 4.2.14

We only consider stabilizing functions, P, such that h is convex and has only one minimum. This way the minimum can be found at the point where the derivative of h is zero.

$$0 = h'(z_2) = 2[P(Q_1 z_1 + Q_2 z_2)]^T (PQ_2)$$

Equation 4.2.15

The solution is obtained by solving

$$(Q_2^T P^T P Q_2) z_2 = -Q_2^T P^T P Q_1 z_1$$

Equation 4.2.16

If P is positive definite, the solution is unique. If P is only positive semi-definite then we find the solution with minimum l_2 norm, by using Singular Value Decomposition (SVD) to solve Equation 4.2.16.

Method 2

The assumption, that the measurements are exact, in general will not be correct. In this case λ_1 should not be set to ∞. Instead it should be set to a finite value. So here we set $\lambda_0 = \lambda$ and $\lambda_1 = 1$, because only the ratio between λ_0 and λ_1 is important. In our implementations of this second method, we experiment with three different values for λ. The three different values are 0.00000001, 0.0001, and 0.1. Essentially here we are minimizing

$$h(x) = \|Ax - b\|^2 + \lambda \|Px\|^2$$

Equation 4.2.17

Again, we only consider stabilizing functions, P, such that h is convex and has only one minimum. The minimum occurs when the derivative of $h(x)$ is equal to zero.

$$0 = h'(x) = 2(Ax - b)^T A + 2\lambda(Px)^T P$$

Equation 4.2.18

$$0 = A^T(Ax - b) + \lambda P^T Px$$

Equation 4.2.19

Therefore

$$(A^T A + \lambda P^T P)x = A^T b$$

Equation 4.2.20

So x may be solved if $(A^T A + \lambda P^T P)$ is invertible. When it is not invertible, the solution x may not be unique, and so we chose the solution with the smallest norm. So Equation 4.2.20 is solved using the standard Singular Value Decomposition algorithm (SVD). One of the problems with this method is that $(A^T A + \lambda P^T P)$ has a large condition number and inverting $(A^T A + \lambda P^T P)$ is ill conditioned.

Stabilizing Functions

In general P can be taken to be any positive semi-definite matrix. In our applications P is a 7 by 7 diagonal matrix with diagonal entries $d_1, d_2, d_3, d_4, d_5, d_6$, and d_7. So

$$\|Px\| = \sqrt{\sum_{i=1..7} d_i^2 x_i^2}$$

Equation 4.2.21

The relative weights of the d_i's determines the contribution weight of the elements of the vector x. Because x corresponds to the 7 by 1 matrix in Equation 3.3.10

$$x = [u, v, \alpha_1, \alpha_2, \alpha_3, a, b]^T$$

Equation 4.2.22

The first two components of the solution, x, describe the translational component of the solution. The middle three components of the solution x, describe the change in the intensity triple, because $(\alpha_1, \alpha_2, \alpha_3) = (\frac{dE_1}{dt}, \frac{dE_2}{dt}, \frac{dE_3}{dt})$. The last two components of the solution x describe the rotational component of the solution, because a and b are equal to the total derivatives of the surface gradients p and q with respect to time. From here on the first two elements will be grouped and referred to as the translational component of the solution, the middle three components as the intensity change component of the solution, and the last two components as the rotational components of the solution.

In our implementations we have implemented four different types of stabilizing functions. The first is a stabilizing function that minimizes the intensity change and the rotational component of the solution. The intensity change and rotational component of

the solution are minimized by placing infinite weight on the intensity change and rotational components with respect to the other components, which are weighted with zero weight. This in effect tries to account for observed motion mainly by translation, and the associated P_1 has the following form.

$$P_1 = \begin{bmatrix} 0 & 0 & 0 & 0 & 0 & 0 & 0 \\ 0 & 0 & 0 & 0 & 0 & 0 & 0 \\ 0 & 0 & 1 & 0 & 0 & 0 & 0 \\ 0 & 0 & 0 & 1 & 0 & 0 & 0 \\ 0 & 0 & 0 & 0 & 1 & 0 & 0 \\ 0 & 0 & 0 & 0 & 0 & 1 & 0 \\ 0 & 0 & 0 & 0 & 0 & 0 & 1 \end{bmatrix}$$

Equation 4.2.23

The second stabilizing function minimizes the translational component of the solution. The translational component of the solution is minimized by placing infinite weight on the translational components with respect to the other components which are weighted with zero weight. This in effect tries to account for the observed motion mainly by rotation, and the associated P_2 has the following form.

$$P_2 = \begin{bmatrix} 1 & 0 & 0 & 0 & 0 & 0 & 0 \\ 0 & 1 & 0 & 0 & 0 & 0 & 0 \\ 0 & 0 & 0 & 0 & 0 & 0 & 0 \\ 0 & 0 & 0 & 0 & 0 & 0 & 0 \\ 0 & 0 & 0 & 0 & 0 & 0 & 0 \\ 0 & 0 & 0 & 0 & 0 & 0 & 0 \\ 0 & 0 & 0 & 0 & 0 & 0 & 0 \end{bmatrix}$$

Equation 4.2.24

The third stabilizing function minimizes the translational, intensity change, and rotational components of the solution. This is accomplished by weighting all components with a weight of one. This has the effect of selecting a solution to the optical flow problem with the minimum amount of translation and rotation, which are equally weighted.

$$P_3 = \begin{bmatrix} 1 & 0 & 0 & 0 & 0 & 0 & 0 \\ 0 & 1 & 0 & 0 & 0 & 0 & 0 \\ 0 & 0 & 1 & 0 & 0 & 0 & 0 \\ 0 & 0 & 0 & 1 & 0 & 0 & 0 \\ 0 & 0 & 0 & 0 & 1 & 0 & 0 \\ 0 & 0 & 0 & 0 & 0 & 1 & 0 \\ 0 & 0 & 0 & 0 & 0 & 0 & 1 \end{bmatrix}$$

Equation 4.2.25

The fourth stabilizing function minimizes the intensity change components of the solution. This is accomplished by weighting the intensity change components with a weight of one. This has the effect of selecting a solution to the optical flow problem with the minimum amount of intensity change. It is expected that the fourth stabilizing function will yield similar results to the minimal intensity change and rotation solution, because the less rotation there is, the less the intensity change will be.

$$P_4 = \begin{bmatrix} 0 & 0 & 0 & 0 & 0 & 0 & 0 \\ 0 & 0 & 0 & 0 & 0 & 0 & 0 \\ 0 & 0 & 1 & 0 & 0 & 0 & 0 \\ 0 & 0 & 0 & 1 & 0 & 0 & 0 \\ 0 & 0 & 0 & 0 & 1 & 0 & 0 \\ 0 & 0 & 0 & 0 & 0 & 0 & 0 \\ 0 & 0 & 0 & 0 & 0 & 0 & 0 \end{bmatrix}$$

Equation 4.2.26

In the four different stabilizing functions, the matrices P_1, P_2, P_3, and P_4 have different null spaces. The local regularization selects the minimum norm solution within these null spaces. The minimal intensity change and rotation solution is correct under translation under distant light sources, and yields a motion estimate which is similar to that obtained had we assumed the classic optical flow constraint equations. The minimal translation solution is correct for deforming surfaces with minimal translation but has significant surface normal changes. The minimal translation, intensity change, and rotation solution is more difficult to analyze. The assumptions on the observed motion for the minimal translation, and the minimal rotation case contradict each other. Hence the minimal translation, intensity change, and rotation solution is likely to be correct under a certain balance of rotation and translation in the scene.

Chapter Five

5 Synthetic Image Data

Experimentation and data collection were accomplished using synthetic image data. The true optical flow for the synthetic data could be calculated and then compared with the estimated optical flow from our algorithm. The motions in the sequences described below include translation, rotation, and deformation.

5.1 Calibration sphere

The synthetic calibration sphere was created using a program called "3D Studio Max 2.0" which is made by Kinetix. This is a three dimensional graphics program which allows one to place objects and light sources at arbitrary locations in a virtual environment, and to render this virtual scene using various shading models. Information on the various shading models can be obtained on the internet at the Uniform Resource Locator (URL), www.ktx.com. In this program, the calibration sphere was created by placing a sphere at the center of the scene, and placing red, green, and blue light sources behind the camera. The light sources were arranged so that they illuminated the sphere from three different directions. In this artificial environment the light sources were separated into the red, green, and blue parts of the spectrum with no overlaps. The calibration sphere was made of a dull white material, and a lambertian or diffuse reflectance model was used. The placement of the light sources illuminated the sphere

from the bottom left, top, and bottom right, for the red, blue, and green light sources respectively.

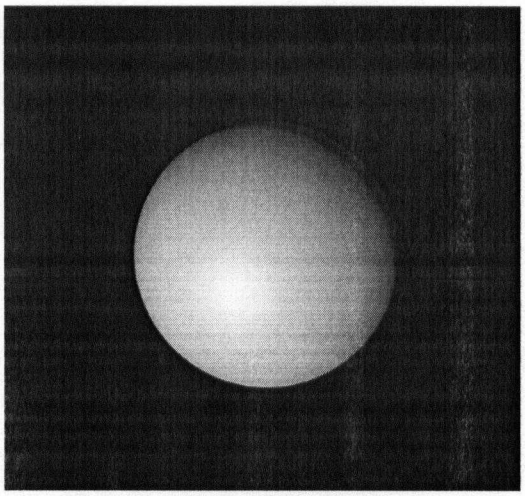

Figure 5.1.1: The calibration sphere under the red illumination.

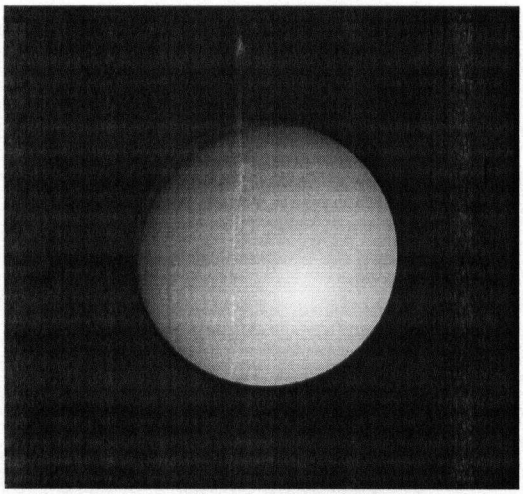

Figure 5.1.2: The calibration sphere under the green illumination.

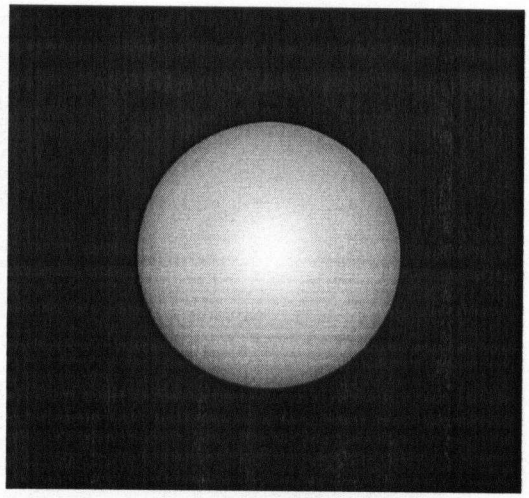

Figure 5.1.3: The calibration sphere under the blue illumination.

5.2 Translation of a Sphere

This sequence shows the synthetic calibration sphere translating horizontally to the right. The translational speed is constant at 1 pixel per frame. The sphere is a doubly curved object and hence the multiple light source optical flow from Siegerist's work [14,15] can be used.

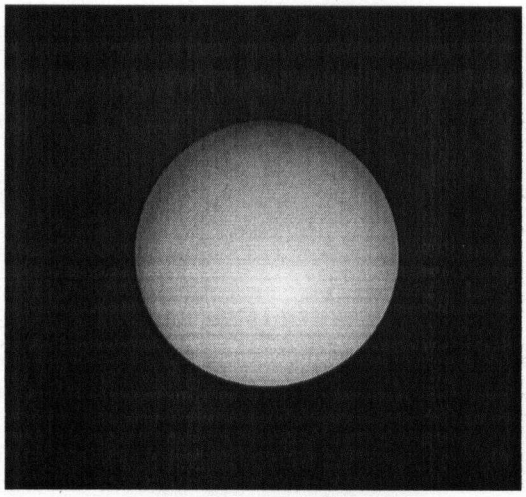

Figure 5.2.1: The first of 11 images in the translating calibration sphere sequence. The red, green, and blue illuminations have been superimposed.

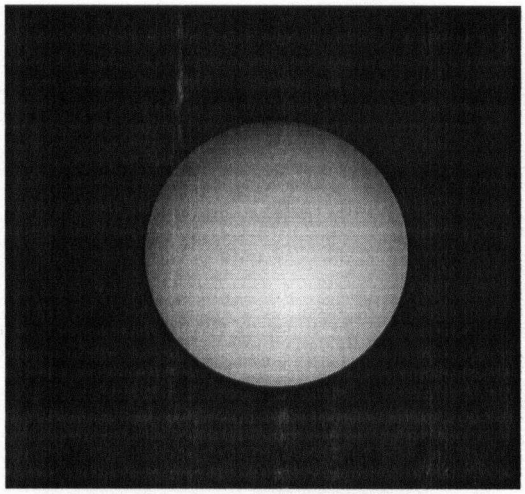

Figure 5.2.2: The last of 11 images in the translating calibration sphere sequence. The red, green, and blue illuminations have been superimposed.

5.3 Curving Sheet

The curving sheet image sequence shows a white sheet gradually curving. The surface normal at the center of the sheet is pointed towards the viewer. At the start of the sequence the sheet is almost flat, but then gradually the edges start curving away from the viewer. In order to determine the true optical flow of the sequence, it is important to understand how the curving sheet deformation was parameterized and formulated.

The curving sheet is parameterized by its length l in pixels, with l=0 representing the vertical line at the center of the sheet. The sheet is also parameterized by its width w in pixels, with w=0 representing the horizontal edge at the top of the sheet.

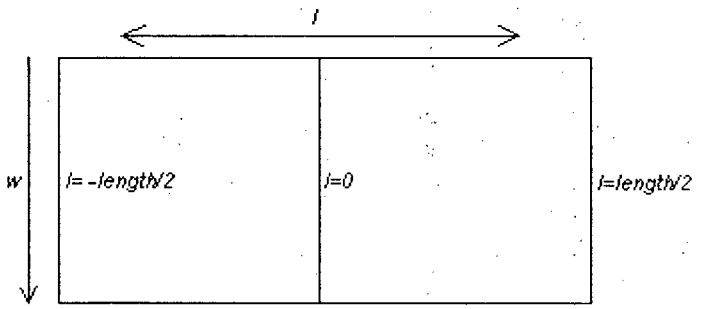

Figure 5.3.1: Diagram depicting the parameterization of curving surface.

The curving deformation on the sheet takes place only along the l axis. Since we are assuming an orthographic projection all horizontal lines represented by w=k, where k is some value, will continue to be projected to horizontal lines in the image sequence as the sheet deforms.

Let x and y be the image coordinates where x increases towards the right from x=0 at the left edge, and y increases downwards from y=0 at the top edge. Also we will

let time be represented by t. If we model the curving of the sheet as being wrapped around a cylinder which decreases in radius, then the radius decreases with time. When the radius is at infinity the sheet is flat, but as time moves on and the radius decreases, and the sheet wrapped around the cylinder appears to curve away from the viewer. We also let the radius $r=k-mt$, where k and m are some constants. Then under orthographic projection the sheet will be represented as

$$x = x_c + r\cos\left(\frac{l}{r} + \frac{\pi}{2}\right)$$
$$y = y_c + w$$
$$z = r\sin\left(\frac{l}{r} + \frac{\pi}{2}\right) - r$$

Equation 5.3.1

where (x_c, y_c) is the center of the image and the z-axis points towards the viewer along the optical center.

The l and w parameters of the sheet represent actual lengths. Since we are modeling a sheet that is deforming but not stretching, at each time step the l and w parameters are constrained to be within certain ranges at all times t in the image sequence.

$$-length/2 \le l \le length/2$$

$$0 \le w \le width$$

Equation 5.3.2

The following proves that l and w represent actual lengths on the sheet surface. Because of orthographic projection and the fact that there is no deformation occurring along the w axis, it is obvious that w represents actual length on the curved sheet. To show that l

represents actual length, we will determine the length along the l axis of the deforming sheet. This is equivalent to finding the arc length of the curve in the x and z plane. From elementary calculus, we know that, if X and Y are parameterized by l, then

$$arclength = \int \sqrt{X'^2 + Y'^2}\, dl$$

Equation 5.3.3

So in our case we have

$$arclength = \int \sqrt{x'^2 + z'^2}\, dl$$

Equation 5.3.4

$$arclength = \int \sqrt{\left(-\sin\left(\frac{l}{r} + \frac{\pi}{2}\right)\right)^2 + \left(\cos\left(\frac{l}{r} + \frac{\pi}{2}\right)\right)^2}\, dl$$

Equation 5.3.5

$$arclength = \int 1 dl = l$$

Equation 5.3.6

Hence it is clear that the parameter, l, is also a parameter which represents actual length in the horizontal direction on the surface of the curved sheet.

In order to synthesize the images of the deforming sheet we have just parameterized, we need to know the surface gradients (p,q), of the curving sheet.

$$p = \frac{\partial z}{\partial x} = \frac{\partial z}{\partial l}\left(\frac{\partial x}{\partial l}\right)^{-1} = -\cos\left(\frac{l}{r}+\frac{\pi}{2}\right) \Big/ \sin\left(\frac{l}{r}+\frac{\pi}{2}\right) = -1 \Big/ \tan\left(\frac{l}{r}+\frac{\pi}{2}\right)$$

Equation 5.3.7

$$q = \frac{\partial z}{\partial y} = 0$$

Equation 5.3.8

as z is constant along y parameter.

Now that we have the gradients, (p,q), at all points on the sheet, we can use the red, green, and blue reflectance maps estimated from the synthetic calibration sphere to convert the gradient (p,q) into red, green, and blue intensity values at all points on the sheet in the image. The image sequence is created by repeating this process for a certain range of time values.

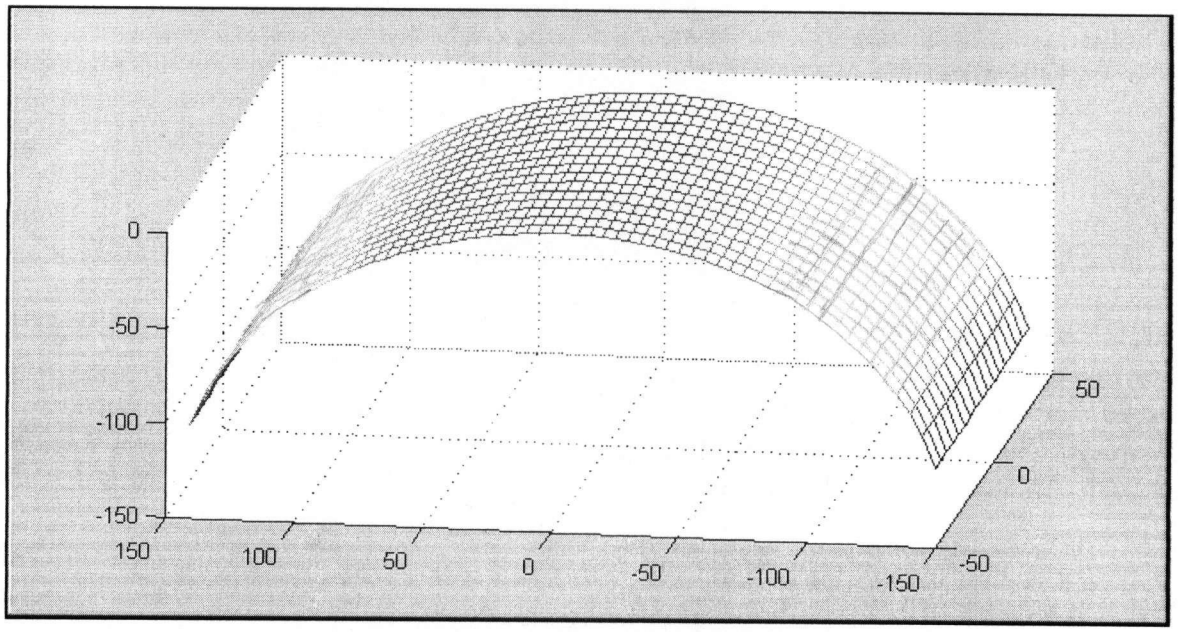

Figure 5.3.2: A wire mesh visualization of the curved sheet, at the end of its deformation. Units are in pixels.

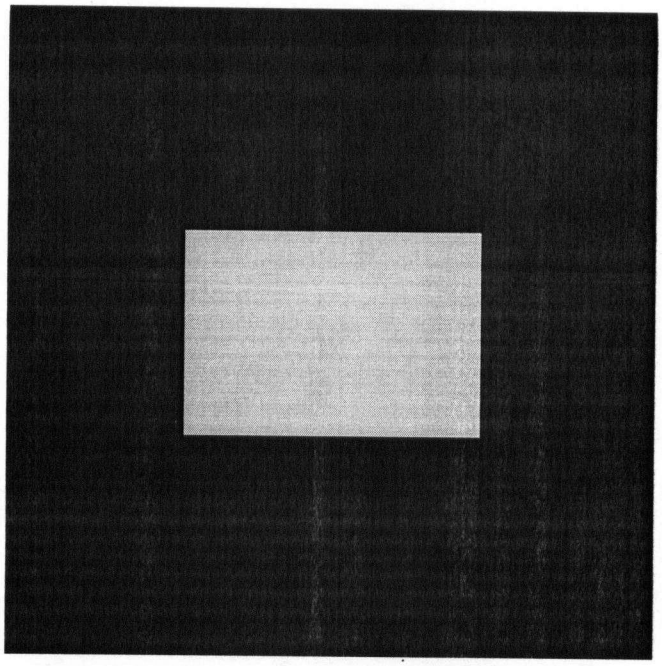

Figure 5.3.3: The first of 11 images in the curving sheet sequence. The red, green, and blue illuminations have been superimposed.

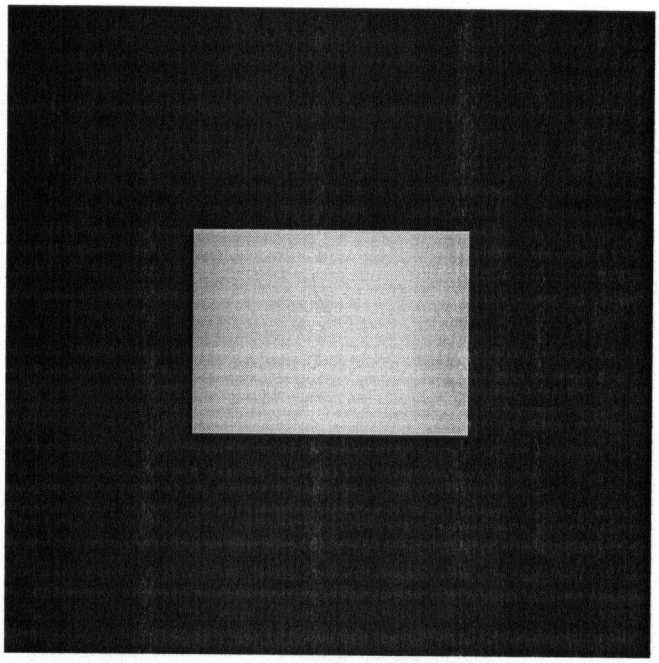

Figure 5.3.4: The last of 11 images in the curving sheet sequence. The red, green, and blue illuminations have been superimposed.

In order to determine how accurate our estimated optical flow is, we determine the known motion field. The known motion field (u,v) for the curving image sequence is given below.

$$u = \frac{dx}{dt} = \frac{\partial x}{\partial r}\frac{\partial r}{\partial t} = -m\left[\cos\left(\frac{l}{r} + \frac{\pi}{2}\right) + \left(\frac{l}{r}\right)\sin\left(\frac{l}{r} + \frac{\pi}{2}\right)\right]$$

Equation 5.3.9

$$v = \frac{dy}{dt} = \frac{dy}{dr}\frac{dr}{dt} = 0$$

Equation 5.3.10

In our actual implementation r deforms according to the following equation.

$r = 210 - 10t$, where t is time.

5.4 Curved Translating Sheet

This translation sequence consists of a non-deforming curved sheet which translates to the right. The curved sheet is parameterized and created in a similar manner to the sequence above, except that it does not deform. The speed of the horizontal motion was set to a constant value of 1 pixel per frame. The curved translating sheet is exactly the same as the curved sheet at the last frame in the curving sheet sequence which is shown in Figure 5.3.4, and has the same wire mesh visualization as in Figure 5.3.2.

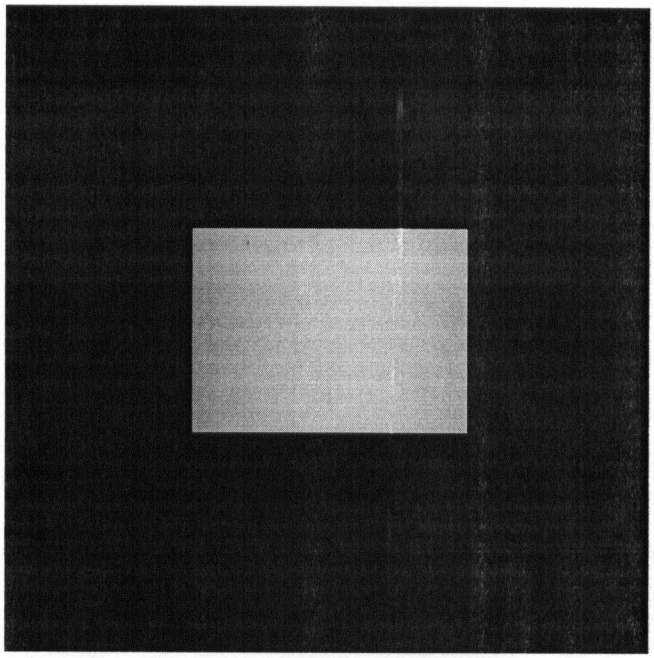

Figure 5.4.1: The first of 11 images in the curved translating sheet sequence. The red, green, and blue illuminations have been superimposed.

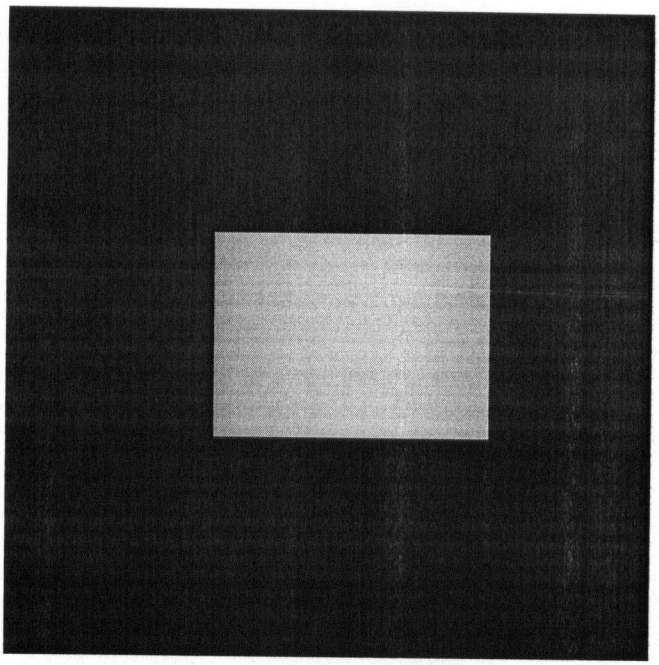

Figure 5.4.2: The last of 11 images in the curved translating sheet sequence. The red, green, and blue illuminations have been superimposed.

5.5 Rotation of a Surface With Negative Gaussian Curvature

This sequence shows a saddle shaped object being rotated around the center of the image at a rate of 0.01 radians per frame. All points on the surface have negative Gaussian curvature. Along the length of the object, the edges curve away from the viewer, while along the width of the object, the edges curve toward the viewer. This can be parameterized in a similar manner to the curved sheet discussed above, and curvature is simply introduced in a perpendicular direction to that which is already present. The effects of inter-reflection which would occur in real life for this saddle shaped object were not taken into account.

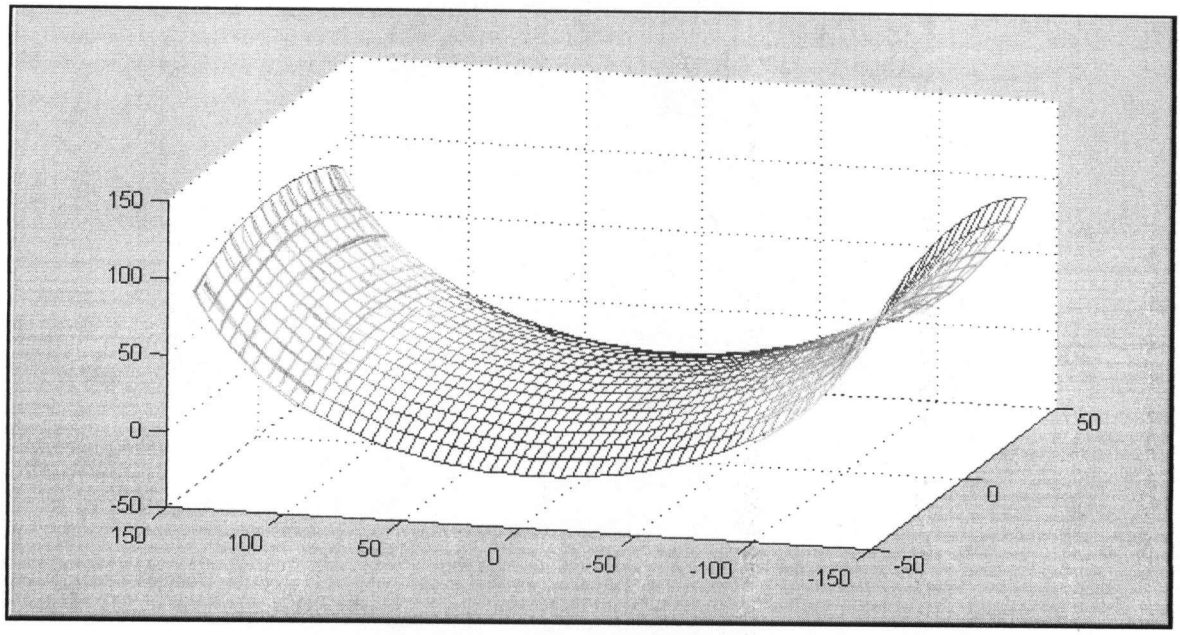

Figure 5.5.1: A wire mesh visualization of the surface with negative Gaussian curvature. Units are in pixels.

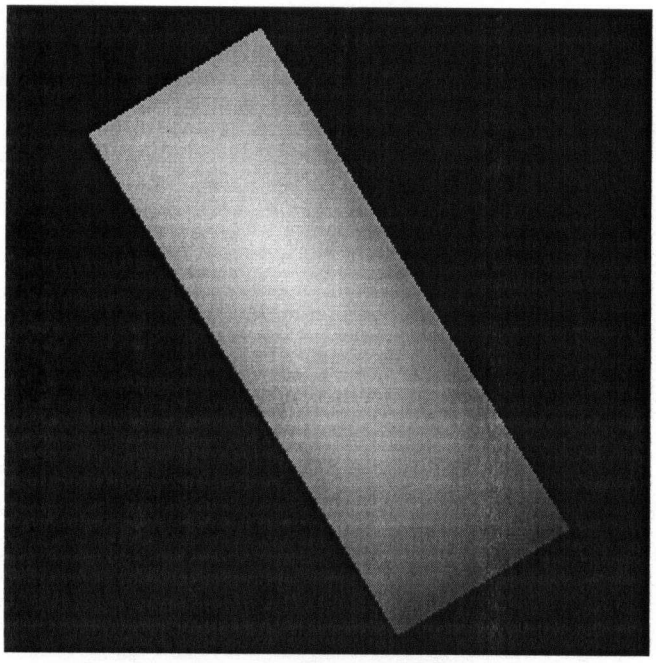

Figure 5.5.2: The first of 11 images in the sequence of a rotating surface with negative Gaussian curvature. The red, green, and blue illuminations have been superimposed.

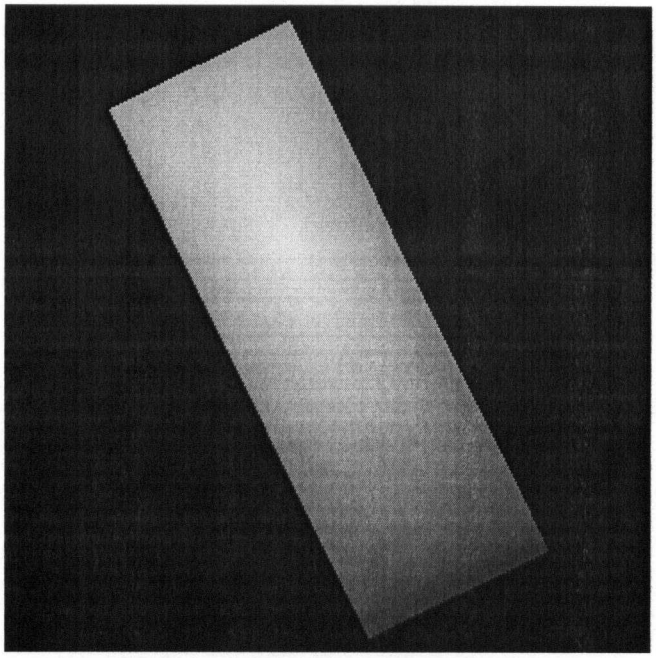

Figure 5.5.3: The last of 11 images in the sequence of a rotating surface with negative Gaussian curvature. The red, green, and blue illuminations have been superimposed.

5.6 Translation of a Surface With Negative Gaussian Curvature

This sequence shows the same saddle shaped object as that depicted in Figure 5.5.1 being translated at a rate of 1 pixel per frame. The effects of inter-reflection, which would occur in real life for this saddle shaped object were not taken into account.

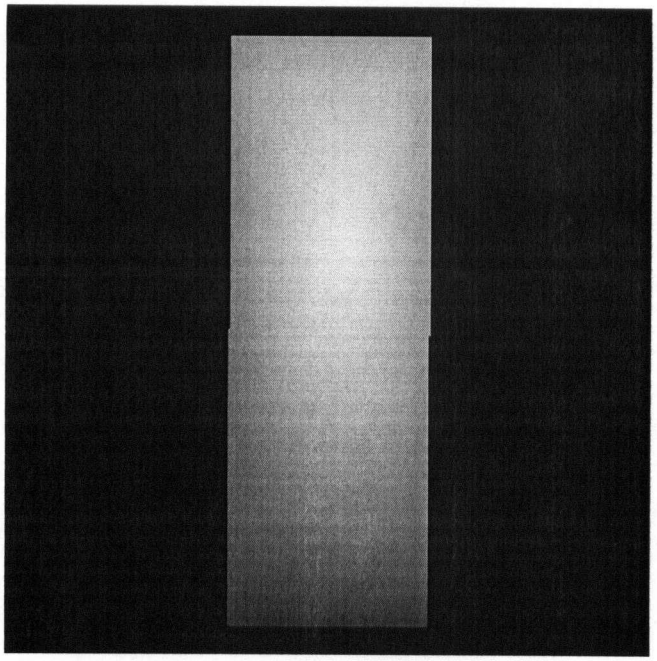

Figure 5.6.1: The first of 11 images in the sequence of a translating surface with negative Gaussian curvature. The red, green, and blue illuminations have been superimposed.

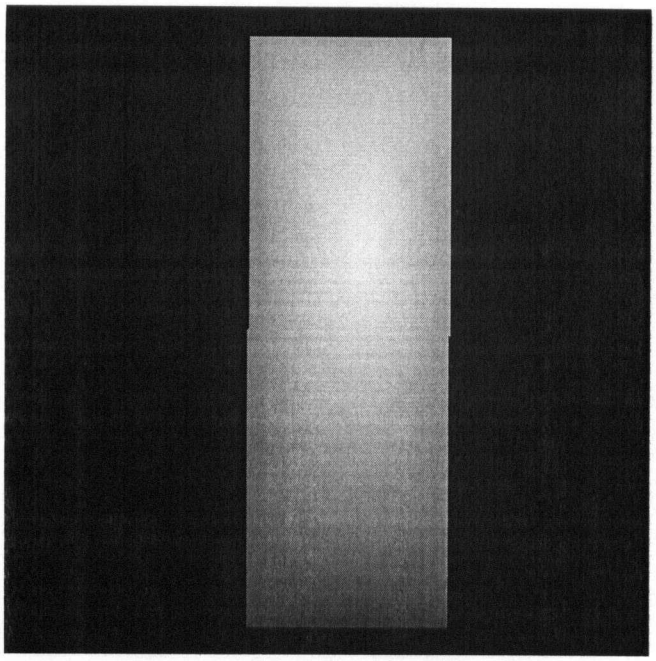

Figure 5.6.2: The last of 11 images in the sequence of a translating surface with negative Gaussian curvature. The red, green, and blue illuminations have been superimposed.

5.7 Rotation and Translation of a Surface With Negative Gaussian Curvature

This sequence shows the same saddle shaped object as that depicted in Figure 5.5.1 being translated at a rate of 0.5 pixels per frame and also being rotated at a rate 0.01 radians per frame. The effects of inter-reflection, which would occur in real life for this saddle shaped object were not taken into account.

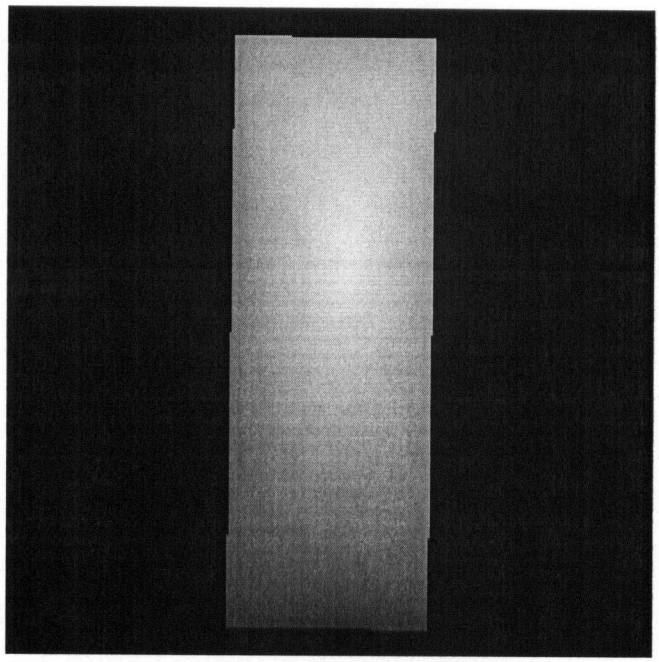

Figure 5.7.1: The first of 11 images in the sequence of a rotating and translating surface with negative Gaussian curvature. The red, green, and blue illuminations have been superimposed.

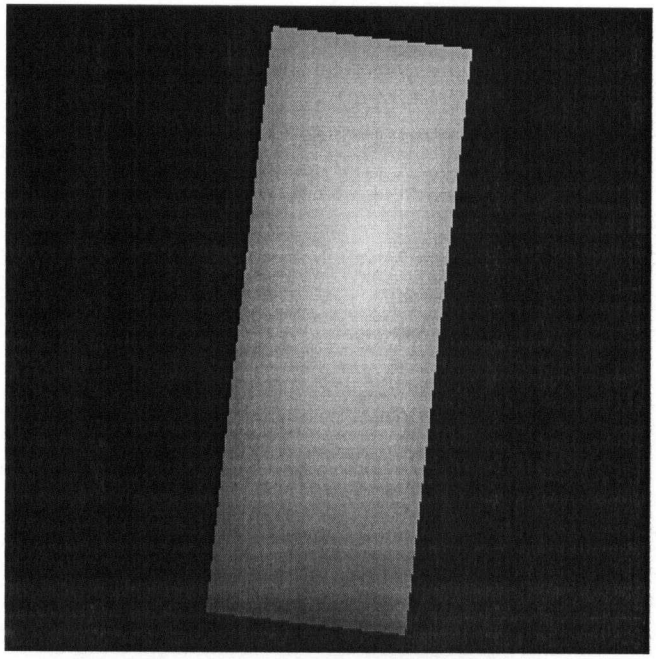

Figure 5.7.2: The last of 11 images in the sequence of a rotating and translating surface with negative Gaussian curvature. The red, green, and blue illuminations have been superimposed.

5.8 Rotation of a Surface With Positive Gaussian Curvature

This sequence shows a surface with positive Gaussian curvature being rotated around the center of the image at a rate of 0.01 radians per frame. Along all the edges of this rectangular object, the surface curves away from the viewer. This can be parameterized in a similar manner to the curved sheet discussed above, and curvature is simply introduced in a perpendicular direction to that which is already present.

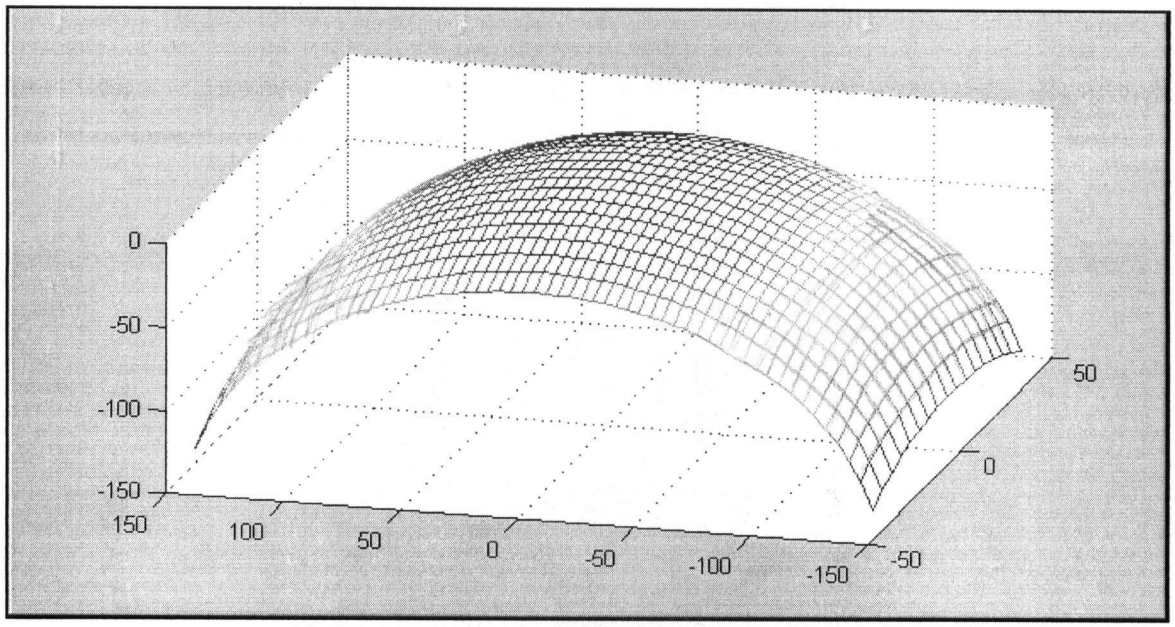

Figure 5.8.1: A wire mesh visualization of the surface with positive Gaussian curvature. Units are in pixels.

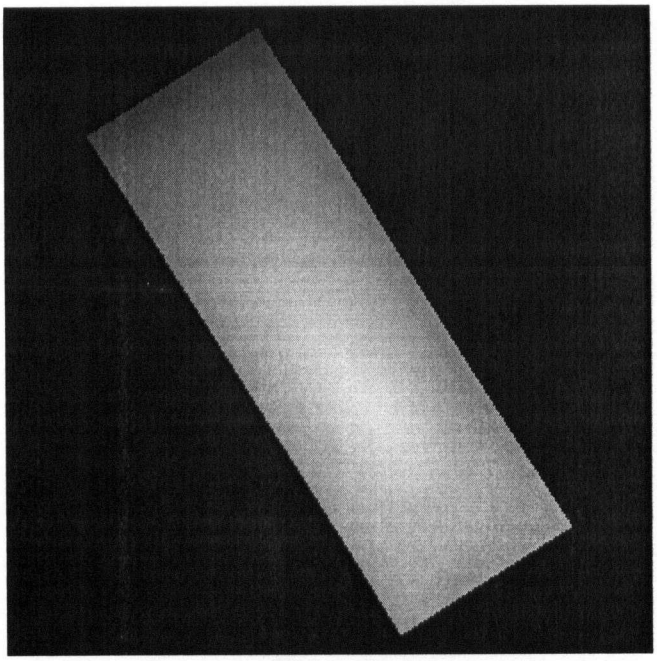

Figure 5.8.2: The first of 11 images in the sequence of a rotating surface with positive Gaussian curvature. The red, green, and blue illuminations have been superimposed.

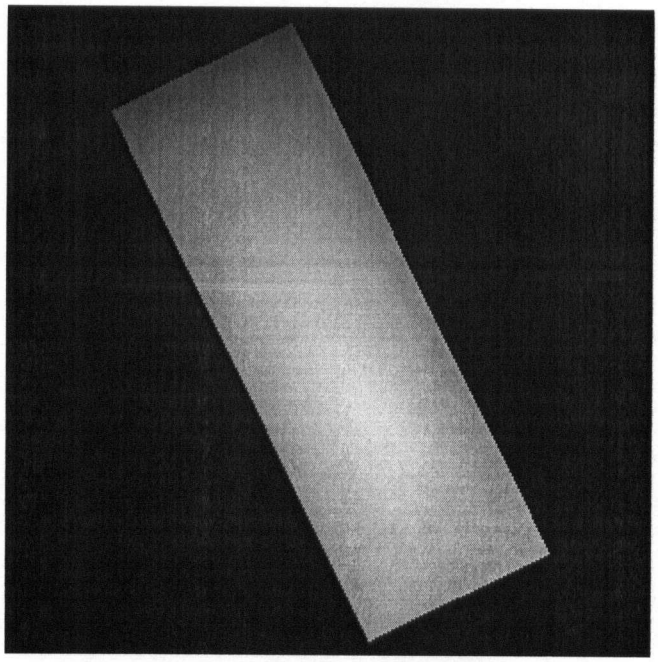

Figure 5.8.3: The last of 11 images in the sequence of a rotating surface with positive Gaussian curvature. The red, green, and blue illuminations have been superimposed.

5.9 Translation of a Surface With Positive Gaussian Curvature

This sequence uses the same surface with positive Gaussian curvature as that depicted in Figure 5.8.1. In this sequence, it is being translated at a rate of 1 pixel per frame.

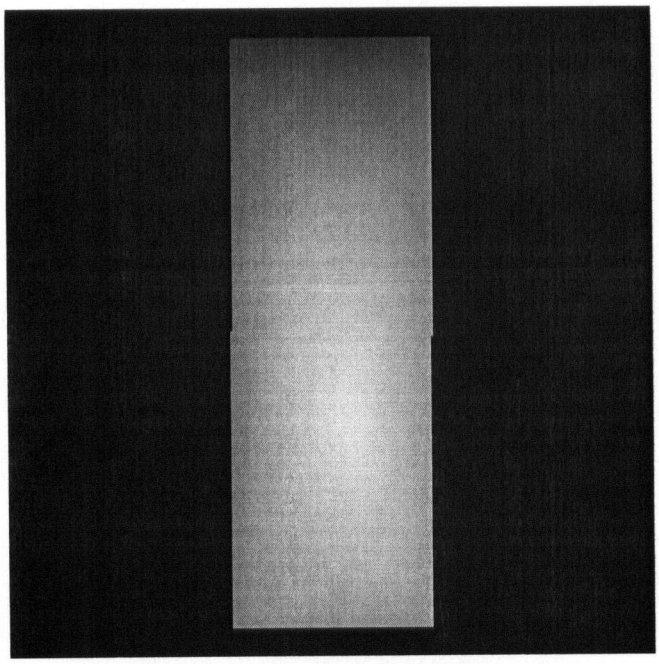

Figure 5.9.1: The first of 11 images in the sequence of a translating surface with positive Gaussian curvature. The red, green, and blue illuminations have been superimposed.

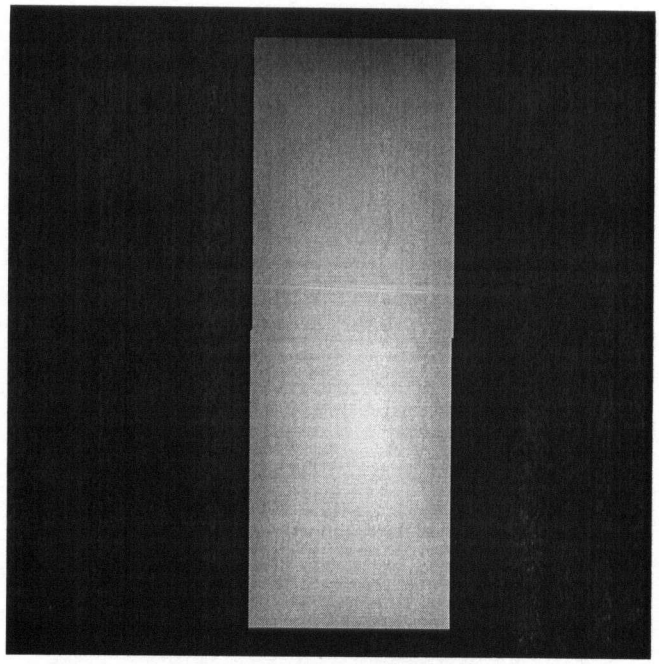

Figure 5.9.2: The last of 11 images in the sequence of a translating surface with positive Gaussian curvature. The red, green, and blue illuminations have been superimposed.

5.10 Rotation and Translation of a Surface With Positive Gaussian Curvature

This sequence uses the same surface with positive Gaussian curvature as that depicted in Figure 5.8.1. It has positive Gaussian curvature at all points and is being translated at a rate of 0.5 pixels per frame and is also being rotated at a rate 0.01 radians per frame.

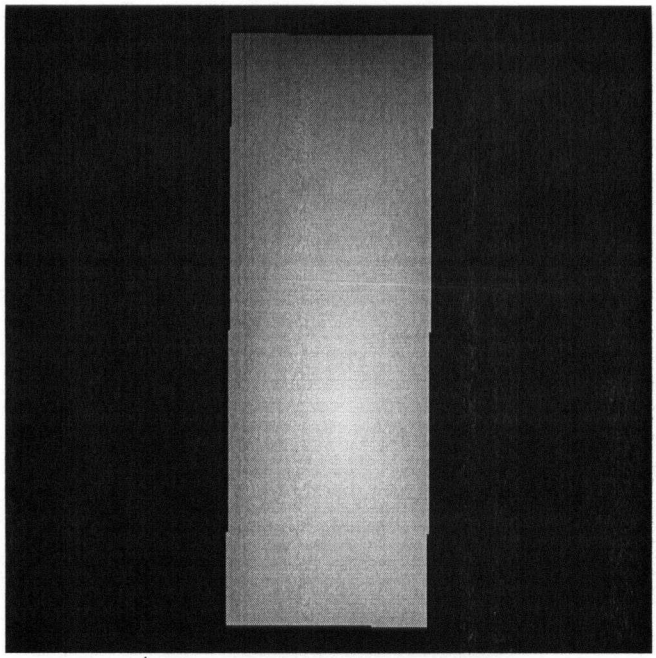

Figure 5.10.1: The first of 11 images in the sequence of a rotating and translating surface with positive Gaussian curvature. The red, green, and blue illuminations have been superimposed.

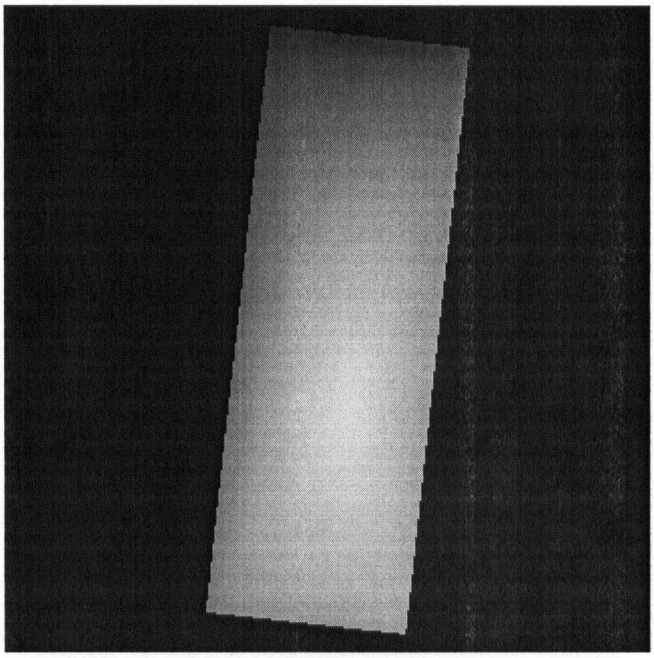

Figure 5.10.2: The last of 11 images in the sequence of a rotating and translating surface with positive Gaussian curvature. The red, green, and blue illuminations have been superimposed.

Chapter Six

6 Results

6.1 Optical Flow Estimation Techniques Tested

Two types of optical flow estimation techniques were implemented and tested. The two types of optical flow will be identified as type 1 and type 2 optical flows. Type 1 is the multiple light source optical flow and solves the optical flow problem by using Equation 2.1.4. Type 2 solves for the optical flow by using Equation 3.3.10.

The type 2 optical flow estimation has sub-types identified as A, B, B′, and B″ according to the type of regularization used. Type A uses method 1 from the discussion on regularization, while type B uses method 2 with λ equal to 0.00000001. Type B′ uses method 2 with λ equal to 0.0001 and Type B″ uses method 2 with λ equal to 0.1. Also all the sub-types of the type 2 optical flow estimation will be further sub-classified based on the stabilizing function used. "Min. A" will refer to the minimum intensity change and rotation stabilizing function, "Min. B" will refer to the minimum translation stabilizing function, "Min. C" will refer to the minimum intensity change, translation and rotation stabilizing function, and "Min. D" will refer to the minimum intensity change stabilizing function.

Algorithm	Equations Used	Regularization Method	Lambda (λ)	Minimize Translation	Minimize Intensity Change	Minimize Rotation
Type 1	Equation 2.1.4	N/A	N/A		N/A	N/A
Type 2A - Min. A	Equation 3.3.10	1	N/A	No	Yes	Yes
Type 2A - Min. B	Equation 3.3.10	1	N/A	Yes	No	No
Type 2A - Min. C	Equation 3.3.10	1	N/A	Yes	Yes	Yes
Type 2A - Min. D	Equation 3.3.10	1	N/A	No	Yes	No
Type 2B – Min. A	Equation 3.3.10	2	0.00000001	No	Yes	Yes
Type 2B - Min. B	Equation 3.3.10	2	0.00000001	Yes	No	No
Type 2B - Min. C	Equation 3.3.10	2	0.00000001	Yes	Yes	Yes
Type 2B - Min. D	Equation 3.3.10	2	0.00000001	No	Yes	No

Type 2B′ – Min. A	Equation 3.3.10	2	0.0001	No	Yes	Yes
Type 2B′ - Min. B	Equation 3.3.10	2	0.0001	Yes	No	No
Type 2B′ - Min. C	Equation 3.3.10	2	0.0001	Yes	Yes	Yes
Type 2B′ - Min. D	Equation 3.3.10	2	0.0001	No	Yes	No
Type 2B″ – Min. A	Equation 3.3.10	2	0.1	No	Yes	Yes
Type 2B″ - Min. B	Equation 3.3.10	2	0.1	Yes	No	No
Type 2B″ - Min. C	Equation 3.3.10	2	0.1	Yes	Yes	Yes
Type 2B″ - Min. D	Equation 3.3.10	2	0.1	No	Yes	No

Table 6.1.1: The different optical flow estimation algorithms implemented and tested.

6.2 Optical Flow Estimation Quality Measures

All the variations on the optical flow estimation techniques described above were tested using the synthetic image sequences described in chapter 5. For each optical flow estimation a number of statistical averages were calculated. At a given pixel (x,y), we denote the u and v components of the estimated optical flow as $u_e(x,y)$, and $v_e(x,y)$. The average of $u_e(x,y)$ is denoted as $\overline{u_e}$ and the average of $v_e(x,y)$ is denoted as $\overline{v_e}$. The averages are calculated by summing over all the pixels corresponding to the object's surface and dividing by the number of pixels considered. The pixel is considered if it is illuminated by all three light sources and has a neighborhood of pixels which are also illuminated by all three sources. This neighborhood condition considers pixels which are far enough away from the edge of the object that the edge effects from image smoothing do not contribute to the statistics. The neighborhood is a 5 by 5 grid with the pixel of interest at the center.

N	N	N	N	N
N	N	N	N	N
N	N	P	N	N
N	N	N	N	N
N	N	N	N	N

Figure 6.2.1 The 5 by 5 neighborhood of the pixel P. All cells labelled "N" are in the 5 by 5 neighborhood.

Here all the cells labeled with "N" are part of the neighborhood of the pixel P. A 5 by 5 neighborhood was used because a 5 by 5 Gaussian smoothing kernel was used in our implementation to smooth the images.

$$\overline{u_e} = \frac{\sum_{(x,y)\ni surface} u_e(x,y)}{\left|\{(x,y)|(x,y)\ni surface\}\right|}$$

Equation 6.2.1

$$\overline{v_e} = \frac{\sum_{(x,y)\ni surface} v_e(x,y)}{\left|\{(x,y)|(x,y)\ni surface\}\right|}$$

Equation 6.2.2

where "$|\ |$" is the "size of" operator which returns the number of elements in a set. The standard deviation of u and v is also calculated and will be denoted as σ_{u_e} and σ_{v_e} respectively. Standard deviations in our analysis are always calculated according to the following formula.

$$\sigma_T = \sqrt{\frac{\sum_{(x,y)\in surface} \left(T(x,y) - \overline{T}\right)^2}{\left|\{(x,y)|(x,y)\in surface\}\right| - 1}}$$

Equation 6.2.3

where T is some quantity at pixel, (x,y), like u_e or v_e. We will denote the u and v components of the known motion field vector at a pixel (x,y), as $u_k(x,y)$ and $v_k(x,y)$.

The averages and standard deviations are also calculated for the known motion field vectors. They will be denoted as $\overline{u_k}$, $\overline{v_k}$, σ_{u_k}, and σ_{v_k} respectively.

$$\overline{u_k} = \frac{\sum_{(x,y)\ni surface} u_k(x,y)}{\left|\{(x,y)|(x,y) \ni surface\}\right|}$$

Equation 6.2.4

$$\overline{v_k} = \frac{\sum_{(x,y)\ni surface} v_k(x,y)}{\left|\{(x,y)|(x,y) \ni surface\}\right|}$$

Equation 6.2.5

These *u* and *v* component averages of the estimated optical flow make sense for translating objects, as all the estimated optical flow vectors should be constant if the estimation is completely accurate. If the estimation is not completely accurate, the averaging tends to get rid of some of the noise that is present in the estimation.

A number of error measures will be used to gauge the quality of the estimated optical flow. Our formulation for the estimation of optical flow is under-constrained and ambiguous. We are simply selecting a solution out of all the ambiguous cases. Hence part of the error is due to the ambiguous nature of the problem. Nonetheless we will still refer to these comparison measures as error measures, and the difference between the known motion field vector and estimated optical flow vectors at a point (x,y) will be referred to as the error vector. The first set of error measures involves the error vectors between the known motion field vectors and the estimated optical flow vectors. Let us denote the error vector as *e* and define it as follows.

$$e(x,y) = \left(u_e(x,y), v_e(x,y)\right) - \left(u_k(x,y), v_k(x,y)\right)$$

Equation 6.2.6

where $u_e(x,y)$ and $v_e(x,y)$ are the u and v components of the estimated optical flow vector at the pixel, (x,y), and $u_k(x,y)$ and $v_k(x,y)$ are the u and v components of the known motion field vector at the pixel, (x,y). The average norm of the error vectors will be denoted as $\overline{\|e\|}$.

$$\overline{\|e\|} = \frac{\sum_{(x,y)\in surface} \|e(x,y)\|}{\left|\{(x,y) | (x,y) \in surface\}\right|}$$

Equation 6.2.7

The standard deviation of the norms of the error vectors will be denoted as $\sigma_{\|e\|}$.

The u component of $e(x,y)$ will be denoted as $e_u(x,y)$ and the v component of $e(x,y)$ will be denoted as $e_v(x,y)$. The average of the magnitude of $e_u(x,y)$ over all the pixels corresponding to the object's surface will be denoted as $\overline{\|e_u\|}$ and the average magnitude of $e_v(x,y)$ over all the pixels corresponding to the object's surface will be denoted as $\overline{\|e_v\|}$. The average of $e_u(x,y)$ over all the pixels corresponding to the object's surface will be denoted as $\overline{e_u}$ and the average of $e_v(x,y)$ over all the pixels corresponding to the object's surface will be denoted as $\overline{e_v}$.

$$\overline{\|e_u\|} = \frac{\sum_{(x,y)\in surface} \|e_u(x,y)\|}{|\{(x,y)|(x,y) \in surface\}|}$$

Equation 6.2.8

$$\overline{\|e_v\|} = \frac{\sum_{(x,y)\in surface} \|e_v(x,y)\|}{|\{(x,y)|(x,y) \in surface\}|}$$

Equation 6.2.9

$$\overline{e_u} = \frac{\sum_{(x,y)\in surface} e_u(x,y)}{|\{(x,y)|(x,y) \in surface\}|}$$

Equation 6.2.10

$$\overline{e_v} = \frac{\sum_{(x,y)\in surface} e_v(x,y)}{|\{(x,y)|(x,y) \in surface\}|}$$

Equation 6.2.11

The standard deviations of $e_u(x,y)$, $e_v(x,y)$, $\|e_u(x,y)\|$ and $\|e_v(x,y)\|$ will be denoted as σ_{e_u}, σ_{e_v}, $\sigma_{\|e_u\|}$ and $\sigma_{\|e_v\|}$ respectively.

At a given pixel (x,y), the norm of the error, e, divided by the norm of the known motion field vector will be denoted as r. This quantity expresses the amount of error per known amount of motion.

$$r(x,y) = \frac{\|e(x,y)\|}{\|(u(x,y), v(x,y))\|}$$

Equation 6.2.12

One of the most informative error measures is the average of r over all pixels that are a part of the object's surface being imaged and will be denoted as $\bar{r}$. This measure $\bar{r}$ expresses the amount of error per known amount of motion on average over all the pixels corresponding to the object's surface.

$$\bar{r} = \frac{\sum_{(x,y)\in surface} r(x,y)}{|\{(x,y)|(x,y) \in surface\}|}$$

Equation 6.2.13

The above measure $\bar{r}$ encodes both the errors in magnitude and direction of the estimated optical flow vectors. In order to measure only the directional error between the estimated optical flow vectors and the known motion field vectors we will introduce one more measure to gage the quality of the directions of the estimated optical flow vectors. At a given pixel (x,y), let $\angle$ denote the angle between estimated optical flow vector and the known motion field vector.

$$\angle(x,y) = \cos^{-1}\left(\frac{(u_e(x,y), v_e(x,y)) \bullet (u_k(x,y), v_k(x,y))}{\|(u_e(x,y), v_e(x,y))\| \|(u_k(x,y), v_k(x,y))\|}\right)$$

Equation 6.2.14

Here we are only interested in the positive angles returned by the inverse cosine function, because our directional measure will be the average magnitude of $\angle(x,y)$ over all pixels

corresponding the object's surface and will be denoted as $\overline{\angle}$. So we assume that the inverse cosine function always returns values in the range of 0 to π.

$$\overline{\angle} = \frac{\sum_{(x,y)\in surface} \angle(x,y)}{\left|\{(x,y)|(x,y) \in surface\}\right|}$$

Equation 6.2.15

The standard deviation of $\angle(x,y)$ over all pixels corresponding the object's surface will be denoted as $\sigma_{\angle}$.

6.3 Translation of the Calibration Sphere

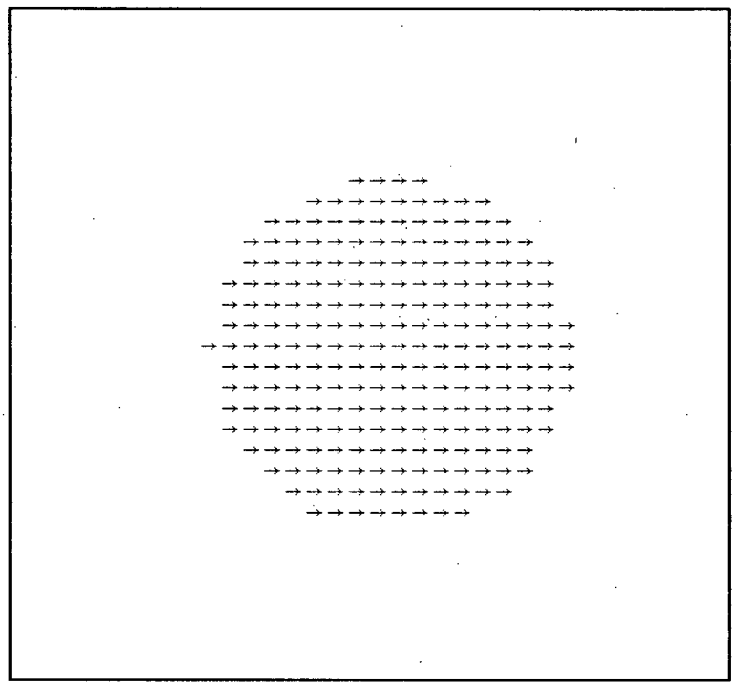

Figure 6.3.1: The known motion field for the translating calibration sphere. Vectors are magnified 10 times and sampled every 20 pixels.

Measure	Average	Standard Deviation
u_k	1.000000	0.000000
v_k	0.000000	0.000000
$\|u_k\|$	1.000000	0.000000
$\|v_k\|$	0.000000	0.000000
$\|(u_k, v_k)\|$	1.000000	0.000000

Table 6.3.1: The averages and standard deviations of measures associated with the known motion field. The units for all measures are pixels.

Type 1 Optical Flow Estimation

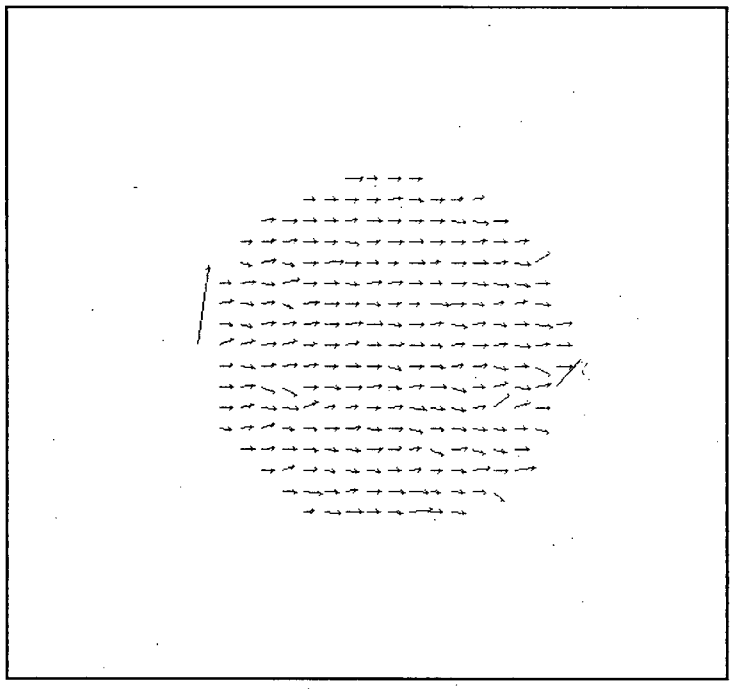

Figure 6.3.2: The type 1 optical flow estimation for the translating calibration sphere. Vectors are magnified 10 times and sampled every 20 pixels.

Measure	Average	Standard Deviation
u_e	1.02011	0.155768
v_e	-0.005898	0.323023
u_k	1	0
v_k	0	0
e_u	0.02011	0.155768
e_v	-0.005898	0.323023
$\|e\|$	0.177143	0.312516
$\|e_u\|$	0.098314	0.122484
$\|e_v\|$	0.122239	0.299058
r	0.177143	0.312516
$\angle$	0.107476	0.142329

Table 6.3.2: The averages and standard deviations of measures associated with the type 1 optical flow estimation. The measure *r* is unitless. The measure $\angle$ is in radians. All other measures are in pixels.

Type 2A Min. A Optical Flow Estimation

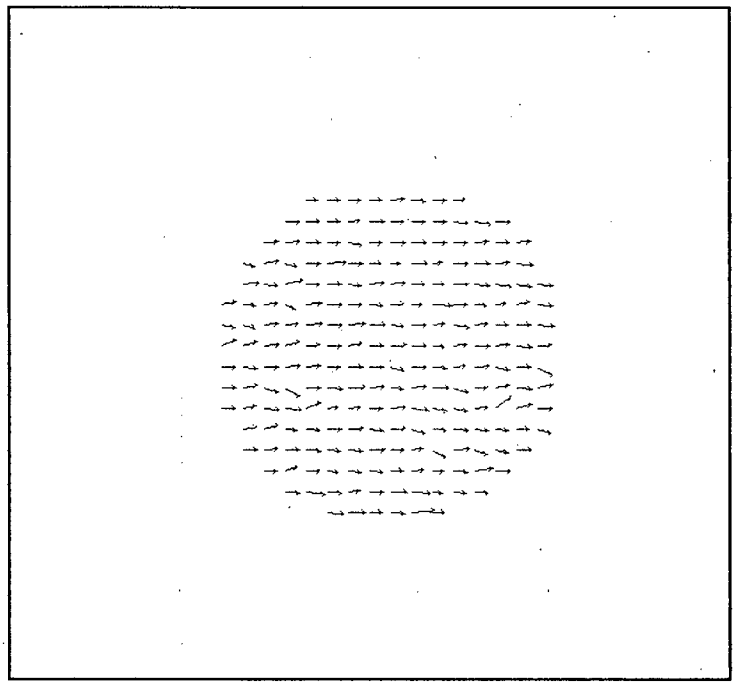

Figure 6.3.3: The type 2A Min. A optical flow estimation for the translating calibration sphere. Vectors are magnified 10 times and sampled every 20 pixels.

Measure	Average	Standard Deviation
u_e	0.965659	0.261974
v_e	-0.001434	0.145695
u_k	1	0
v_k	0	0
e_u	-0.034341	0.261974
e_v	-0.001434	0.145695
$\|e\|$	0.198312	0.227399
$\|e_u\|$	0.141533	0.223109
$\|e_v\|$	0.095068	0.110413
r	0.198312	0.227399
$\angle$	0.097455	0.099299

Table 6.3.3: The averages and standard deviations of measures associated with the type 2A Min. A optical flow estimation. The measure *r* is unitless. The measure $\angle$ is in radians. All other measures are in pixels.

Type 2A Min. B Optical Flow Estimation

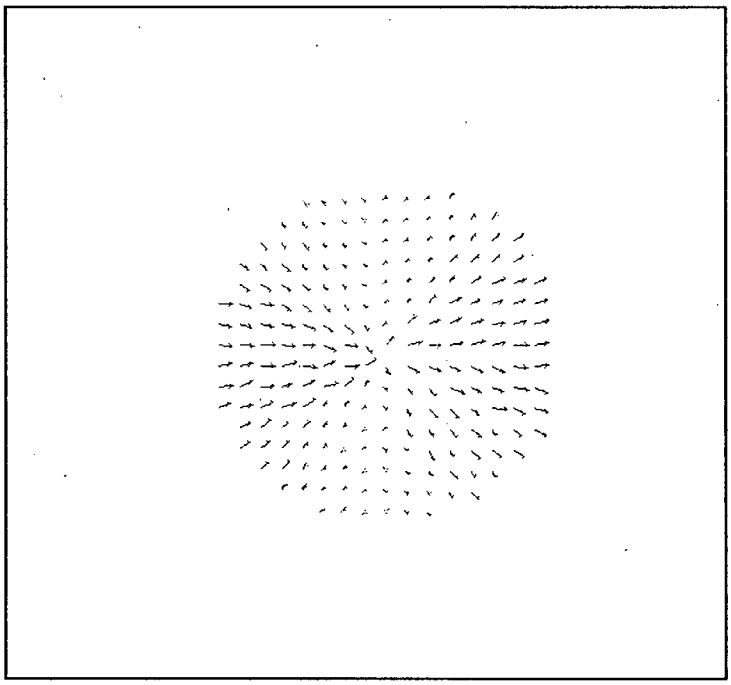

Figure 6.3.4: The type 2A Min. B optical flow estimation for the translating calibration sphere. Vectors are magnified 10 times and sampled every 20 pixels.

Measure	Average	Standard Deviation
u_e	0.484021	0.373708
v_e	0.005511	0.355688
u_k	1	0
v_k	0	0
e_u	-0.515979	0.373708
e_v	0.005511	0.355688
$\|e\|$	0.663219	0.30426
$\|e_u\|$	0.526835	0.358241
$\|e_v\|$	0.308737	0.176704
r	0.663219	0.30426
$\angle$	0.784984	0.457188

Table 6.3.4: The averages and standard deviations of measures associated with the type 2A Min. B optical flow estimation. The measure *r* is unitless. The measure $\angle$ is in radians. All other measures are in pixels.

Type 2A Min. C Optical Flow Estimation

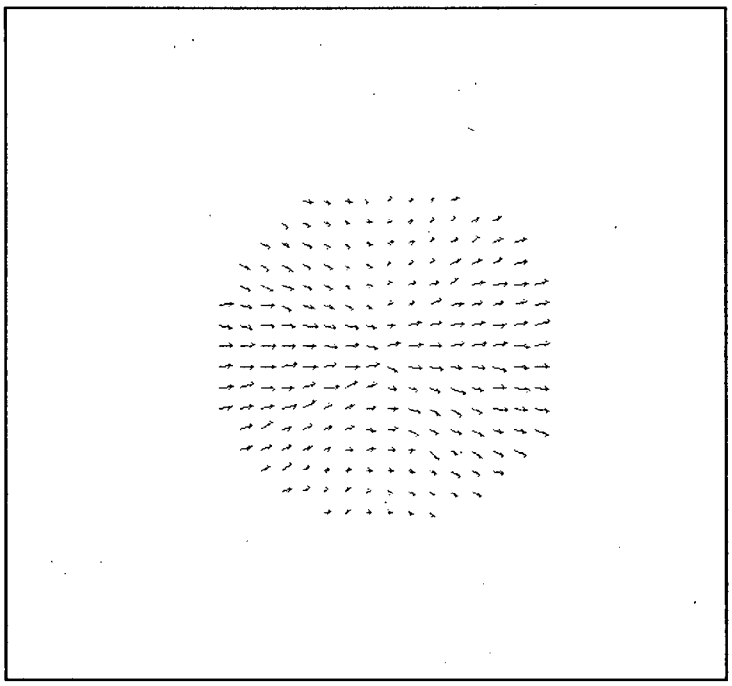

Figure 6.3.5: The type 2A Min. C optical flow estimation for the translating calibration sphere. Vectors are magnified 10 times and sampled every 20 pixels.

Measure	Average	Standard Deviation
u_e	0.682772	0.284131
v_e	0.003327	0.222653
u_k	1	0
v_k	0	0
e_u	-0.317228	0.284131
e_v	0.003327	0.222653
$\|e\|$	0.417219	0.238487
$\|e_u\|$	0.333361	0.265018
$\|e_v\|$	0.185223	0.1236
r	0.417219	0.238487
$\angle$	0.285751	0.18296

Table 6.3.5: The averages and standard deviations of measures associated with the type 2A Min. C optical flow estimation. The measure *r* is unitless. The measure $\angle$ is in radians. All other measures are in pixels.

Type 2A Min. D Optical Flow Estimation

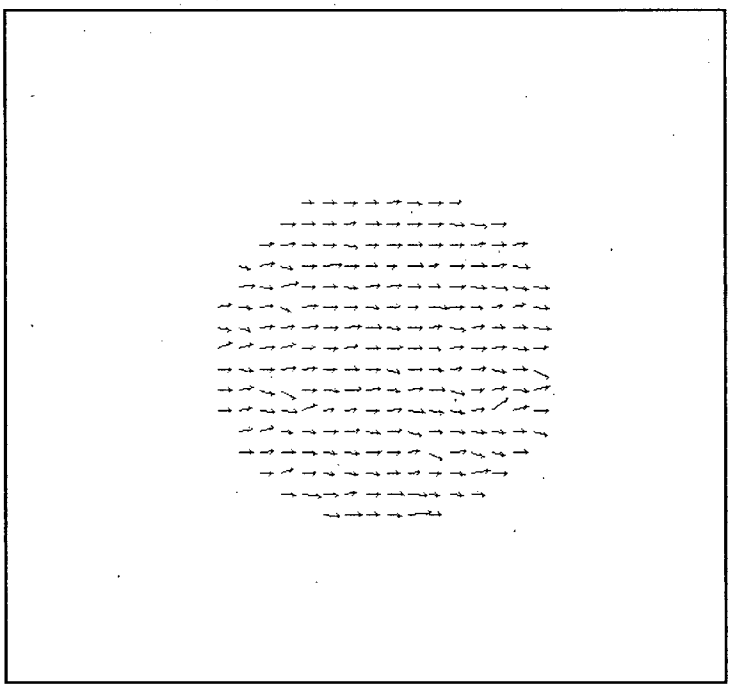

Figure 6.3.6: The type 2A Min. D optical flow estimation for the translating calibration sphere. Vectors are magnified 10 times and sampled every 20 pixels.

Measure	Average	Standard Deviation
u_e	0.965658	0.261973
v_e	-0.001434	0.145695
u_k	1	0
v_k	0	0
e_u	-0.034342	0.261973
e_v	-0.001434	0.145695
$\|e\|$	0.198312	0.227399
$\|e_u\|$	0.141533	0.223109
$\|e_v\|$	0.095068	0.110413
r	0.198312	0.227399
$\angle$	0.097455	0.0993

Table 6.3.6: The averages and standard deviations of measures associated with the type 2A Min. D optical flow estimation. The measure *r* is unitless. The measure $\angle$ is in radians. All other measures are in pixels.

Type 2B, 2B′, and 2B″ Min. A Optical Flow Estimation

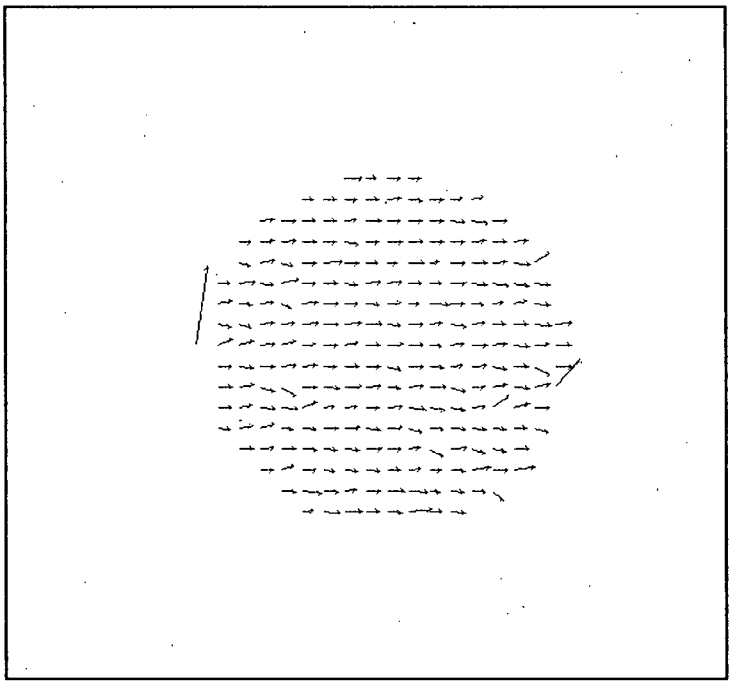

Figure 6.3.7: The type 2B Min. A optical flow estimation for the translating calibration sphere. Vectors are magnified 10 times and sampled every 20 pixels.

	2B Min. A		2B′ Min. A		2B″ Min. A	
Measure	**Average**	**Standard Deviation**	**Average**	**Standard Deviation**	**Average**	**Standard Deviation**
u_e	1.021277	0.15875	1.020507	0.158327	1.020034	0.156021
v_e	-0.005378	0.32523	-0.005464	0.324829	-0.005825	0.323202
u_k	1	0	1	0	1	0
v_k	0	0	0	0	0	0
e_u	0.021277	0.15875	0.020507	0.158327	0.020034	0.156021
e_v	-0.005378	0.32523	-0.005464	0.324829	-0.005825	0.323202
$\|e\|$	0.17975	0.314876	0.178938	0.314662	0.177393	0.31268
$\|e_u\|$	0.099899	0.125198	0.099435	0.124901	0.098472	0.122666
$\|e_v\|$	0.12404	0.300694	0.123464	0.300499	0.12242	0.299177
r	0.17975	0.314876	0.178938	0.314662	0.177393	0.31268
$\angle$	0.109054	0.145002	0.108604	0.144731	0.107693	0.142775

Table 6.3.7: The averages and standard deviations of measures associated with the type 2B, 2B′, and 2B″ Min. A optical flow estimation. The measure r is unitless. The measure $\angle$ is in radians. All other measures are in pixels.

Type 2B, 2B′, and 2B″ Min. B Optical Flow Estimation

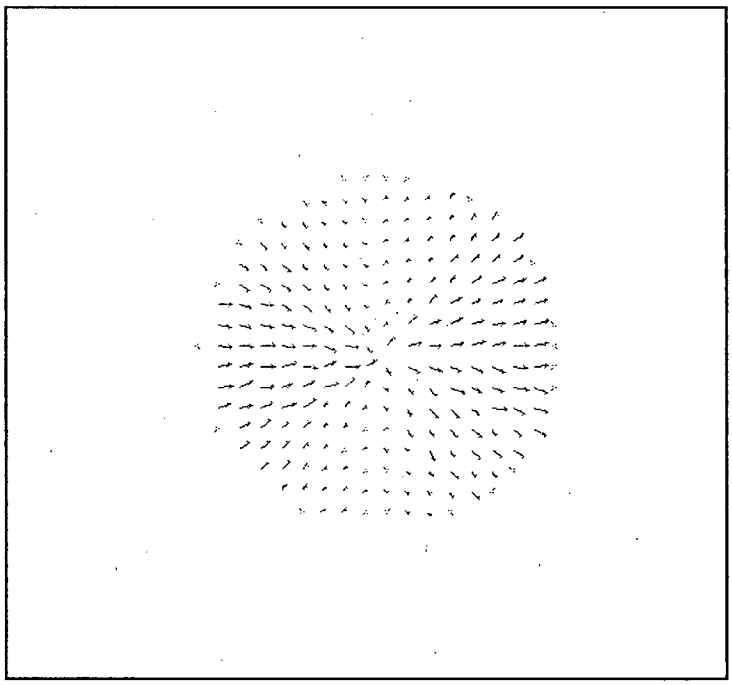

Figure 6.3.8: The type 2B Min. B optical flow estimation for the translating calibration sphere. Vectors are magnified 10 times and sampled every 20 pixels.

	2B Min. B		2B′ Min. B		2B″ Min. B	
Measure	**Average**	**Standard Deviation**	**Average**	**Standard Deviation**	**Average**	**Standard Deviation**
u_e	0.483421	0.373345	0.307274	0.323476	0.044637	0.134728
v_e	0.005507	0.355188	0.003949	0.256898	0.001246	0.079468
u_k	1	0	1	0	1	0
v_k	0	0	0	0	0	0
e_u	-0.516579	0.373345	-0.692726	0.323476	-0.955363	0.134728
e_v	0.005507	0.355188	0.003949	0.256898	0.001246	0.079468
$\|e\|$	0.663223	0.304238	0.762045	0.264203	0.961342	0.11405
$\|e_u\|$	0.527273	0.358082	0.695771	0.316874	0.955566	0.133278
$\|e_v\|$	0.308259	0.176533	0.194651	0.167697	0.027216	0.074672
r	0.663223	0.304238	0.762045	0.264203	0.961342	0.11405
$\angle$	0.826019	0.546009	0.828912	0.549546	0.827237	0.547405

Table 6.3.8: The averages and standard deviations of measures associated with the type 2B, 2B′, and 2B″ Min. B optical flow estimation. The measure r is unitless. The measure $\angle$ is in radians. All other measures are in pixels.

Type 2B, 2B′, and 2B″ Min. C Optical Flow Estimation

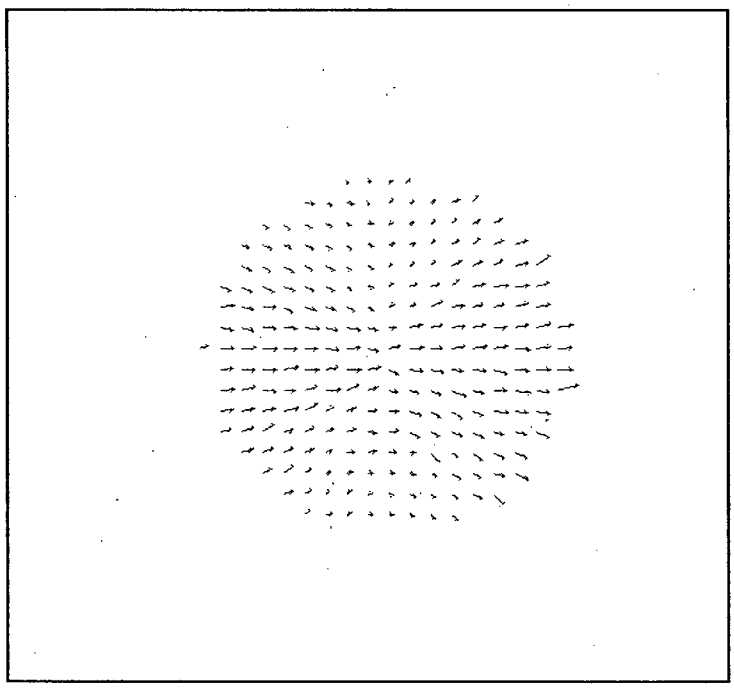

Figure 6.3.9: The type 2B Min. C optical flow estimation for the translating calibration sphere. Vectors are magnified 10 times and sampled every 20 pixels.

	2B Min. C		2B′ Min. C		2B″ Min. C	
Measure	**Average**	**Standard Deviation**	**Average**	**Standard Deviation**	**Average**	**Standard Deviation**
u_e	0.715898	0.246847	0.635354	0.214035	0.574245	0.194891
v_e	0.006586	0.234884	0.004522	0.201468	-0.000261	0.1951
u_k	1	0	1	0	1	0
v_k	0	0	0	0	0	0
e_u	-0.284102	0.246847	-0.364646	0.214035	-0.425755	0.194891
e_v	0.006586	0.234884	0.004522	0.201468	-0.000261	0.1951
$\|e\|$	0.393332	0.205306	0.430975	0.183432	0.47691	0.172831
$\|e_u\|$	0.30395	0.221951	0.37373	0.197746	0.430625	0.183882
$\|e_v\|$	0.197835	0.126784	0.16277	0.118808	0.158475	0.113795
r	0.393332	0.205306	0.430975	0.183432	0.47691	0.172831
$\angle$	0.291177	0.190262	0.263782	0.186978	0.281585	0.194536

Table 6.3.9: The averages and standard deviations of measures associated with the type 2B, 2B′, and 2B″ Min. C optical flow estimation. The measure r is unitless. The measure $\angle$ is in radians. All other measures are in pixels.

Type 2B, 2B′, and 2B″ Min. D Optical Flow Estimation

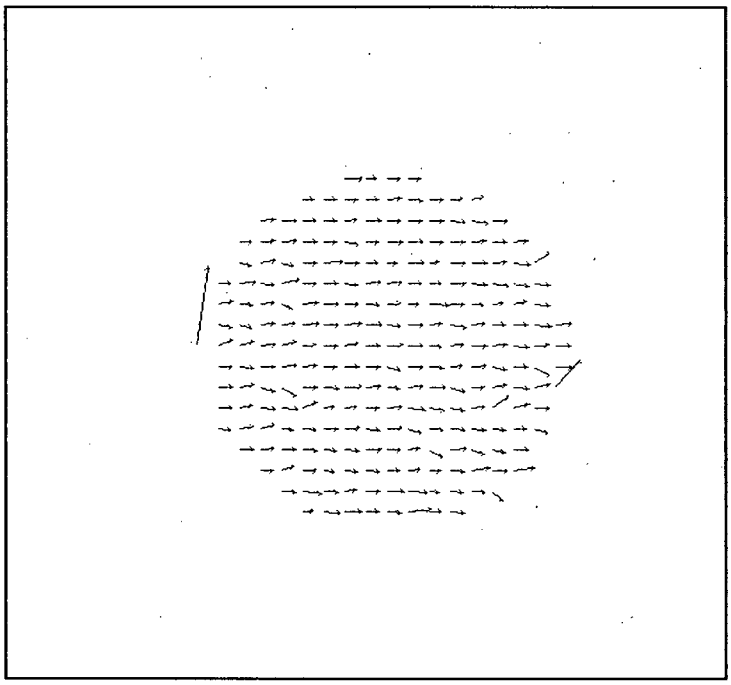

Figure 6.3.10: The type 2B Min. D optical flow estimation for the translating calibration sphere. Vectors are magnified 10 times and sampled every 20 pixels.

	2B Min. D		2B′ Min. D		2B″ Min. D	
Measure	**Average**	**Standard Deviation**	**Average**	**Standard Deviation**	**Average**	**Standard Deviation**
u_e	1.021276	0.15875	1.020506	0.158326	1.020033	0.156019
v_e	-0.005377	0.32523	-0.005464	0.324829	-0.005826	0.323202
u_k	1	0	1	0	1	0
v_k	0	0	0	0	0	0
e_u	0.021276	0.15875	0.020506	0.158326	0.020033	0.156019
e_v	-0.005377	0.32523	-0.005464	0.324829	-0.005826	0.323202
$\|e\|$	0.17975	0.314876	0.178938	0.314662	0.177392	0.312679
$\|e_u\|$	0.099899	0.125197	0.099435	0.124901	0.098471	0.122665
$\|e_v\|$	0.12404	0.300694	0.123464	0.300499	0.122419	0.299176
r	0.17975	0.314876	0.178938	0.314662	0.177392	0.312679
$\angle$	0.109054	0.145002	0.108604	0.144732	0.107692	0.142773

Table 6.3.10: The averages and standard deviations of measures associated with the type 2B, 2B′, and 2B″ Min. D optical flow estimation. The measure *r* is unitless. The measure $\angle$ is in radians. All other measures are in pixels.

6.4 Curving Sheet

The type 1 multiple light source optical flow method cannot estimate the flow properly for developable surfaces, so only the type 2 estimation technique for optical flow will be shown.

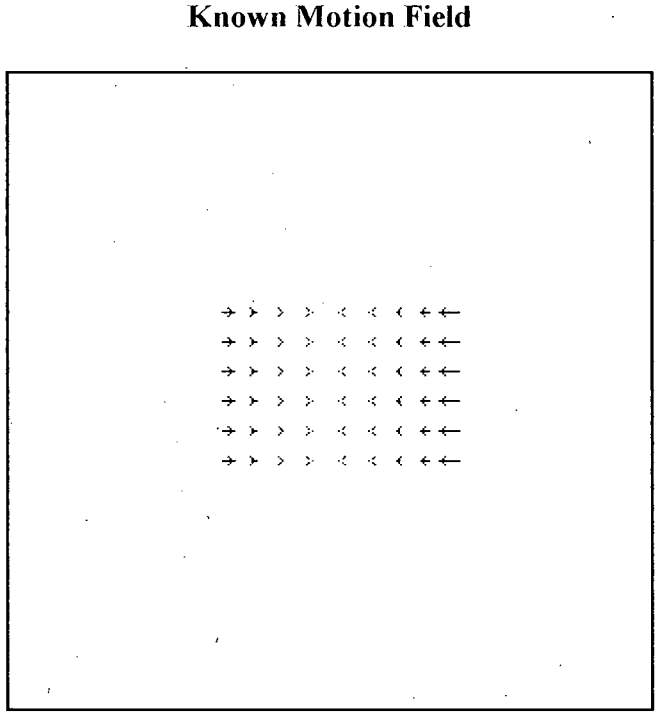

Figure 6.4.1: The known motion field for the curving sheet. Vectors are magnified 35 times and sampled every 20 pixels.

Measure	Average	Standard Deviation
u_k	0	0.134642
v_k	0	0
$\|u_k\|$	0.088119	0.101799
$\|v_k\|$	0	0
$\|(u_k, v_k)\|$	0.088119	0.101799

Table 6.4.1: The averages and standard deviations of measures associated with the known motion field. The measure *r* is unitless. All measures are in pixels.

Type 2A Min. A Optical Flow Estimation

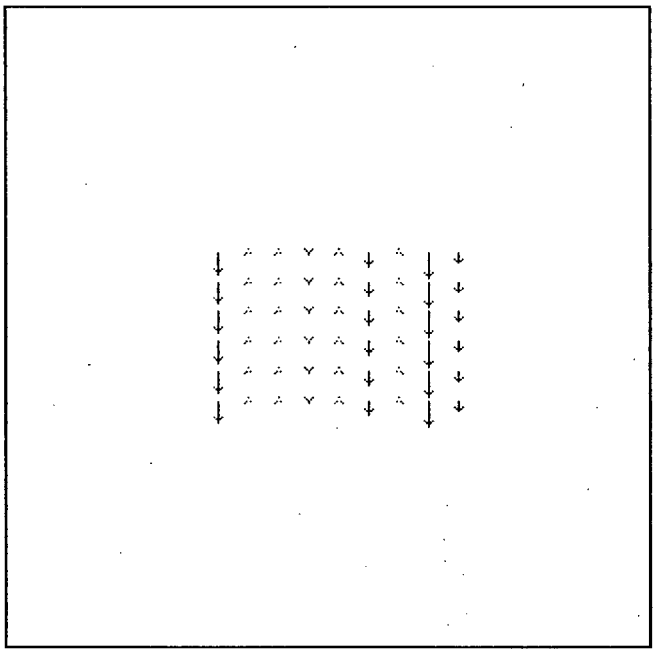

Figure 6.4.2: The type 2A Min. A optical flow estimation for the curving sheet. Vectors are magnified 0.000000000000004 times and sampled every 20 pixels.

Measure	Average	Standard Deviation
u_e	-0.162539	3.240363
v_e	3.45929E+14	2.82933E+15
u_k	0	0.134642
v_k	0	0
e_u	-0.162539	3.1258
e_v	3.45929E+14	2.82933E+15
$\|e\|$	1.45225E+15	2.45266E+15
$\|e_u\|$	2.63142	1.694745
$\|e_v\|$	1.45225E+15	2.45266E+15
r	1.00325E+28	1.20386E+29
$\angle$	1.51226	0.289457

Table 6.4.2: The averages and standard deviations of measures associated with the type 2A Min. A optical flow estimation. The measure *r* is unitless. The measure $\angle$ is in radians. All other measures are in pixels.

Type 2A Min. B Optical Flow Estimation

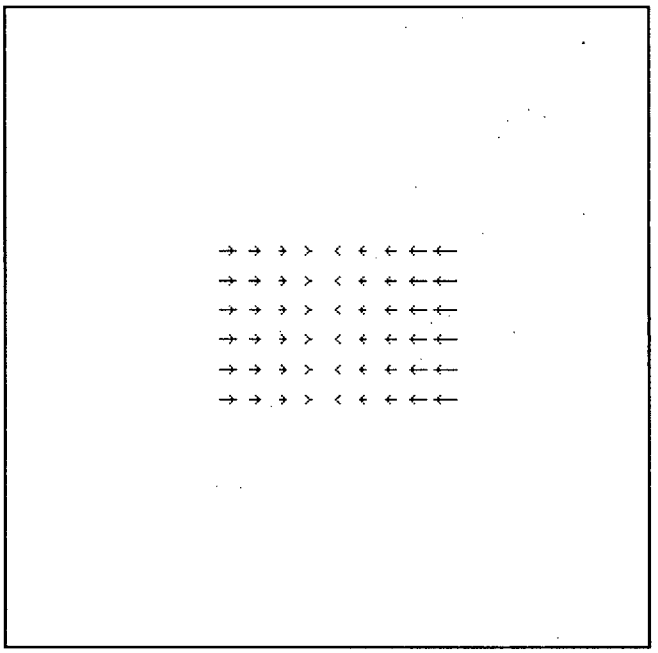

Figure 6.4.3: The type 2A Min. B optical flow estimation for the curving sheet. Vectors are magnified 2 times and sampled every 20 pixels.

Measure	Average	Standard Deviation
u_e	-0.14445	3.205273
v_e	0	0.287939
u_k	0	0.134642
v_k	0	0
e_u	-0.14445	3.090808
e_v	0	0.287939
$\|e\|$	2.613752	1.680674
$\|e_u\|$	2.591166	1.690954
$\|e_v\|$	0.048586	0.28381
r	2.01542E+12	2.36781E+13
$\angle$	0.053333	0.30824

Table 6.4.3: The averages and standard deviations of measures associated with the type 2A Min. B optical flow estimation. The measure *r* is unitless. The measure $\angle$ is in radians. All other measures are in pixels.

Type 2A Min. C Optical Flow Estimation

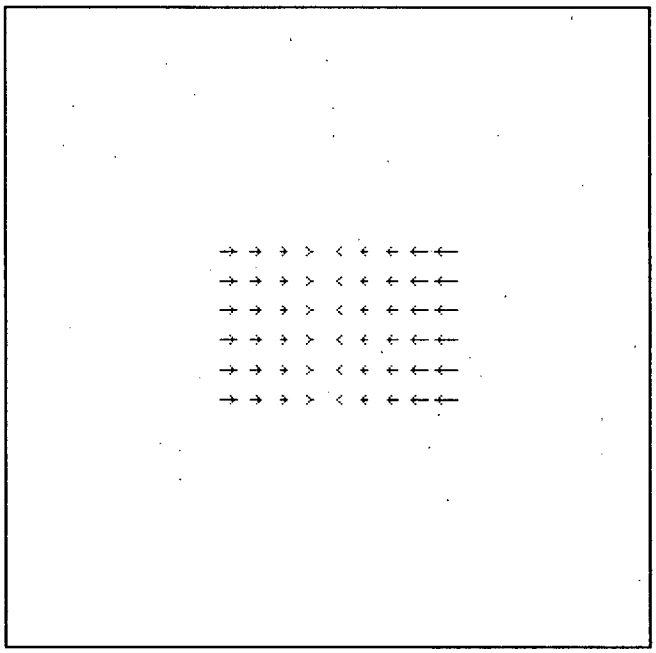

Figure 6.4.4: The type 2A Min. C optical flow estimation for the curving sheet. Vectors are magnified 2 times and sampled every 20 pixels.

Measure	Average	Standard Deviation
u_e	-0.145185	3.218087
v_e	0	0.202182
u_k	0	0.134642
v_k	0	0
e_u	-0.145185	3.103231
e_v	0	0.202182
$\|e\|$	2.623962	1.675204
$\|e_u\|$	2.617133	1.673686
$\|e_v\|$	0.029572	0.200007
r	2.0171E+12	2.36968E+13
$\angle$	0.03445	0.272545

Table 6.4.4: The averages and standard deviations of measures associated with the type 2A Min. C optical flow estimation. The measure *r* is unitless. The measure $\angle$ is in radians. All other measures are in pixels.

Type 2A Min. D Optical Flow Estimation

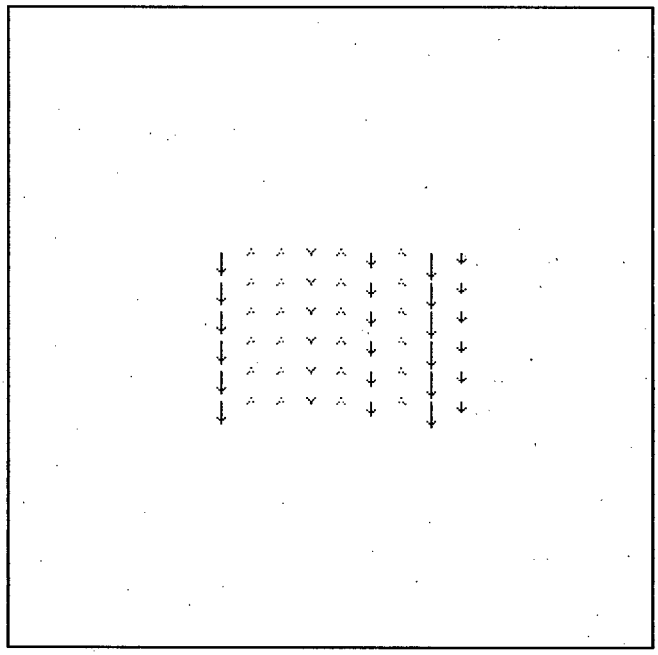

Figure 6.4.5: The type 2A Min. D optical flow estimation for the curving sheet. Vectors are magnified 0.000000000000004 times and sampled every 20 pixels.

Measure	Average	Standard Deviation
u_e	-0.162539	3.240363
v_e	3.45929E+14	2.82933E+15
u_k	0	0.134642
v_k	0	0
e_u	-0.162539	3.1258
e_v	3.45929E+14	2.82933E+15
$\|e\|$	1.45225E+15	2.45266E+15
$\|e_u\|$	2.63142	1.694745
$\|e_v\|$	1.45225E+15	2.45266E+15
r	1.00325E+28	1.20386E+29
$\angle$	1.51226	0.289457

Table 6.4.5: The averages and standard deviations of measures associated with the type 2A Min. D optical flow estimation. The measure *r* is unitless. The measure $\angle$ is in radians. All other measures are in pixels.

Type 2B, 2B′, and 2B″ Min. A Optical Flow Estimation

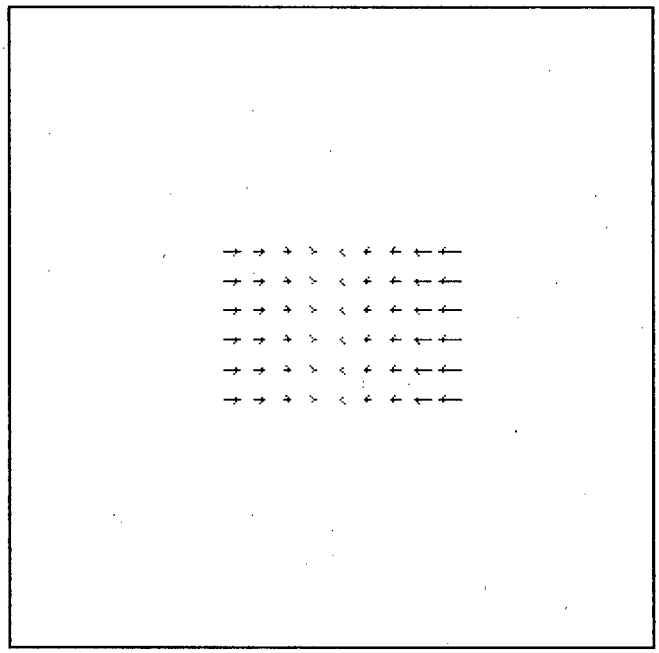

Figure 6.4.6: The type 2B Min. A optical flow estimation for the curving sheet. Vectors are magnified 2 times and sampled every 20 pixels.

	2B Min. A		2B′ Min. A		2B″ Min. A	
Measure	Average	Standard Deviation	Average	Standard Deviation	Average	Standard Deviation
u_e	-0.142662	3.257643	-0.160225	3.247889	-0.162388	3.250522
v_e	0	1.320262	0	1.150765	0	1.078429
u_k	0	0.134642	0	0.134642	0	0.134642
v_k	0	0	0	0	0	0
e_u	-0.142662	3.142417	-0.160225	3.132997	-0.162388	3.135713
e_v	0	1.320262	0	1.150765	0	1.078429
$\|e\|$	2.678971	2.112064	2.656735	2.026534	2.655547	1.992391
$\|e_u\|$	2.652187	1.691308	2.632291	1.706421	2.632132	1.711852
$\|e_v\|$	0.040767	1.319633	0.038561	1.150119	0.037602	1.077773
r	1.69259E+12	1.98869E+13	1.55237E+12	1.82432E+13	1.55235E+12	1.82429E+13
$\angle$	0.028017	0.269778	0.028054	0.269747	0.028064	0.269748

Table 6.4.6: The averages and standard deviations of measures associated with the type 2B, 2B′, and 2B″ Min. A optical flow estimation. The measure r is unitless. The measure $\angle$ is in radians. All other measures are in pixels.

Type 2B, 2B′, and 2B″ Min. B Optical Flow Estimation

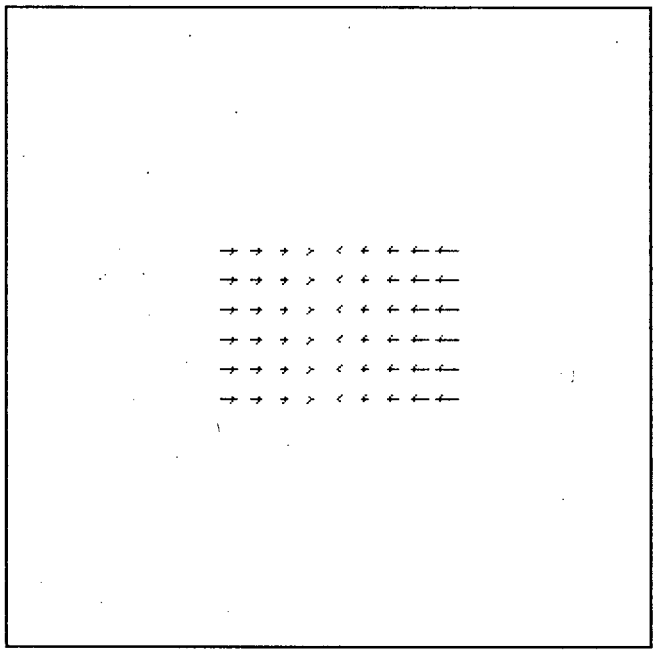

Figure 6.4.7: The type 2B Min. B optical flow estimation for the curving sheet. Vectors are magnified 2 times and sampled every 20 pixels.

	2B Min. B		2B′ Min. B		2B″ Min. B	
Measure	**Average**	**Standard Deviation**	**Average**	**Standard Deviation**	**Average**	**Standard Deviation**
u_e	-0.139623	3.201663	-0.014633	0.73972	-0.005184	0.04495
v_e	0	0.287783	0	0.11293	0	0.000502
u_k	0	0.134642	0	0.134642	0	0.134642
v_k	0	0	0	0	0	0
e_u	-0.139623	3.087124	-0.014633	0.612937	-0.005184	0.127064
e_v	0	0.287783	0	0.11293	0	0.000502
$\|e\|$	2.6024	1.691053	0.360718	0.50846	0.083905	0.09556
$\|e_u\|$	2.579842	1.701104	0.352401	0.501707	0.083904	0.09556
$\|e_v\|$	0.048487	0.283668	0.01442	0.112005	0.000039	0.000501
r	7.4112E+11	8.70654E+12	117229792.8	1377282367	117237.5699	1377362.236
$\angle$	0.053333	0.30824	0.053333	0.30824	0.053333	0.30824

Table 6.4.7: The averages and standard deviations of measures associated with the type 2B, 2B′, and 2B″ Min. B optical flow estimation. The measure r is unitless. The measure $\angle$ is in radians. All other measures are in pixels.

Type 2B, 2B′, and 2B″ Min. C Optical Flow Estimation

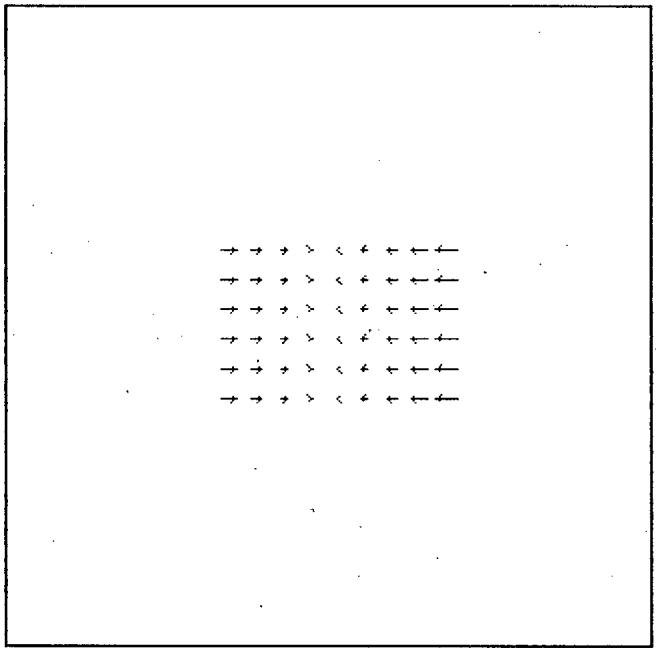

Figure 6.4.8: The type 2B Min. C optical flow estimation for the curving sheet. Vectors are magnified 2 times and sampled every 20 pixels.

	2B Min. C		2B′ Min. C		2B″ Min. C	
Measure	**Average**	**Standard Deviation**	**Average**	**Standard Deviation**	**Average**	**Standard Deviation**
u_e	-0.142102	3.214436	-0.093626	2.195431	-0.092035	2.055316
v_e	0	0.202111	0	0.172778	0	0.169902
u_k	0	0.134642	0	0.134642	0	0.134642
v_k	0	0	0	0	0	0
e_u	-0.142102	3.099506	-0.093626	2.077482	-0.092035	1.937986
e_v	0	0.202111	0	0.172778	0	0.169902
$\|e\|$	2.614689	1.68252	1.773133	1.100143	1.668613	1.004318
$\|e_u\|$	2.60786	1.68098	1.766003	1.098043	1.661131	1.002349
$\|e_v\|$	0.02954	0.199941	0.024846	0.170982	0.024666	0.168102
r	1.11357E+12	1.30834E+13	8.89828E+11	1.04562E+13	8.53426E+11	1.00285E+13
$\angle$	0.034504	0.272319	0.036308	0.275083	0.037047	0.276253

Table 6.4.8: The averages and standard deviations of measures associated with the type 2B, 2B′, and 2B″ Min. C optical flow estimation. The measure r is unitless. The measure $\angle$ is in radians. All other measures are in pixels.

Type 2B, 2B′, and 2B″ Min. D Optical Flow Estimation

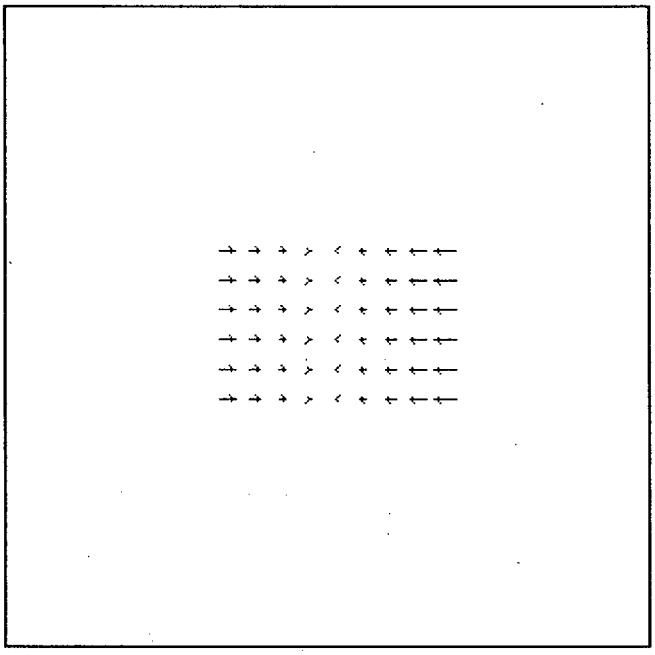

Figure 6.4.9: The type 2B Min. D optical flow estimation for the curving sheet. Vectors are magnified 2 times and sampled every 20 pixels.

	2B Min. D		2B′ Min. D		2B″ Min. D	
Measure	**Average**	**Standard Deviation**	**Average**	**Standard Deviation**	**Average**	**Standard Deviation**
u_e	-0.142662	3.257643	-0.160225	3.247891	-0.162389	3.250524
v_e	0	1.320274	0	1.150754	0	1.078398
u_k	0	0.134642	0	0.134642	0	0.134642
v_k	0	0	0	0	0	0
e_u	-0.142662	3.142418	-0.160225	3.132999	-0.162389	3.135716
e_v	0	1.320274	0	1.150754	0	1.078398
$\|e\|$	2.678972	2.112071	2.656735	2.02653	2.655548	1.992378
$\|e_u\|$	2.652187	1.691308	2.632292	1.706424	2.632133	1.711855
$\|e_v\|$	0.040767	1.319645	0.038561	1.150108	0.037602	1.077742
R	1.69259E+12	1.98869E+13	1.55237E+12	1.82432E+13	1.55235E+12	1.8243E+13
$\angle$	0.028017	0.269778	0.028054	0.269747	0.028064	0.269748

Table 6.4.9: The averages and standard deviations of measures associated with the type 2B, 2B′, and 2B″ Min. D optical flow estimation. The measure *r* is unitless. The measure $\angle$ is in radians. All other measures are in pixels.

6.5 Curved Translating Sheet

The type 1 multiple light source optical flow method cannot determine the flow for developable surfaces, so only the type 2 optical flow estimation technique results will be shown.

Known Motion Field

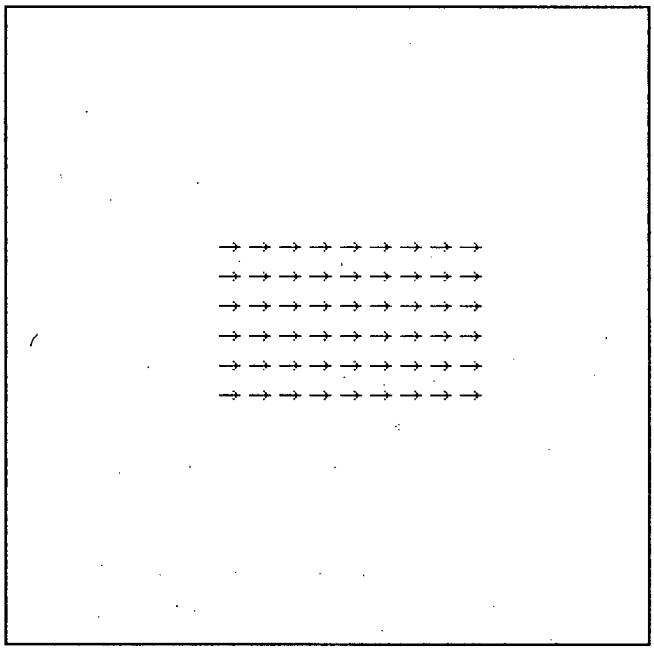

Figure 6.5.1: The known motion field for the translating curved sheet. Vectors are magnified 10 times and sampled every 20 pixels.

Measure	Average	Standard Deviation
u_k	1.000000	0.000000
v_k	0.000000	0.000000
$\|u_k\|$	1.000000	0.000000
$\|v_k\|$	0.000000	0.000000
$\|(u_k, v_k)\|$	1.000000	0.000000

Table 6.5.1: The averages and standard deviations of measures associated with the known motion field. All measures are in pixels.

Type 2A Min. A Optical Flow Estimation

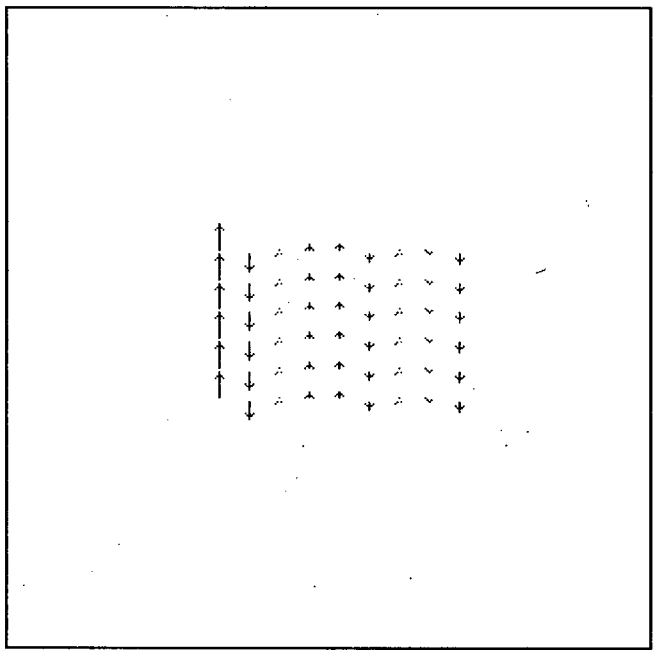

Figure 6.5.2: The type 2A Min. A optical flow estimation for the translating curved sheet. Vectors are magnified 0.00000000000001 times and sampled every 20 pixels.

Measure	Average	Standard Deviation
u_e	1.036104	0.263672
v_e	-2.66135E+13	9.60369E+14
u_k	1	0
v_k	0	0
e_u	0.036104	0.263672
e_v	-2.66135E+13	9.60369E+14
$\|e\|$	4.14421E+14	8.66752E+14
$\|e_u\|$	0.104323	0.244831
$\|e_v\|$	4.14421E+14	8.66752E+14
r	4.14421E+14	8.66752E+14
$\angle$	1.46612	0.38511

Table 6.5.2: The averages and standard deviations of measures associated with the type 2A Min. A optical flow estimation. The measure r is unitless. The measure $\angle$ is in radians. All other measures are in pixels.

Type 2A Min. B Optical Flow Estimation

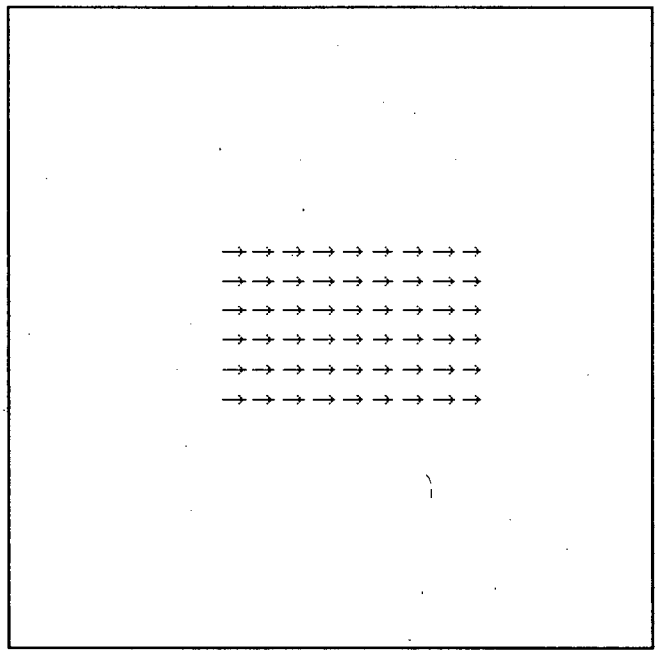

Figure 6.5.3: The type 2A Min. B optical flow estimation for the translating curved sheet. Vectors are magnified 10 times and sampled every 20 pixels.

Measure	Average	Standard Deviation
u_e	1.019631	0.271611
v_e	0	0.090596
u_k	1	0
v_k	0	0
e_u	0.019631	0.271611
e_v	0	0.090596
$\|e\|$	0.118612	0.261335
$\|e_u\|$	0.109976	0.249123
$\|e_v\|$	0.017412	0.088907
R	0.118612	0.261335
$\angle$	0.026161	0.138672

Table 6.5.3: The averages and standard deviations of measures associated with the type 2A Min. B optical flow estimation. The measure r is unitless. The measure $\angle$ is in radians. All other measures are in pixels.

Type 2A Min. C Optical Flow Estimation

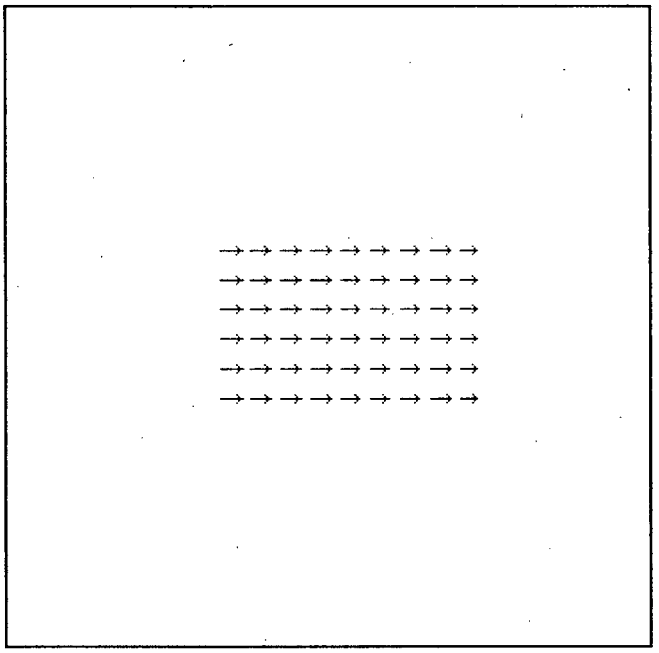

Figure 6.5.4: The type 2A Min. C optical flow estimation for the translating curved sheet. Vectors are magnified 10 times and sampled every 20 pixels.

Measure	Average	Standard Deviation
u_e	1.028629	0.257969
v_e	0	0.059492
u_k	1	0
v_k	0	0
e_u	0.028629	0.257969
e_v	0	0.059492
$\|e\|$	0.106015	0.244268
$\|e_u\|$	0.101082	0.239059
$\|e_v\|$	0.009012	0.058805
r	0.106015	0.244268
$\angle$	0.010296	0.059511

Table 6.5.4: The averages and standard deviations of measures associated with the type 2A Min. C optical flow estimation. The measure *r* is unitless. The measure $\angle$ is in radians. All other measures are in pixels.

Type 2A Min. D Optical Flow Estimation

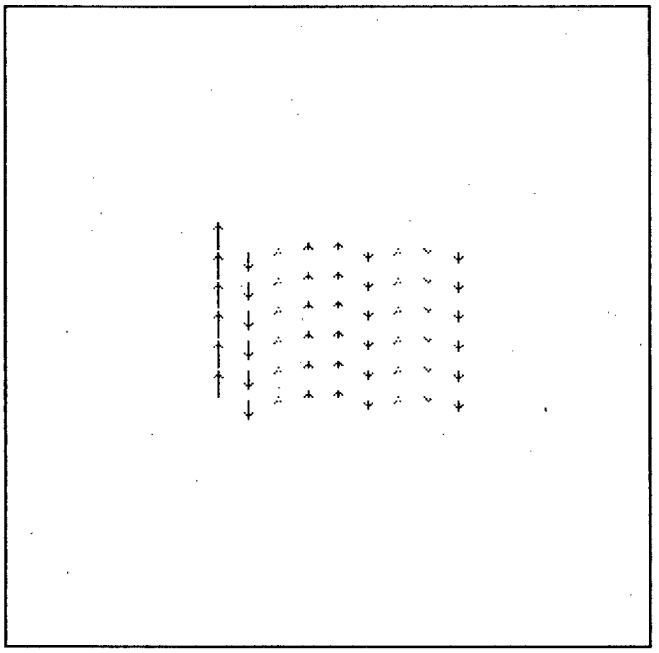

Figure 6.5.5: The type 2A Min. D optical flow estimation for the translating curved sheet. Vectors are magnified 0.00000000000001 times and sampled every 20 pixels.

Measure	Average	Standard Deviation
u_e	1.036104	0.263671
v_e	-2.66135E+13	9.60369E+14
u_k	1	0
v_k	0	0
e_u	0.036104	0.263671
e_v	-2.66135E+13	9.60369E+14
$\|e\|$	4.14421E+14	8.66752E+14
$\|e_u\|$	0.104323	0.244831
$\|e_v\|$	4.14421E+14	8.66752E+14
r	4.14421E+14	8.66752E+14
$\angle$	1.46612	0.38511

Table 6.5.5: The averages and standard deviations of measures associated with the type 2A Min. D optical flow estimation. The measure r is unitless. The measure $\angle$ is in radians. All other measures are in pixels.

Type 2B, 2B′, and 2B″ Min. A Optical Flow Estimation

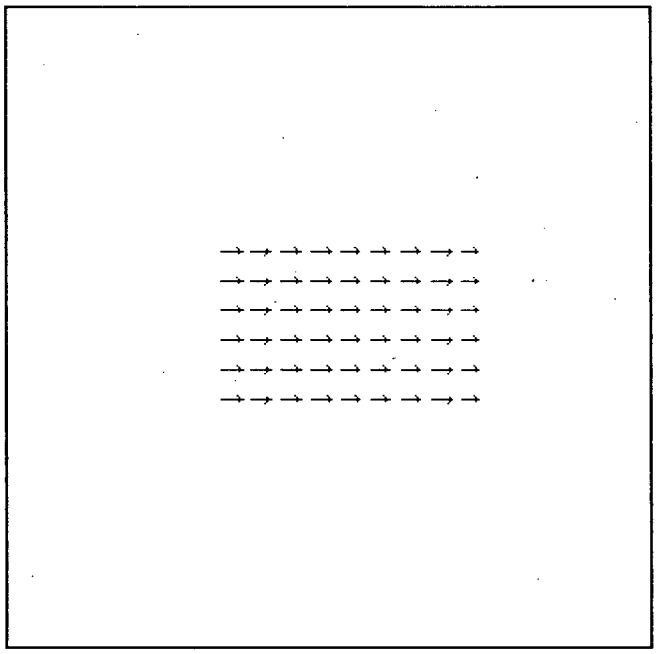

Figure 6.5.6: The type 2B Min. A optical flow estimation for the translating curved sheet. Vectors are magnified 10 times and sampled every 20 pixels.

	2B Min. A		2B′ Min. A		2B″ Min. A	
Measure	Average	Standard Deviation	Average	Standard Deviation	Average	Standard Deviation
u_e	1.03519	0.253348	1.033541	0.263507	1.033738	0.270427
v_e	0	0.342174	0	0.34486	0	0.351724
u_k	1	0	1	0	1	0
v_k	0	0	0	0	0	0
e_u	0.03519	0.253348	0.033541	0.263507	0.033738	0.270427
e_v	0	0.342174	0	0.34486	0	0.351724
$\|e\|$	0.109014	0.413064	0.108739	0.421503	0.109902	0.43116
$\|e_u\|$	0.098012	0.236255	0.097678	0.247021	0.098678	0.25403
$\|e_v\|$	0.013043	0.341925	0.012938	0.344617	0.013015	0.351483
r	0.109014	0.413064	0.108739	0.421503	0.109902	0.43116
$\angle$	0.005392	0.057209	0.005237	0.056437	0.005165	0.056098

Table 6.5.6: The averages and standard deviations of measures associated with the type 2B, 2B′, and 2B″ Min. A optical flow estimation. The measure r is unitless. The measure $\angle$ is in radians. All other measures are in pixels.

Type 2B, 2B′, and 2B″ Min. B Optical Flow Estimation

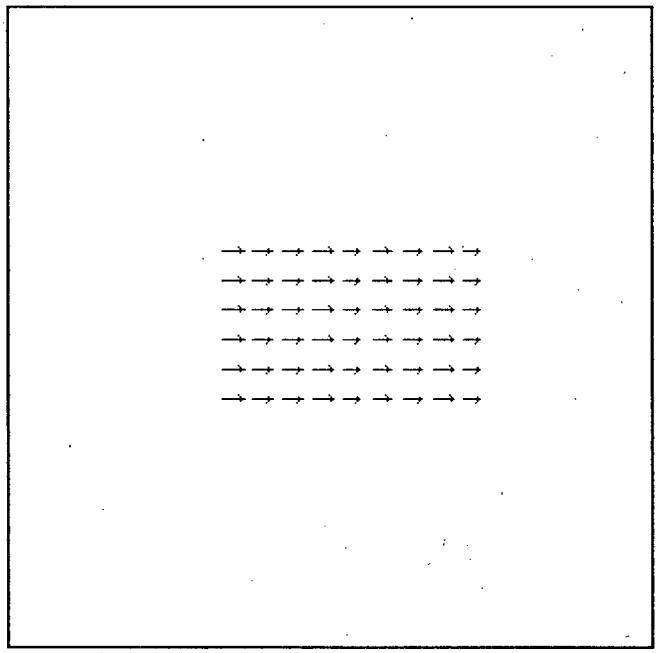

Figure 6.5.7: The type 2B Min. B optical flow estimation for the translating curved sheet. Vectors are magnified 10 times and sampled every 20 pixels.

	2B Min. B		2B′ Min. B		2B″ Min. B	
Measure	Average	Standard Deviation	Average	Standard Deviation	Average	Standard Deviation
u_e	1.004322	0.279711	0.281178	0.378537	0.002568	0.015323
v_e	0	0.090325	0	0.047219	0	0.00052
u_k	1	0	1	0	1	0
v_k	0	0	0	0	0	0
e_u	0.004322	0.279711	-0.718822	0.378537	-0.997432	0.015323
e_v	0	0.090325	0	0.047219	0	0.00052
$\|e\|$	0.128627	0.264328	0.761678	0.286473	0.997432	0.015323
$\|e_u\|$	0.120163	0.25262	0.760147	0.286649	0.997432	0.015323
$\|e_v\|$	0.017311	0.08865	0.006504	0.046769	0.000033	0.000519
r	0.128627	0.264328	0.761678	0.286473	0.997432	0.015323
$\angle$	0.026161	0.138672	0.026161	0.138672	0.026161	0.138672

Table 6.5.7: The averages and standard deviations of measures associated with the type 2B, 2B′, and 2B″ Min. B optical flow estimation. The measure r is unitless. The measure $\angle$ is in radians. All other measures are in pixels.

Type 2B, 2B′, and 2B″ Min. C Optical Flow Estimation

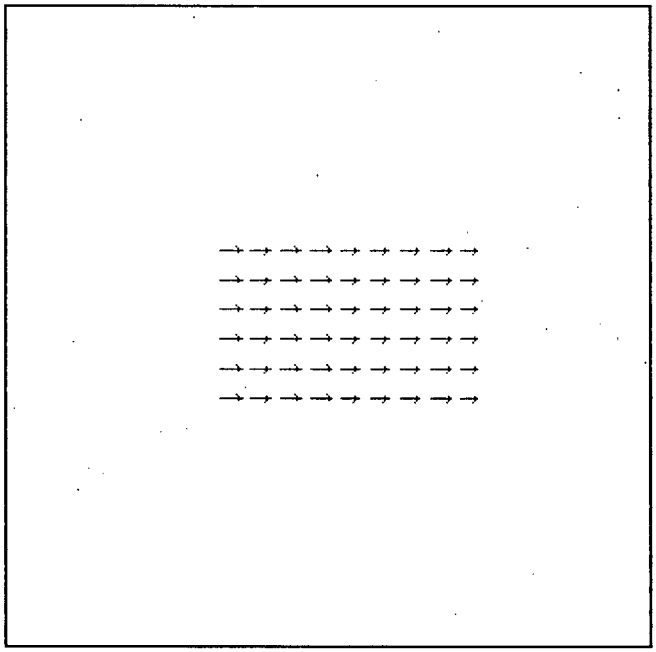

Figure 6.5.8: The type 2B Min. C optical flow estimation for the translating curved sheet. Vectors are magnified 10 times and sampled every 20 pixels.

	2B Min. C		2B′ Min. C		2B″ Min. C	
Measure	**Average**	**Standard Deviation**	**Average**	**Standard Deviation**	**Average**	**Standard Deviation**
u_e	1.019292	0.260423	0.823345	0.267081	0.789354	0.26337
v_e	0	0.059477	0	0.056755	0	0.056336
u_k	1	0	1	0	1	0
v_k	0	0	0	0	0	0
e_u	0.019292	0.260423	-0.176655	0.267081	-0.210646	0.26337
e_v	0	0.059477	0	0.056755	0	0.056336
$\|e\|$	0.110236	0.244084	0.232095	0.227795	0.26196	0.219738
$\|e_u\|$	0.105329	0.23895	0.229212	0.223605	0.259287	0.215647
$\|e_v\|$	0.009011	0.05879	0.00827	0.056149	0.008293	0.055722
r	0.110236	0.244084	0.232095	0.227795	0.26196	0.219738
$\angle$	0.010318	0.059533	0.011658	0.067029	0.01235	0.070991

Table 6.5.8: The averages and standard deviations of measures associated with the type 2B, 2B′, and 2B″ Min. C optical flow estimation. The measure r is unitless. The measure $\angle$ is in radians. All other measures are in pixels.

Type 2B, 2B′, and 2B″ Min. D Optical Flow Estimation

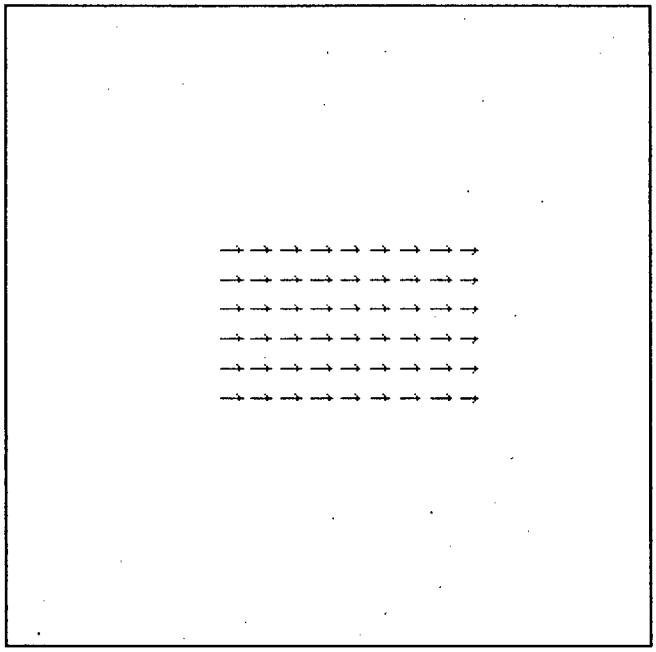

Figure 6.5.9: The type 2B Min. D optical flow estimation for the translating curved sheet. Vectors are magnified 10 times and sampled every 20 pixels.

	2B Min. D		2B′ Min. D		2B″ Min. D	
Measure	Average	Standard Deviation	Average	Standard Deviation	Average	Standard Deviation
u_e	1.03519	0.253348	1.033541	0.263507	1.033738	0.270428
v_e	0	0.342174	0	0.344861	0	0.351729
u_k	1	0	1	0	1	0
v_k	0	0	0	0	0	0
e_u	0.03519	0.253348	0.033541	0.263507	0.033738	0.270428
e_v	0	0.342174	0	0.344861	0	0.351729
$\|e\|$	0.109014	0.413064	0.108739	0.421504	0.109902	0.431165
$\|e_u\|$	0.098012	0.236255	0.097678	0.247022	0.098678	0.254031
$\|e_v\|$	0.013043	0.341926	0.012938	0.344619	0.013015	0.351488
r	0.109014	0.413064	0.108739	0.421504	0.109902	0.431165
$\angle$	0.005392	0.057209	0.005237	0.056437	0.005165	0.056098

Table 6.5.9: The averages and standard deviations of measures associated with the type 2B, 2B′, and 2B″ Min. D optical flow estimation. The measure r is unitless. The measure $\angle$ is in radians. All other measures are in pixels.

6.6 Rotation of a Surface With Negative Gaussian Curvature

Known Motion Field

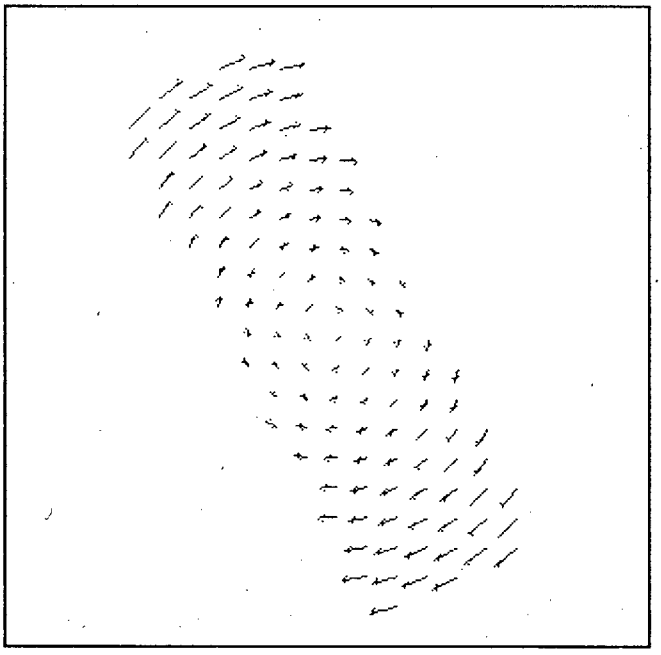

Figure 6.6.1: The known motion field for the rotating surface with negative Gaussian curvature. Vectors are magnified 10 times and sampled every 20 pixels.

Measure	Average	Standard Deviation
u_k	0	0.732816
v_k	0	0.468766
$\|u_k\|$	0.631154	0.372356
$\|v_k\|$	0.390208	0.259756
$\|(u_k, v_k)\|$	0.784106	0.376717

Table 6.6.1: The averages and standard deviations of measures associated with the known motion field. The measure *r* is unitless. The measure $\angle$ is in radians. All other measures are in pixels.

Type 1 Optical Flow Estimation

Figure 6.6.2: The type 1 optical flow estimation for the rotating surface with negative Gaussian curvature. Vectors are magnified 10 times and sampled every 20 pixels.

Measure	Average	Standard Deviation
u_e	-0.026634	1.207233
v_e	-0.003204	1.200599
u_k	0	0.732816
v_k	0	0.468766
e_u	-0.026634	0.622309
e_v	-0.003204	0.889667
$\|e\|$	0.77432	0.761513
$\|e_u\|$	0.445683	0.435129
$\|e_v\|$	0.573548	0.680109
r	1.294162	1.580457
$\angle$	0.283987	0.231137

Table 6.6.2: The averages and standard deviations of measures associated with the type 1 optical flow estimation. The measure *r* is unitless. The measure $\angle$ is in radians. All other measures are in pixels.

Type 2A Min. A Optical Flow Estimation

Figure 6.6.3: The type 2A Min. A optical flow estimation for the rotating surface with negative Gaussian curvature. Vectors are magnified 10 times and sampled every 20 pixels.

Measure	Average	Standard Deviation
u_e	-0.020448	1.233756
v_e	-0.004997	1.291821
u_k	0	0.732816
v_k	0	0.468766
e_u	-0.020448	0.67678
e_v	-0.004997	1.016785
$\|e\|$	0.805597	0.918322
$\|e_u\|$	0.462881	0.494148
$\|e_v\|$	0.600366	0.820624
r	1.34301	1.76883
$\angle$	0.290014	0.238149

Table 6.6.3: The averages and standard deviations of measures associated with the type 2A Min. A optical flow estimation. The measure *r* is unitless. The measure $\angle$ is in radians. All other measures are in pixels.

Type 2A Min. B Optical Flow Estimation

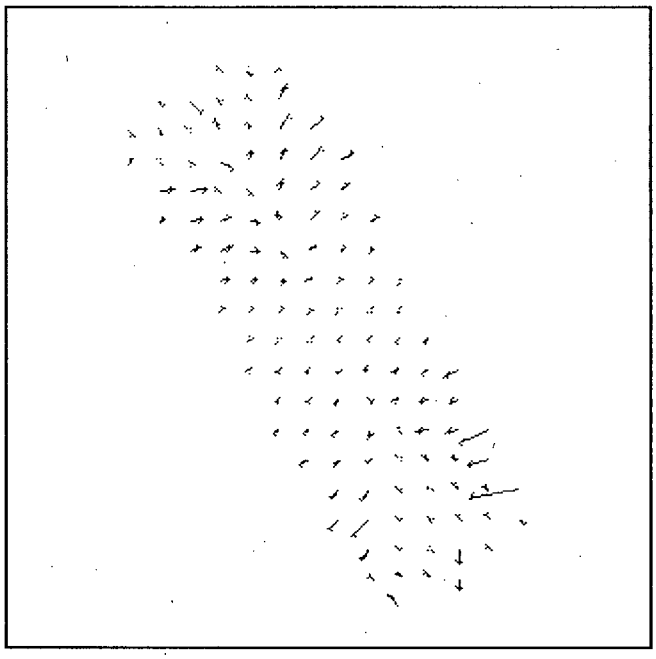

Figure 6.6.4: The type 2A Min. B optical flow estimation for the rotating surface with negative Gaussian curvature. Vectors are magnified 10 times and sampled every 20 pixels.

Measure	Average	Standard Deviation
u_e	-0.012674	0.415968
v_e	-0.011052	0.31971
u_k	0	0.732816
v_k	0	0.468766
e_u	-0.012674	0.603756
e_v	-0.011052	0.495564
$\|e\|$	0.672638	0.397403
$\|e_u\|$	0.450845	0.401764
$\|e_v\|$	0.41674	0.268378
r	0.837118	0.177931
$\angle$	1.03181	0.348888

Table 6.6.4: The averages and standard deviations of measures associated with the type 2A Min. B optical flow estimation. The measure r is unitless. The measure $\angle$ is in radians. All other measures are in pixels.

Type 2A Min. C Optical Flow Estimation

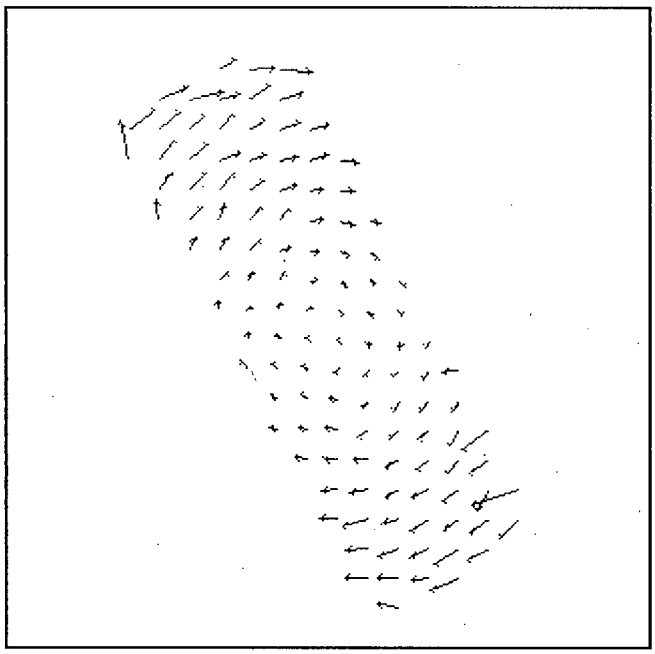

Figure 6.6.5: The type 2A Min. C optical flow estimation for the rotating surface with negative Gaussian curvature. Vectors are magnified 10 times and sampled every 20 pixels.

Measure	Average	Standard Deviation
u_e	-0.013993	0.777264
v_e	-0.02398	0.519127
u_k	0	0.732816
v_k	0	0.468766
e_u	-0.013993	0.230545
e_v	-0.02398	0.217927
$\|e\|$	0.212287	0.237374
$\|e_u\|$	0.131485	0.189888
$\|e_v\|$	0.143358	0.165876
r	0.321901	0.337653
$\angle$	0.175804	0.16936

Table 6.6.5: The averages and standard deviations of measures associated with the type 2A Min. C optical flow estimation. The measure r is unitless. The measure $\angle$ is in radians. All other measures are in pixels.

Type 2A Min. D Optical Flow Estimation

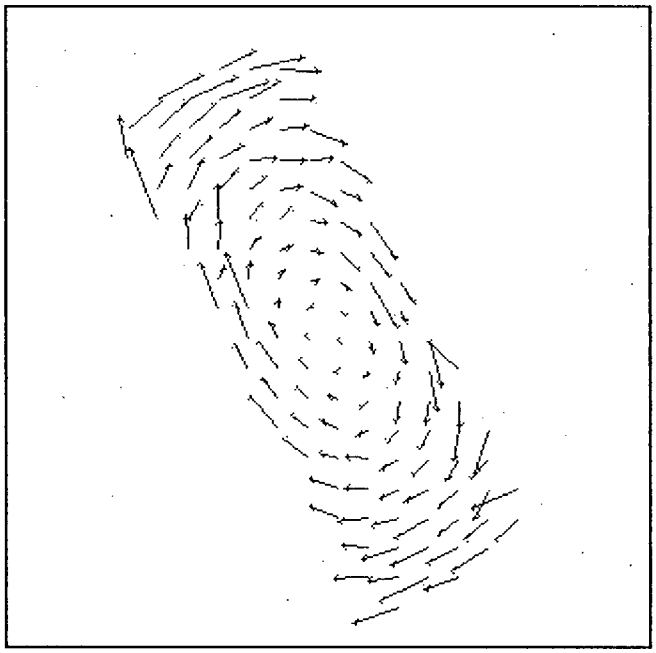

Figure 6.6.6: The type 2A Min. D optical flow estimation for the rotating surface with negative Gaussian curvature. Vectors are magnified 10 times and sampled every 20 pixels.

Measure	Average	Standard Deviation
u_e	-0.020448	1.233743
v_e	-0.004993	1.291802
u_k	0	0.732816
v_k	0	0.468766
e_u	-0.020448	0.676764
e_v	-0.004993	1.016762
$\|e\|$	0.805586	0.918294
$\|e_u\|$	0.462874	0.494133
$\|e_v\|$	0.600359	0.820601
r	1.342995	1.768789
$\angle$	0.290012	0.238148

Table 6.6.6: The averages and standard deviations of measures associated with the type 2A Min. D optical flow estimation. The measure r is unitless. The measure $\angle$ is in radians. All other measures are in pixels.

Type 2B, 2B′, and 2B″ Min. A Optical Flow Estimation

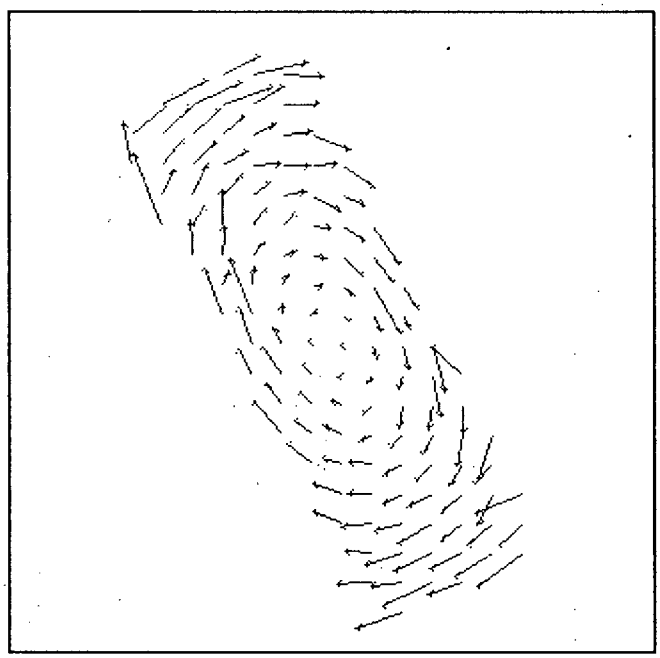

Figure 6.6.7: The type 2B Min. A optical flow estimation for the rotating surface with negative Gaussian curvature. Vectors are magnified 10 times and sampled every 20 pixels.

	2B Min. A		2B′ Min. A		2B″ Min. A	
Measure	Average	Standard Deviation	Average	Standard Deviation	Average	Standard Deviation
u_e	-0.028704	1.240773	-0.027702	1.227127	-0.026708	1.209576
v_e	0.001175	1.298493	-0.000047	1.241082	-0.002604	1.202041
u_k	0	0.732816	0	0.732816	0	0.732816
v_k	0	0.468766	0	0.468766	0	0.468766
e_u	-0.028704	0.676498	-0.027702	0.651597	-0.026708	0.625467
e_v	0.001175	1.014995	-0.000047	0.941671	-0.002604	0.891089
$\|e\|$	0.802091	0.919411	0.79199	0.827538	0.775465	0.764591
$\|e_u\|$	0.46076	0.496151	0.456399	0.465873	0.446551	0.438757
$\|e_v\|$	0.597054	0.820811	0.58768	0.735774	0.574218	0.681401
r	1.340487	1.770217	1.321145	1.66008	1.295127	1.581188
$\angle$	0.290073	0.238385	0.287389	0.234418	0.284067	0.231103

Table 6.6.7: The averages and standard deviations of measures associated with the type 2B, 2B′, and 2B″ Min. A optical flow estimation. The measure r is unitless. The measure $\angle$ is in radians. All other measures are in pixels.

Type 2B, 2B′, and 2B″ Min. B Optical Flow Estimation

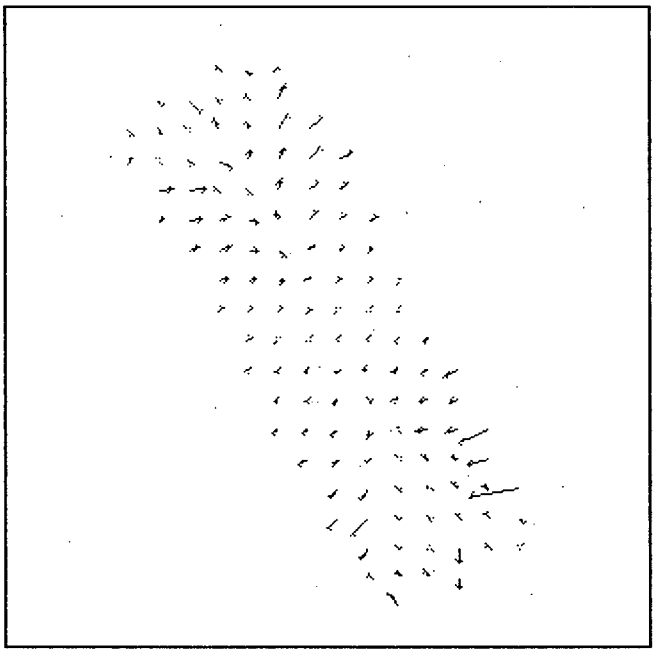

Figure 6.6.8: The type 2B Min. B optical flow estimation for the rotating surface with negative Gaussian curvature. Vectors are magnified 10 times and sampled every 20 pixels.

	2B Min. B		2B′ Min. B		2B″ Min. B	
Measure	Average	Standard Deviation	Average	Standard Deviation	Average	Standard Deviation
u_e	-0.012845	0.416126	-0.011902	0.374295	-0.005776	0.120229
v_e	-0.011035	0.31977	-0.007854	0.282625	0.000868	0.087973
u_k	0	0.732816	0	0.732816	0	0.732816
v_k	0	0.468766	0	0.468766	0	0.468766
e_u	-0.012845	0.603585	-0.011902	0.618994	-0.005776	0.716097
e_v	-0.011035	0.495566	-0.007854	0.482088	0.000868	0.464062
$\|e\|$	0.672501	0.397383	0.6824	0.3874	0.770124	0.367517
$\|e_u\|$	0.450686	0.401689	0.48155	0.389097	0.616056	0.365089
$\|e_v\|$	0.416741	0.268381	0.398224	0.271813	0.385168	0.258833
r	0.836891	0.176773	0.862873	0.153251	0.987626	0.055354
$\angle$	1.035537	0.358807	1.035809	0.359235	1.035719	0.358924

Table 6.6.8: The averages and standard deviations of measures associated with the type 2B, 2B′, and 2B″ Min. B optical flow estimation. The measure r is unitless. The measure $\angle$ is in radians. All other measures are in pixels.

Type 2B, 2B′, and 2B″ Min. C Optical Flow Estimation

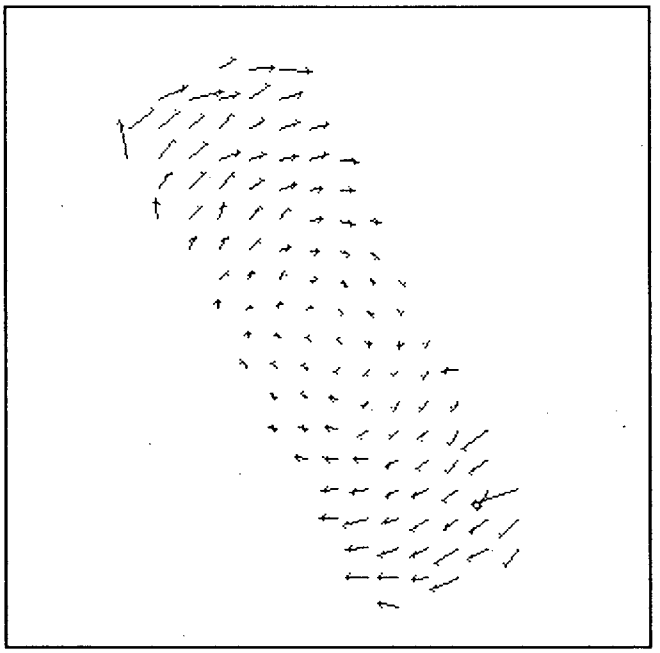

Figure 6.6.9: The type 2B Min. C optical flow estimation for the rotating surface with negative Gaussian curvature. Vectors are magnified 10 times and sampled every 20 pixels.

	2B Min. C		2B′ Min. C		2B″ Min. C	
Measure	**Average**	**Standard Deviation**	**Average**	**Standard Deviation**	**Average**	**Standard Deviation**
u_e	-0.019062	0.781198	-0.002108	0.770561	0.019229	0.695406
v_e	-0.020856	0.525582	-0.04164	0.506823	-0.071462	0.455809
u_k	0	0.732816	0	0.732816	0	0.732816
v_k	0	0.468766	0	0.468766	0	0.468766
e_u	-0.019062	0.219673	-0.002108	0.212329	0.019229	0.206943
e_v	-0.020856	0.203386	-0.04164	0.179475	-0.071462	0.152258
$\|e\|$	0.206308	0.218759	0.188312	0.208736	0.20242	0.174669
$\|e_u\|$	0.127724	0.179738	0.117953	0.176563	0.129566	0.162503
$\|e_v\|$	0.13817	0.150695	0.123363	0.136843	0.128487	0.108537
r	0.317293	0.33171	0.285666	0.303132	0.305908	0.281594
$\angle$	0.176481	0.169816	0.162721	0.159338	0.191072	0.180111

Table 6.6.9: The averages and standard deviations of measures associated with the type 2B, 2B′, and 2B″ Min. C optical flow estimation. The measure r is unitless. The measure $\angle$ is in radians. All other measures are in pixels.

Type 2B, 2B′, and 2B″ Min. D Optical Flow Estimation

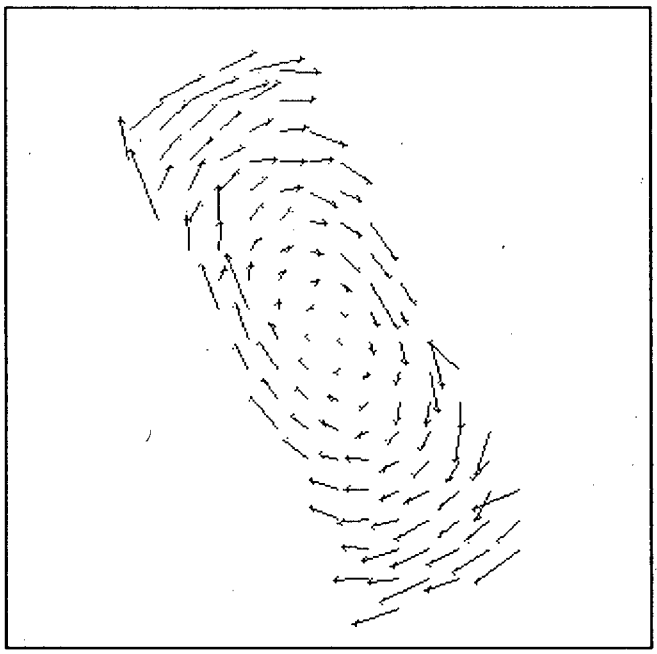

Figure 6.6.10: The type 2B Min. D optical flow estimation for the rotating surface with negative Gaussian curvature. Vectors are magnified 10 times and sampled every 20 pixels.

	2B Min. D		2B′ Min. D		2B″ Min. D	
Measure	**Average**	**Standard Deviation**	**Average**	**Standard Deviation**	**Average**	**Standard Deviation**
u_e	-0.028703	1.240757	-0.027701	1.227115	-0.026706	1.209543
v_e	0.001179	1.298459	-0.000044	1.241064	-0.002605	1.202019
u_k	0	0.732816	0	0.732816	0	0.732816
v_k	0	0.468766	0	0.468766	0	0.468766
e_u	-0.028703	0.676476	-0.027701	0.651581	-0.026706	0.625427
e_v	0.001179	1.014954	-0.000044	0.94165	-0.002605	0.891064
$\|e\|$	0.80208	0.919358	0.791978	0.827513	0.775441	0.764553
$\|e_u\|$	0.460753	0.496128	0.456391	0.465859	0.446532	0.438719
$\|e_v\|$	0.597046	0.820765	0.587672	0.735754	0.574204	0.68138
r	1.340471	1.770151	1.321126	1.660039	1.295093	1.581133
$\angle$	0.290072	0.238384	0.287387	0.234417	0.284065	0.231105

Table 6.6.10: The averages and standard deviations of measures associated with the type 2B, 2B′, and 2B″ Min. D optical flow estimation. The measure r is unitless. The measure $\angle$ is in radians. All other measures are in pixels.

6.7 Translation of a Surface With Negative Gaussian Curvature

Known Motion Field

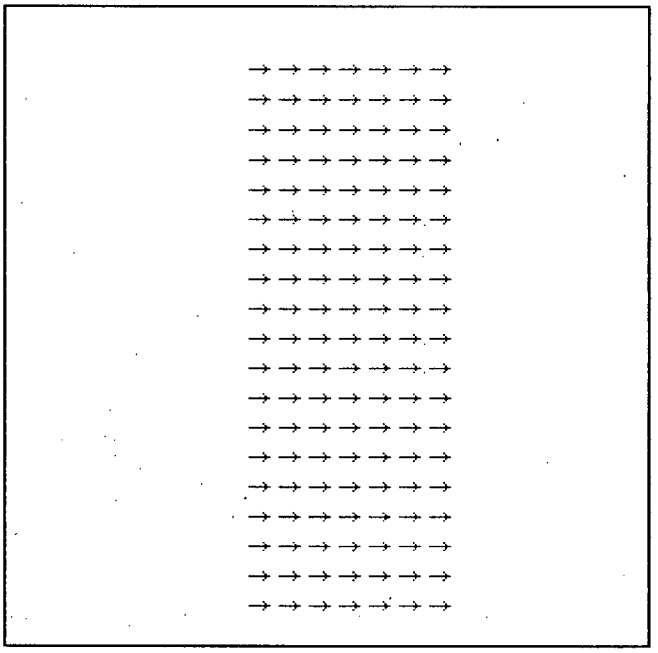

Figure 6.7.1: The known motion field for the translating surface with negative Gaussian curvature. Vectors are magnified 10 times and sampled every 20 pixels.

Measure	Average	Standard Deviation
u_k	1.000000	0.000000
v_k	0.000000	0.000000
$\|u_k\|$	1.000000	0.000000
$\|v_k\|$	0.000000	0.000000
$\|(u_k, v_k)\|$	1.000000	0.000000

Table 6.7.1: The averages and standard deviations of measures associated with the known motion field. The measure *r* is unitless. The measure $\angle$ is in radians. All other measures are in pixels.

Type 1 Optical Flow

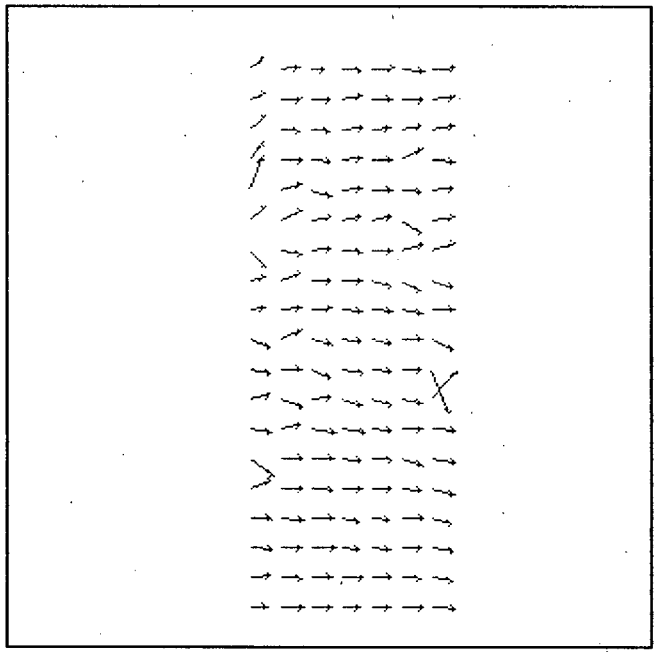

Figure 6.7.2: The type 1optical flow estimation for the translating surface with negative Gaussian curvature. Vectors are magnified 10 times and sampled every 20 pixels.

Measure	Average	Standard Deviation
u_e	1.026016	0.22315
v_e	-0.0031	1.253734
u_k	1	0
v_k	0	0
e_u	0.026016	0.22315
e_v	-0.0031	1.253734
$\|e\|$	0.302459	1.237274
$\|e_u\|$	0.09086	0.205467
$\|e_v\|$	0.266413	1.225104
r	0.302459	1.237274
$\angle$	0.165259	0.242102

Table 6.7.2: The averages and standard deviations of measures associated with the type 1 optical flow estimation. The measure *r* is unitless. The measure $\angle$ is in radians. All other measures are in pixels.

Type 2A Min. A Optical Flow

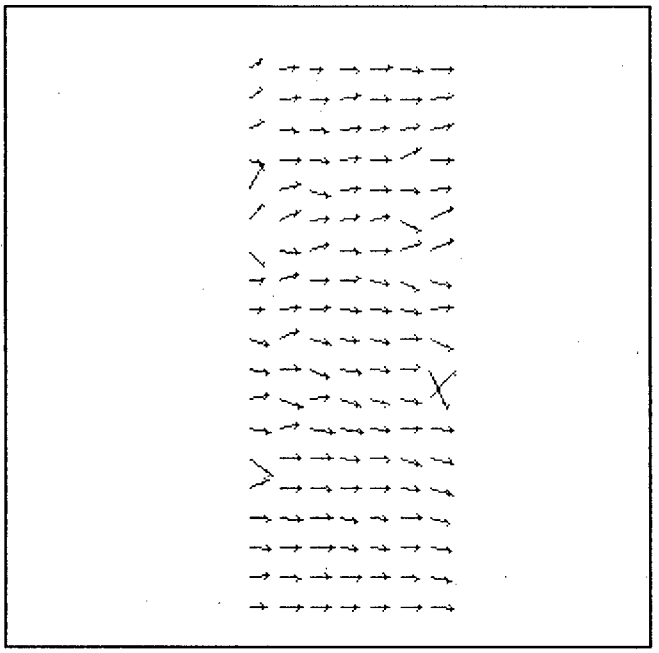

Figure 6.7.3: The type 2A Min. A optical flow estimation for the translating surface with negative Gaussian curvature. Vectors are magnified 10 times and sampled every 20 pixels.

Measure	Average	Standard Deviation
u_e	1.015535	0.21744
v_e	0.019208	1.198455
u_k	1	0
v_k	0	0
e_u	0.015535	0.21744
e_v	0.019208	1.198455
$\|e\|$	0.30576	1.179276
$\|e_u\|$	0.093898	0.196734
$\|e_v\|$	0.263546	1.169275
r	0.30576	1.179276
$\angle$	0.166728	0.241619

Table 6.7.3: The averages and standard deviations of measures associated with the type 2A Min. A optical flow estimation. The measure *r* is unitless. The measure $\angle$ is in radians. All other measures are in pixels.

Type 2A Min. B Optical Flow

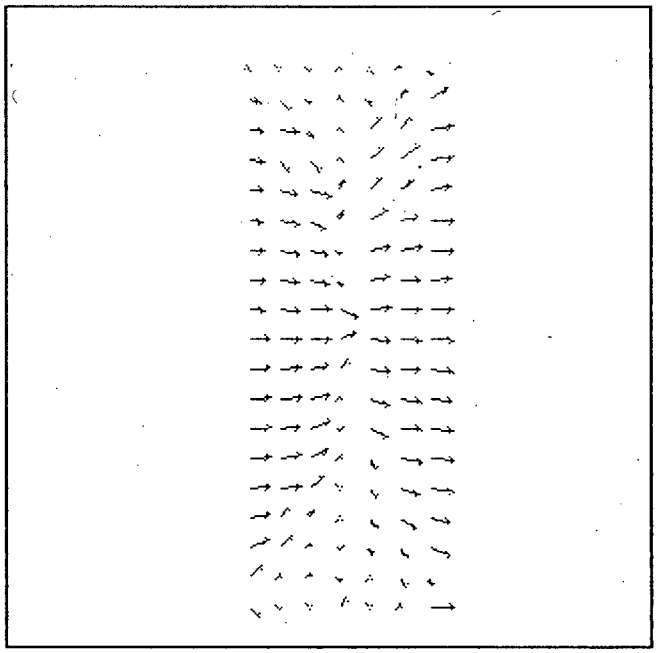

Figure 6.7.4: The type 2A Min. B optical flow estimation for the translating surface with negative Gaussian curvature. Vectors are magnified 10 times and sampled every 20 pixels.

Measure	Average	Standard Deviation
u_e	0.643305	0.454303
v_e	-0.005065	0.295743
u_k	1	0
v_k	0	0
e_u	-0.356695	0.454303
e_v	-0.005065	0.295743
$\|e\|$	0.52506	0.381338
$\|e_u\|$	0.415091	0.401648
$\|e_v\|$	0.228468	0.187856
r	0.52506	0.381338
$\angle$	0.607632	0.546113

Table 6.7.4: The averages and standard deviations of measures associated with the type 2A Min. B optical flow estimation. The measure *r* is unitless. The measure $\angle$ is in radians. All other measures are in pixels.

Type 2A Min. C Optical Flow

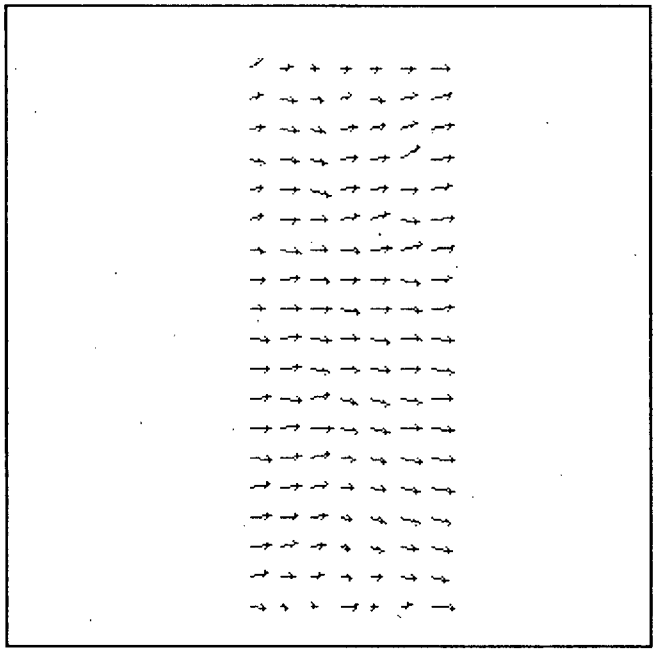

Figure 6.7.5: The type 2A Min. C optical flow estimation for the translating surface with negative Gaussian curvature. Vectors are magnified 10 times and sampled every 20 pixels.

Measure	Average	Standard Deviation
u_e	0.885491	0.265396
v_e	0.003547	0.234221
u_k	1	0
v_k	0	0
e_u	-0.114509	0.265396
e_v	0.003547	0.234221
$\|e\|$	0.252921	0.272853
$\|e_u\|$	0.17713	0.228412
$\|e_v\|$	0.133488	0.192489
r	0.252921	0.272853
$\angle$	0.141913	0.13829

Table 6.7.5: The averages and standard deviations of measures associated with the type 2A Min. C optical flow estimation. The measure *r* is unitless. The measure $\angle$ is in radians. All other measures are in pixels.

Type 2A Min. D Optical Flow

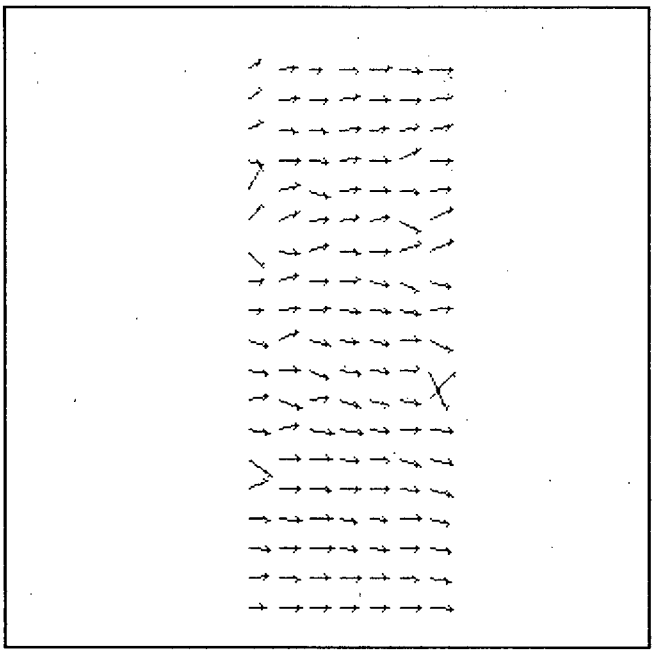

Figure 6.7.6: The type 2A Min. D optical flow estimation for the translating surface with negative Gaussian curvature. Vectors are magnified 10 times and sampled every 20 pixels.

Measure	Average	Standard Deviation
u_e	1.015535	0.217443
v_e	0.019201	1.19849
u_k	1	0
v_k	0	0
e_u	0.015535	0.217443
e_v	0.019201	1.19849
$\|e\|$	0.305764	1.179311
$\|e_u\|$	0.093899	0.196737
$\|e_v\|$	0.26355	1.16931
r	0.305764	1.179311
$\angle$	0.166729	0.241621

Table 6.7.6: The averages and standard deviations of measures associated with the type 2A Min. D optical flow estimation. The measure *r* is unitless. The measure $\angle$ is in radians. All other measures are in pixels.

Type 2B, 2B′, and 2B″ Min. A Optical Flow

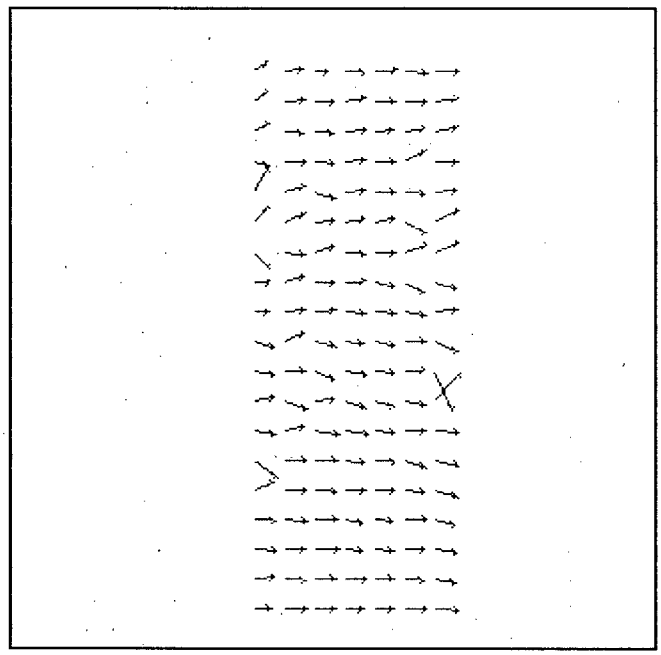

Figure 6.7.7: The type 2B Min. A optical flow estimation for the translating surface with negative Gaussian curvature. Vectors are magnified 10 times and sampled every 20 pixels.

	2B Min. A		2B′ Min. A		2B″ Min. A	
Measure	**Average**	**Standard Deviation**	**Average**	**Standard Deviation**	**Average**	**Standard Deviation**
u_e	1.023672	0.196776	1.023972	0.200033	1.025944	0.222412
v_e	0.019119	1.198595	0.016228	1.193974	-0.003017	1.251757
u_k	1	0	1	0	1	0
v_k	0	0	0	0	0	0
e_u	0.023672	0.196776	0.023972	0.200033	0.025944	0.222412
e_v	0.019119	1.198595	0.016228	1.193974	-0.003017	1.251757
$\|e\|$	0.2988	1.177707	0.296611	1.174071	0.302286	1.235178
$\|e_u\|$	0.086637	0.178256	0.08703	0.181695	0.090726	0.204716
$\|e_v\|$	0.26434	1.169238	0.26204	1.164976	0.266409	1.223082
r	0.2988	1.177707	0.296611	1.174071	0.302286	1.235178
$\angle$	0.166417	0.241852	0.165343	0.241126	0.165451	0.242477

Table 6.7.7: The averages and standard deviations of measures associated with the type 2B, 2B′, and 2B″ Min. A optical flow estimation. The measure r is unitless. The measure $\angle$ is in radians. All other measures are in pixels.

Type 2B, 2B′, and 2B″ Min. B Optical Flow

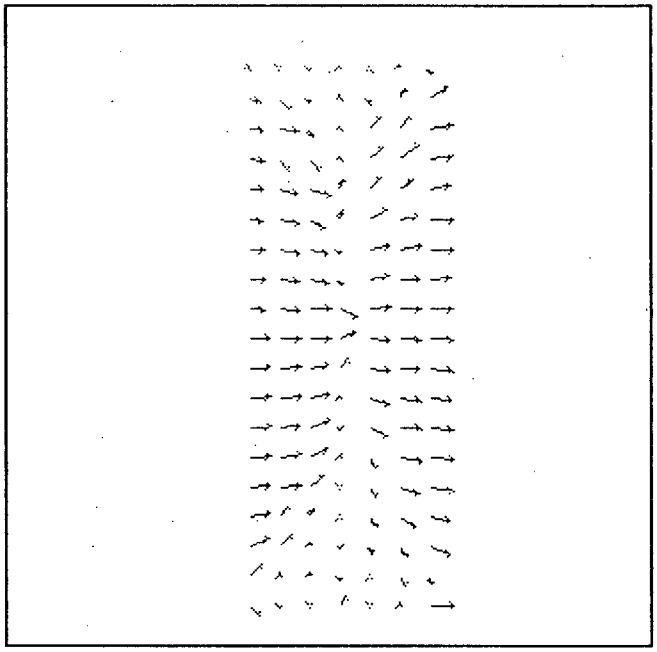

Figure 6.7.8: The type 2B Min. B optical flow estimation for the translating surface with negative Gaussian curvature. Vectors are magnified 10 times and sampled every 20 pixels.

	2B Min. B		2B′ Min. B		2B″ Min. B	
Measure	**Average**	**Standard Deviation**	**Average**	**Standard Deviation**	**Average**	**Standard Deviation**
u_e	0.643225	0.454243	0.463769	0.427441	0.022268	0.084161
v_e	-0.004903	0.295401	-0.004165	0.21493	-0.000826	0.042337
u_k	1	0	1	0	1	0
v_k	0	0	0	0	0	0
e_u	-0.356775	0.454243	-0.536231	0.427441	-0.977732	0.084161
e_v	-0.004903	0.295401	-0.004165	0.21493	-0.000826	0.042337
$\|e\|$	0.524843	0.381374	0.625652	0.353578	0.979886	0.068252
$\|e_u\|$	0.415127	0.401613	0.5785	0.368219	0.978909	0.069136
$\|e_v\|$	0.228161	0.187687	0.150371	0.153623	0.007963	0.04159
r	0.524843	0.381374	0.625652	0.353578	0.979886	0.068252
$\angle$	0.615816	0.556611	0.616878	0.55712	0.613821	0.554227

Table 6.7.8: The averages and standard deviations of measures associated with the type 2B, 2B′, and 2B″ Min. B optical flow estimation. The measure r is unitless. The measure $\angle$ is in radians. All other measures are in pixels.

Type 2B, 2B′, and 2B″ Min. C Optical Flow

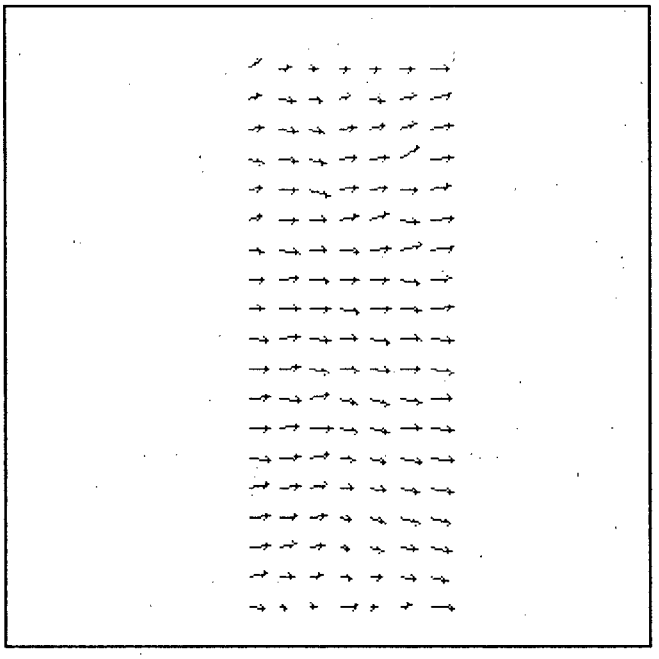

Figure 6.7.9: The type 2B Min. C optical flow estimation for the translating surface with negative Gaussian curvature. Vectors are magnified 10 times and sampled every 20 pixels.

	2B Min. C		2B′ Min. C		2B″ Min. C	
Measure	**Average**	**Standard Deviation**	**Average**	**Standard Deviation**	**Average**	**Standard Deviation**
u_e	0.888538	0.257078	0.854424	0.250651	0.808472	0.262075
v_e	0.003804	0.234443	0.007841	0.208503	0.011213	0.158672
u_k	1	0	1	0	1	0
v_k	0	0	0	0	0	0
e_u	-0.111462	0.257078	-0.145576	0.250651	-0.191528	0.262075
e_v	0.003804	0.234443	0.007841	0.208503	0.011213	0.158672
$\|e\|$	0.249805	0.26662	0.241806	0.262835	0.264099	0.246819
$\|e_u\|$	0.174002	0.219625	0.192678	0.216548	0.233544	0.22544
$\|e_v\|$	0.134093	0.192345	0.106851	0.179214	0.08487	0.134534
r	0.249805	0.26662	0.241806	0.262835	0.264099	0.246819
$\angle$	0.14243	0.139455	0.117646	0.129043	0.100125	0.107209

Table 6.7.9: The averages and standard deviations of measures associated with the type 2B, 2B′, and 2B″ Min. C optical flow estimation. The measure r is unitless. The measure $\angle$ is in radians. All other measures are in pixels.

Type 2B, 2B′, and 2B″ Min. D Optical Flow

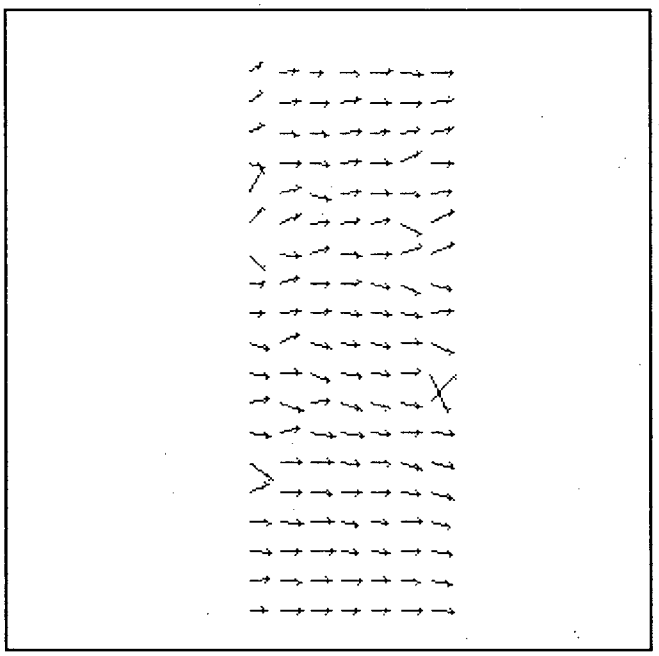

Figure 6.7.10: The type 2B Min. D optical flow estimation for the translating surface with negative Gaussian curvature. Vectors are magnified 10 times and sampled every 20 pixels.

	2B Min. D		2B′ Min. D		2B″ Min. D	
Measure	Average	Standard Deviation	Average	Standard Deviation	Average	Standard Deviation
u_e	1.023672	0.19678	1.023972	0.200036	1.025945	0.222433
v_e	0.019112	1.198631	0.016221	1.194017	-0.003035	1.251958
u_k	1	0	1	0	1	0
v_k	0	0	0	0	0	0
e_u	0.023672	0.19678	0.023972	0.200036	0.025945	0.222433
e_v	0.019112	1.198631	0.016221	1.194017	-0.003035	1.251958
$\|e\|$	0.298804	1.177742	0.296616	1.174114	0.30231	1.23538
$\|e_u\|$	0.086638	0.178259	0.087031	0.181698	0.09073	0.204737
$\|e_v\|$	0.264344	1.169274	0.262045	1.165019	0.266429	1.223283
r	0.298804	1.177742	0.296616	1.174114	0.30231	1.23538
$\angle$	0.166417	0.241853	0.165343	0.241128	0.165448	0.242478

Table 6.7.10: The averages and standard deviations of measures associated with the type 2B, 2B′, and 2B″ Min. D optical flow estimation. The measure r is unitless. The measure $\angle$ is in radians. All other measures are in pixels.

6.8 Rotation and Translation of a Surface with Negative Gaussian Curvature

Known Motion Field

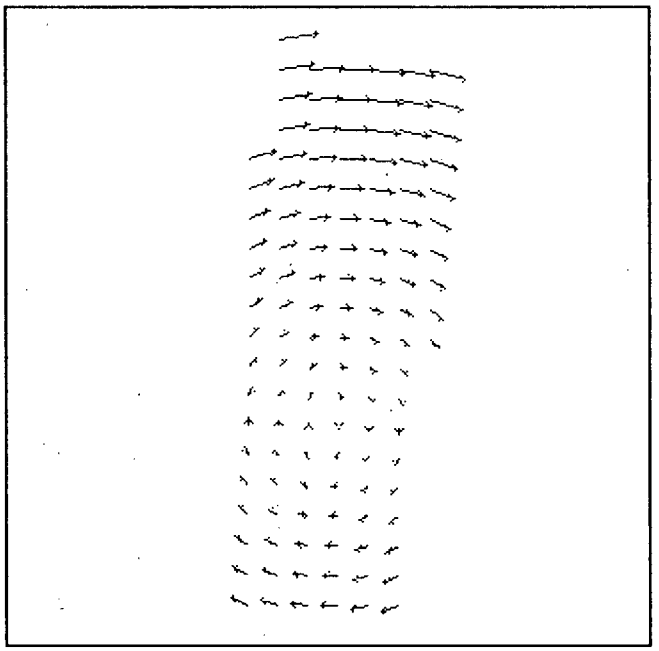

Figure 6.8.1: The known motion field for the rotating and translating surface with negative Gaussian curvature. Vectors are magnified 10 times and sampled every 20 pixels.

Measure	Average	Standard Deviation
u_k	0.5	0.828117
v_k	0	0.280359
$\|u_k\|$	0.80427	0.537506
$\|v_k\|$	0.241545	0.142319
$\|(u_k, v_k)\|$	0.873972	0.500532

Table 6.8.1: The averages and standard deviations of measures associated with the known motion field. All measures are in pixels.

Type 1 Optical Flow

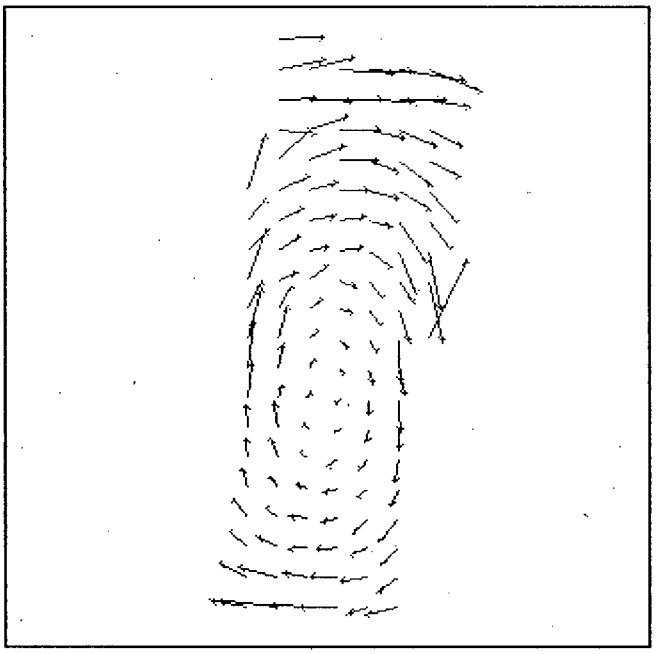

Figure 6.8.2: The type 1 optical flow estimation for the rotating and translating surface with negative Gaussian curvature. Vectors are magnified 10 times and sampled every 20 pixels.

Measure	Average	Standard Deviation
u_e	0.513119	1.252835
v_e	-0.064763	1.500357
u_k	0.5	0.828117
v_k	0	0.280359
e_u	0.013119	0.502478
e_v	-0.064763	1.360187
$\|e\|$	0.829368	1.191253
$\|e_u\|$	0.337401	0.372575
$\|e_v\|$	0.63273	1.205795
r	1.295993	1.822922
$\angle$	0.311989	0.312019

Table 6.8.2: The averages and standard deviations of measures associated with the type 1 optical flow estimation. The measure *r* is unitless. The measure $\angle$ is in radians. All other measures are in pixels.

Type 2A Min. A Optical Flow

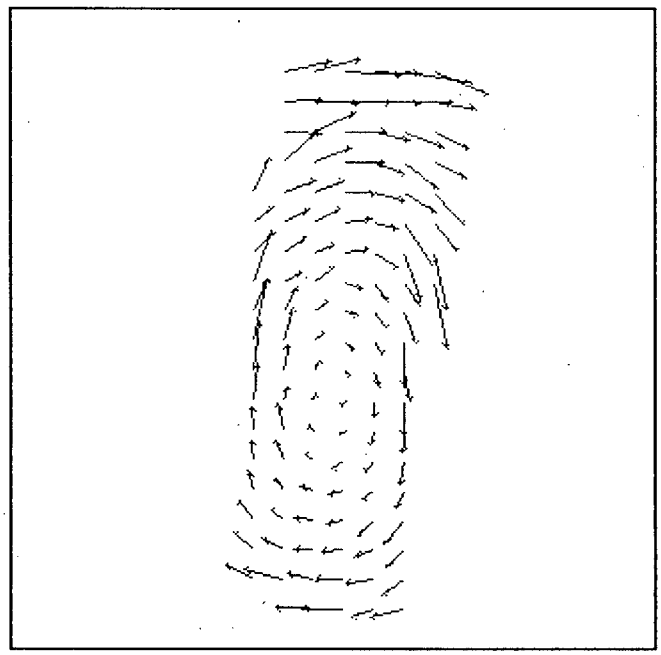

Figure 6.8.3: The type 2A Min. A optical flow estimation for the rotating and translating surface with negative Gaussian curvature. Vectors are magnified 10 times and sampled every 20 pixels.

Measure	Average	Standard Deviation
u_e	0.49656	1.223665
v_e	-0.05245	1.583047
u_k	0.5	0.828117
v_k	0	0.280359
e_u	-0.00344	0.515875
e_v	-0.05245	1.448678
$\|e\|$	0.855991	1.278597
$\|e_u\|$	0.345342	0.383241
$\|e_v\|$	0.652982	1.294225
r	1.33508	2.025876
$\angle$	0.320975	0.323646

Table 6.8.3: The averages and standard deviations of measures associated with the type 2A Min. A optical flow estimation. The measure r is unitless. The measure $\angle$ is in radians. All other measures are in pixels.

Type 2A Min. B Optical Flow

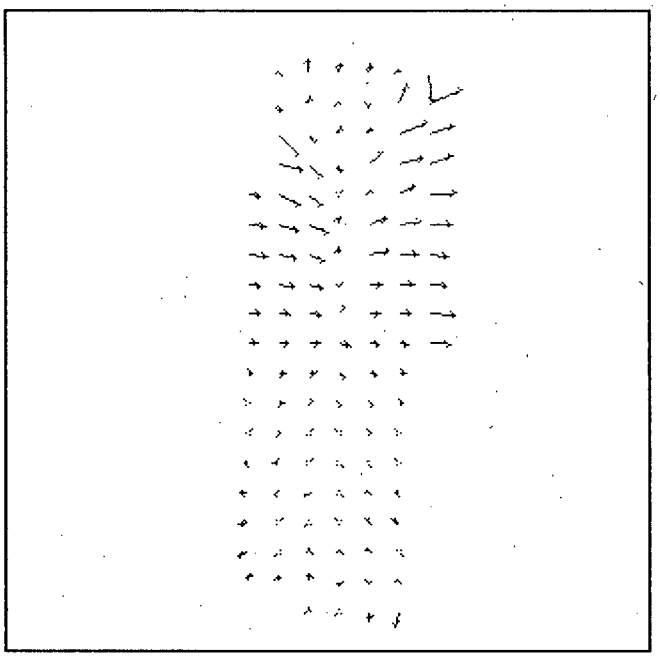

Figure 6.8.4: The type 2A Min. B optical flow estimation for the rotating and translating surface with negative Gaussian curvature. Vectors are magnified 10 times and sampled every 20 pixels.

Measure	Average	Standard Deviation
u_e	0.321193	0.527403
v_e	-0.002764	0.288226
u_k	0.5	0.828117
v_k	0	0.280359
e_u	-0.178807	0.697287
e_v	-0.002764	0.453419
$\|e\|$	0.686994	0.501798
$\|e_u\|$	0.472894	0.54272
$\|e_v\|$	0.371909	0.259375
r	0.787508	0.32358
$\angle$	0.962267	0.467942

Table 6.8.4: The averages and standard deviations of measures associated with the type 2A Min. B optical flow estimation. The measure *r* is unitless. The measure $\angle$ is in radians. All other measures are in pixels.

Type 2A Min. C Optical Flow

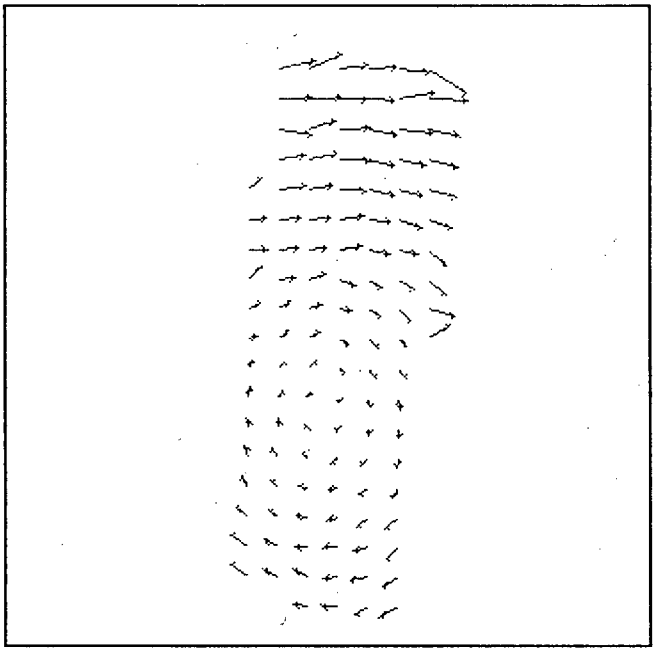

Figure 6.8.5: The type 2A Min. C optical flow estimation for the rotating and translating surface with negative Gaussian curvature. Vectors are magnified 10 times and sampled every 20 pixels.

Measure	Average	Standard Deviation
u_e	0.449203	0.863007
v_e	-0.007631	0.40771
u_k	0.5	0.828117
v_k	0	0.280359
e_u	-0.050797	0.302624
e_v	-0.007631	0.293145
$\|e\|$	0.26348	0.332761
$\|e_u\|$	0.156646	0.263861
$\|e_v\|$	0.172373	0.237232
r	0.396028	0.705978
$\angle$	0.200626	0.237431

Table 6.8.5: The averages and standard deviations of measures associated with the type 2A Min. C optical flow estimation. The measure *r* is unitless. The measure $\angle$ is in radians. All other measures are in pixels.

Type 2A Min. D Optical Flow

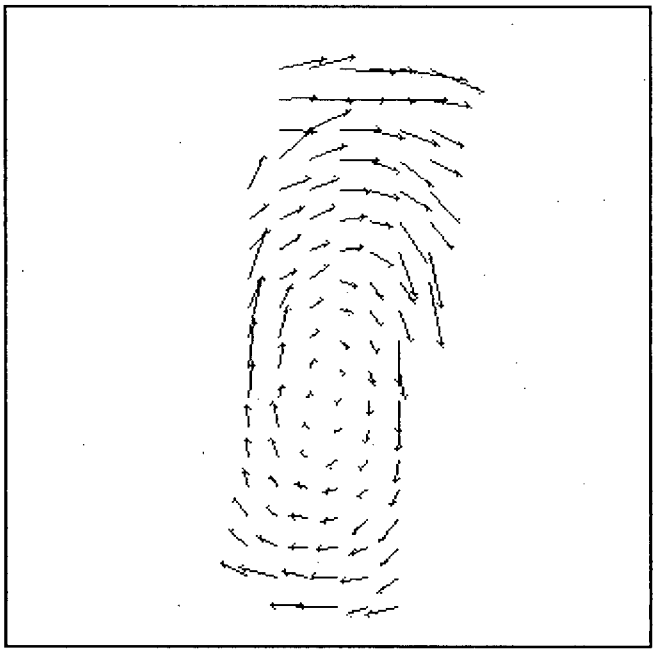

Figure 6.8.6: The type 2A Min. D optical flow estimation for the rotating and translating surface with negative Gaussian curvature. Vectors are magnified 10 times and sampled every 20 pixels.

Measure	Average	Standard Deviation
u_e	0.496559	1.223656
v_e	-0.052447	1.58304
u_k	0.5	0.828117
v_k	0	0.280359
e_u	-0.003441	0.515865
e_v	-0.052447	1.448674
$\|e\|$	0.855979	1.278596
$\|e_u\|$	0.345337	0.383231
$\|e_v\|$	0.652974	1.294224
r	1.335063	2.025853
$\angle$	0.320975	0.323646

Table 6.8.6: The averages and standard deviations of measures associated with the type 2A Min. D optical flow estimation. The measure *r* is unitless. The measure $\angle$ is in radians. All other measures are in pixels.

Type 2B, 2B′, and 2B″ Min. A Optical Flow

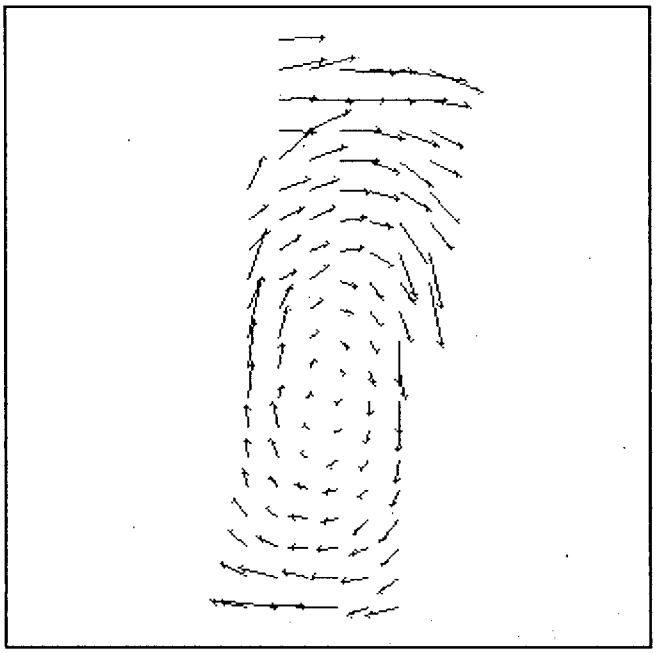

Figure 6.8.7: The type 2B Min. A optical flow estimation for the rotating and translating surface with negative Gaussian curvature. Vectors are magnified 10 times and sampled every 20 pixels.

	2B Min. A		2B′ Min. A		2B″ Min. A	
Measure	**Average**	**Standard Deviation**	**Average**	**Standard Deviation**	**Average**	**Standard Deviation**
u_e	0.508156	1.252049	0.509795	1.252176	0.513128	1.253075
v_e	-0.060525	1.603328	-0.058934	1.568129	-0.06535	1.503125
u_k	0.5	0.828117	0.5	0.828117	0.5	0.828117
v_k	0	0.280359	0	0.280359	0	0.280359
e_u	0.008156	0.500724	0.009795	0.50053	0.013128	0.502684
e_v	-0.060525	1.467881	-0.058934	1.431114	-0.06535	1.363113
$\|e\|$	0.854805	1.295535	0.844671	1.260434	0.830347	1.194031
$\|e_u\|$	0.336659	0.370739	0.336445	0.370711	0.337452	0.372808
$\|e_v\|$	0.659103	1.312976	0.648693	1.277006	0.633654	1.208642
r	1.3352	2.032264	1.319977	1.9745	1.296579	1.823741
$\angle$	0.320373	0.323518	0.317202	0.320135	0.312157	0.312289

Table 6.8.7: The averages and standard deviations of measures associated with the type 2B, 2B′, and 2B″ Min. A optical flow estimation. The measure r is unitless. The measure $\angle$ is in radians. All other measures are in pixels.

Type 2B, 2B′, and 2B″ Min. B Optical Flow

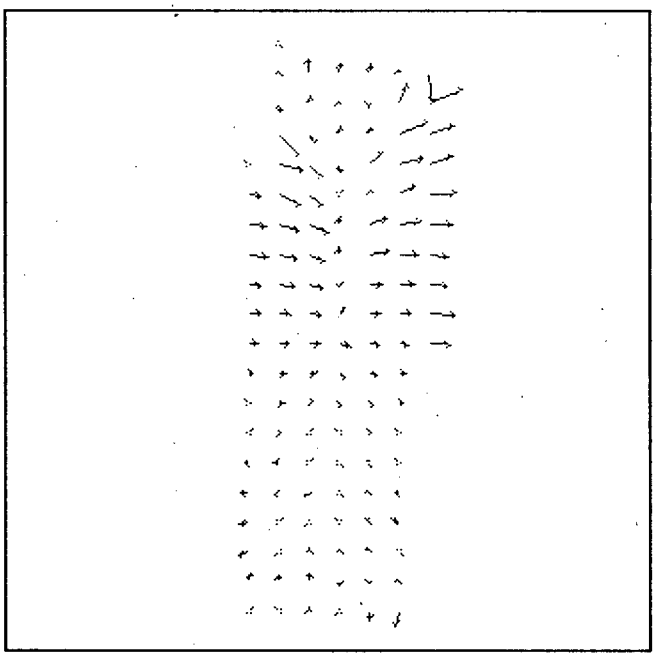

Figure 6.8.8: The type 2B Min. B optical flow estimation for the rotating and translating surface with negative Gaussian curvature. Vectors are magnified 10 times and sampled every 20 pixels.

	2B Min. B		2B′ Min. B		2B″ Min. B	
Measure	**Average**	**Standard Deviation**	**Average**	**Standard Deviation**	**Average**	**Standard Deviation**
u_e	0.320937	0.527756	0.230534	0.481639	0.007905	0.126686
v_e	-0.002787	0.288014	-0.002414	0.239796	-0.001839	0.072969
u_k	0.5	0.828117	0.5	0.828117	0.5	0.828117
v_k	0	0.280359	0	0.280359	0	0.280359
e_u	-0.179063	0.697319	-0.269466	0.712076	-0.492095	0.806567
e_v	-0.002787	0.453241	-0.002414	0.413926	-0.001839	0.287376
$\|e\|$	0.686977	0.501796	0.71983	0.482528	0.857747	0.489437
$\|e_u\|$	0.473039	0.54272	0.550749	0.525673	0.783811	0.527575
$\|e_v\|$	0.37171	0.259349	0.332621	0.246373	0.244238	0.151439
r	0.787473	0.323461	0.835815	0.214807	0.987001	0.056331
$\angle$	0.97095	0.48489	0.969691	0.483186	0.969523	0.483958

Table 6.8.8: The averages and standard deviations of measures associated with the type 2B, 2B′, and 2B″ Min. B optical flow estimation. The measure r is unitless. The measure $\angle$ is in radians. All other measures are in pixels.

Type 2B, 2B′, and 2B″ Min. C Optical Flow

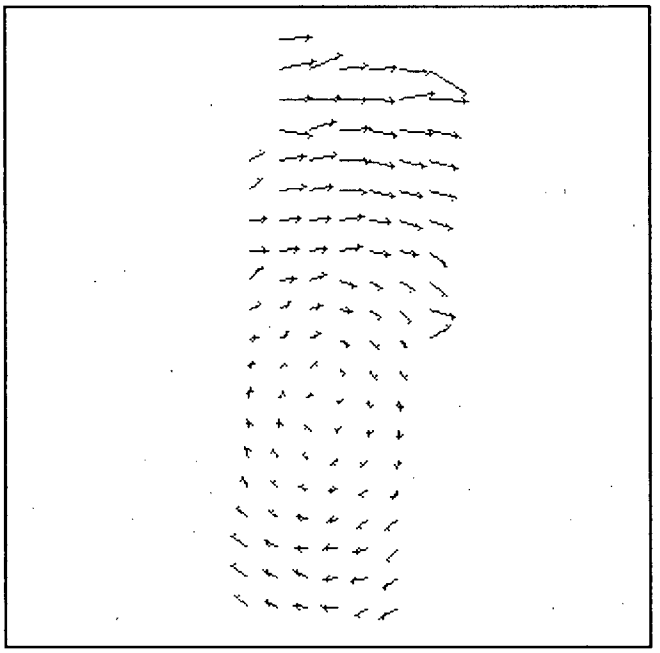

Figure 6.8.9: The type 2B Min. C optical flow estimation for the rotating and translating surface with negative Gaussian curvature. Vectors are magnified 10 times and sampled every 20 pixels.

	2B Min. C		2B′ Min. C		2B″ Min. C	
Measure	**Average**	**Standard Deviation**	**Average**	**Standard Deviation**	**Average**	**Standard Deviation**
u_e	0.456767	0.869273	0.46346	0.86489	0.468949	0.809016
v_e	-0.010012	0.41121	0.001592	0.372644	0.02336	0.308418
u_k	0.5	0.828117	0.5	0.828117	0.5	0.828117
v_k	0	0.280359	0	0.280359	0	0.280359
e_u	-0.043233	0.250047	-0.03654	0.24857	-0.031051	0.257685
e_v	-0.010012	0.291751	0.001592	0.24948	0.02336	0.183147
$\|e\|$	0.249407	0.295644	0.227504	0.271302	0.216301	0.233809
$\|e_u\|$	0.142346	0.21007	0.139035	0.209263	0.14382	0.216058
$\|e_v\|$	0.170508	0.236949	0.147312	0.201348	0.12619	0.134774
r	0.386666	0.702356	0.354518	0.65066	0.335881	0.620093
$\angle$	0.20077	0.236467	0.184561	0.238145	0.189116	0.228745

Table 6.8.9: The averages and standard deviations of measures associated with the type 2B, 2B′, and 2B″ Min. C optical flow estimation. The measure r is unitless. The measure $\angle$ is in radians. All other measures are in pixels.

Type 2B, 2B′, and 2B″ Min. D Optical Flow

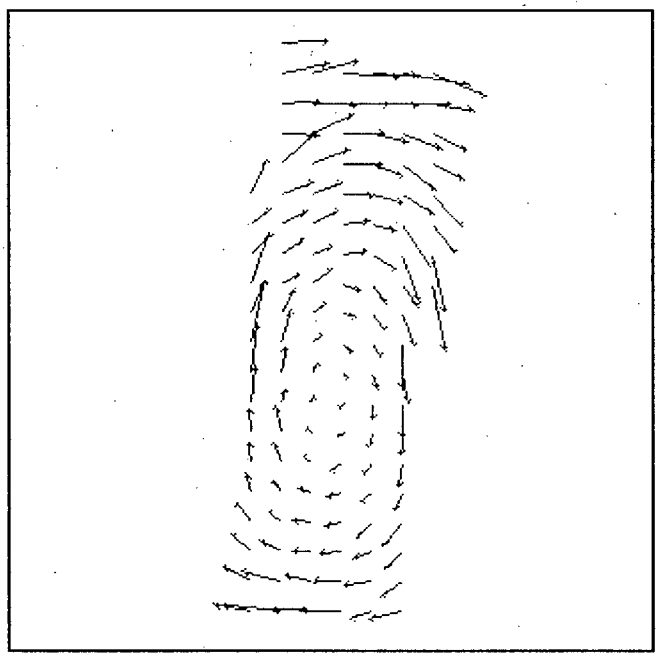

Figure 6.8.10: The type 2B Min. D optical flow estimation for the rotating and translating surface with negative Gaussian curvature. Vectors are magnified 10 times and sampled every 20 pixels.

	2B Min. D		2B′ Min. D		2B″ Min. D	
Measure	Average	Standard Deviation	Average	Standard Deviation	Average	Standard Deviation
u_e	0.508155	1.252039	0.509794	1.252167	0.513129	1.253066
v_e	-0.060522	1.603315	-0.058931	1.568119	-0.065345	1.503139
u_k	0.5	0.828117	0.5	0.828117	0.5	0.828117
v_k	0	0.280359	0	0.280359	0	0.280359
e_u	0.008155	0.500713	0.009794	0.500519	0.013129	0.502676
e_v	-0.060522	1.467869	-0.058931	1.431107	-0.065345	1.363136
$\|e\|$	0.854793	1.295526	0.844657	1.260431	0.83033	1.194065
$\|e_u\|$	0.336655	0.370729	0.33644	0.370702	0.337446	0.372802
$\|e_v\|$	0.659094	1.312967	0.648683	1.277003	0.633641	1.208674
r	1.335183	2.032226	1.319958	1.974473	1.296556	1.823716
$\angle$	0.320373	0.323518	0.317201	0.320134	0.312152	0.312288

Table 6.8.10: The averages and standard deviations of measures associated with the type 2B, 2B′, and 2B″ Min. D optical flow estimation. The measure r is unitless. The measure $\angle$ is in radians. All other measures are in pixels.

6.9 Rotation of a Surface With Positive Gaussian Curvature

Known Motion Field

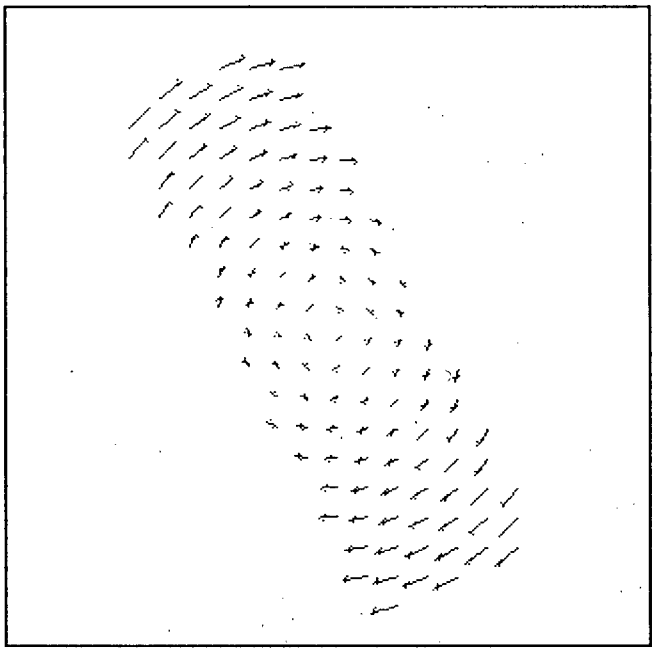

Figure 6.9.1: The known motion field for the rotating surface with positive Gaussian curvature. Vectors are magnified 10 times and sampled every 20 pixels.

Measure	Average	Standard Deviation
u_k	0	0.732816
v_k	0	0.468766
$\|u_k\|$	0.631154	0.372356
$\|v_k\|$	0.390208	0.259756
$\|(u_k, v_k)\|$	0.784106	0.376717

Table 6.9.1: The averages and standard deviations of measures associated with the known motion field. All measures are in pixels.

Type 1 Optical Flow Estimation

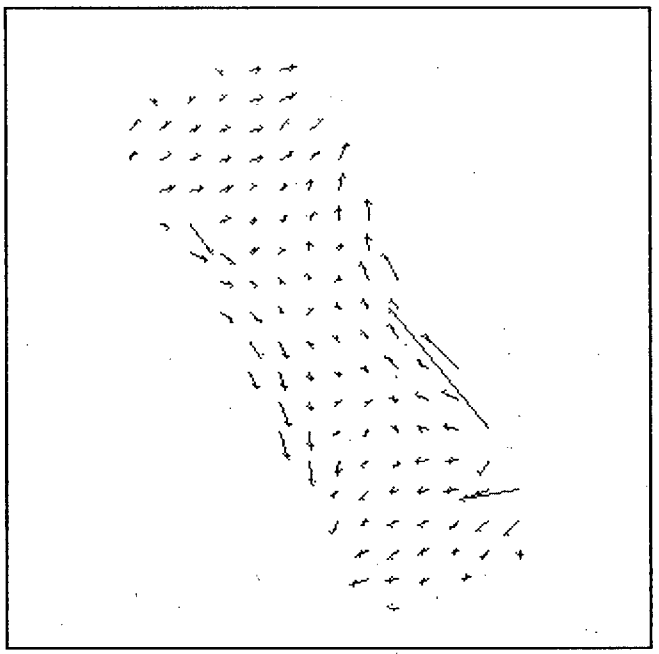

Figure 6.9.2: The type 1 optical flow estimation for the rotating surface with positive Gaussian curvature. Vectors are magnified 20 times and sampled every 20 pixels.

Measure	Average	Standard Deviation
u_e	-0.041499	0.655506
v_e	-0.049725	0.77928
u_k	0	0.732816
v_k	0	0.468766
e_u	-0.041499	0.608952
e_v	-0.049725	0.902984
$\|e\|$	0.754114	0.788472
$\|e_u\|$	0.435246	0.4279
$\|e_v\|$	0.562232	0.708334
r	1.25925	1.490273
$\angle$	0.986764	0.876978

Table 6.9.2: The averages and standard deviations of measures associated with the type 1 optical flow estimation. The measure *r* is unitless. The measure $\angle$ is in radians. All other measures are in pixels.

Type 2A Min. A Optical Flow Estimation

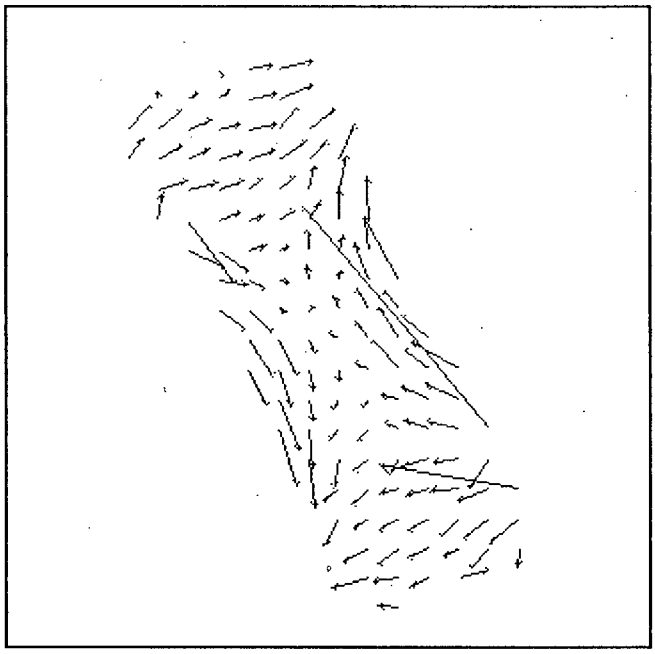

Figure 6.9.3: The type 2A Min. A optical flow estimation for the rotating surface with positive Gaussian curvature. Vectors are magnified 20 times and sampled every 20 pixels.

Measure	Average	Standard Deviation
u_e	-0.03137	0.609187
v_e	-0.033372	0.72762
u_k	0	0.732816
v_k	0	0.468766
e_u	-0.03137	0.574276
e_v	-0.033372	0.847721
$\|e\|$	0.752568	0.695803
$\|e_u\|$	0.433163	0.378338
$\|e_v\|$	0.561019	0.636389
r	1.264576	1.381854
$\angle$	0.986883	0.878407

Table 6.9.3: The averages and standard deviations of measures associated with the type 2A Min. A optical flow estimation. The measure *r* is unitless. The measure $\angle$ is in radians. All other measures are in pixels.

Type 2A Min. B Optical Flow Estimation

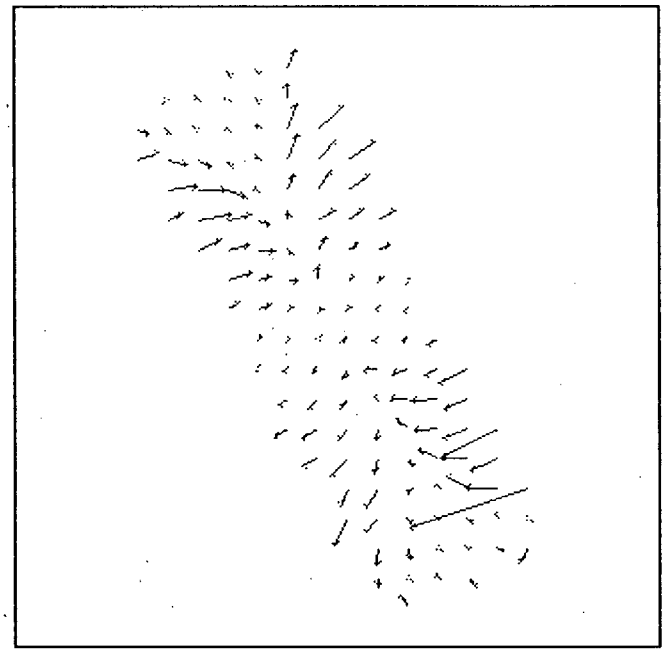

Figure 6.9.4: The type 2A Min. B optical flow estimation for the rotating surface with positive Gaussian curvature. Vectors are magnified 20 times and sampled every 20 pixels.

Measure	Average	Standard Deviation
u_e	-0.017124	0.3845
v_e	-0.004853	0.254874
u_k	0	0.732816
v_k	0	0.468766
e_u	-0.017124	0.616834
e_v	-0.004853	0.475946
$\|e\|$	0.671933	0.394735
$\|e_u\|$	0.46289	0.408047
$\|e_v\|$	0.407473	0.245983
r	0.837352	0.178655
$\angle$	1.037083	0.356841

Table 6.9.4: The averages and standard deviations of measures associated with the type 2A Min. B optical flow estimation. The measure r is unitless. The measure $\angle$ is in radians. All other measures are in pixels.

Type 2A Min. C Optical Flow Estimation

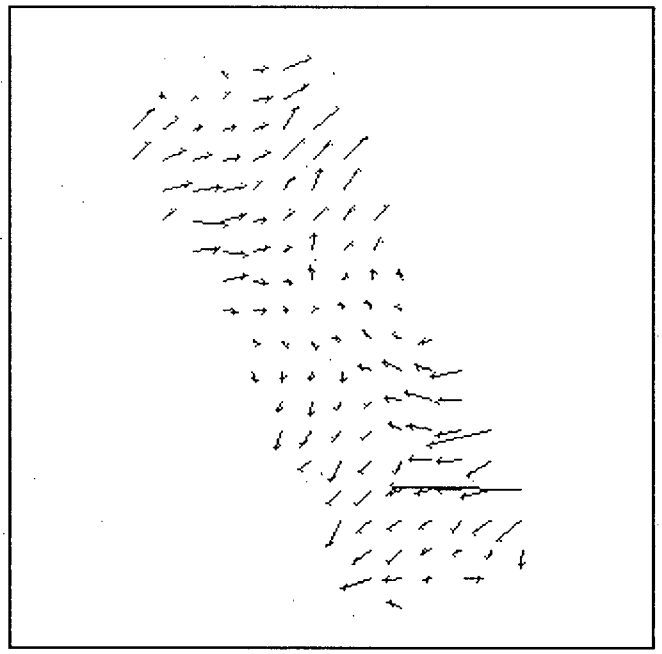

Figure 6.9.5: The type 2A Min. C optical flow estimation for the rotating surface with positive Gaussian curvature. Vectors are magnified 20 times and sampled every 20 pixels.

Measure	Average	Standard Deviation
u_e	-0.023736	0.453832
v_e	-0.015198	0.304343
u_k	0	0.732816
v_k	0	0.468766
e_u	-0.023736	0.490333
e_v	-0.015198	0.460246
$\|e\|$	0.609	0.286621
$\|e_u\|$	0.389686	0.298544
$\|e_v\|$	0.406519	0.216317
r	0.88026	0.418327
$\angle$	0.876148	0.694527

Table 6.9.5: The averages and standard deviations of measures associated with the type 2A Min. C optical flow estimation. The measure *r* is unitless. The measure $\angle$ is in radians. All other measures are in pixels.

Type 2A Min. D Optical Flow Estimation

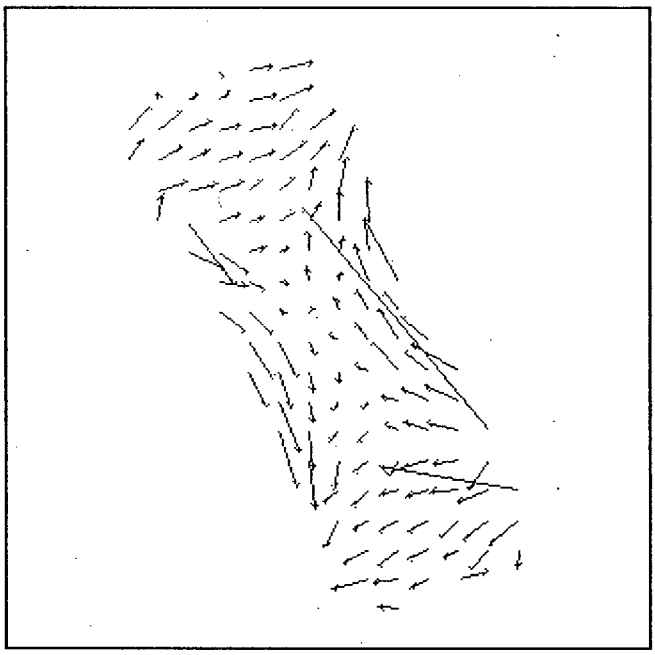

Figure 6.9.6: The type 2A Min. D optical flow estimation for the rotating surface with positive Gaussian curvature. Vectors are magnified 20 times and sampled every 20 pixels.

Measure	Average	Standard Deviation
u_e	-0.031369	0.609194
v_e	-0.033371	0.727648
u_k	0	0.732816
v_k	0	0.468766
e_u	-0.031369	0.574285
e_v	-0.033371	0.847745
$\|e\|$	0.752569	0.695839
$\|e_u\|$	0.433163	0.378352
$\|e_v\|$	0.561019	0.636421
r	1.264574	1.381895
$\angle$	0.986882	0.878406

Table 6.9.6: The averages and standard deviations of measures associated with the type 2A Min. D optical flow estimation. The measure *r* is unitless. The measure $\angle$ is in radians. All other measures are in pixels.

Type 2B, 2B′, and 2B″ Min. A Optical Flow Estimation

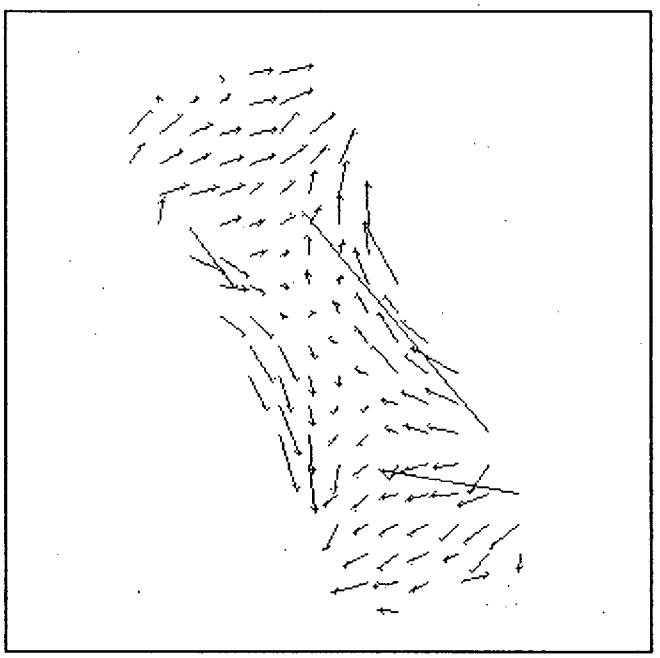

Figure 6.9.7: The type 2B Min. A optical flow estimation for the rotating surface with positive Gaussian curvature. Vectors are magnified 20 times and sampled every 20 pixels.

	2B Min. A		2B′ Min. A		2B″ Min. A	
Measure	**Average**	**Standard Deviation**	**Average**	**Standard Deviation**	**Average**	**Standard Deviation**
u_e	-0.034119	0.618244	-0.034284	0.619814	-0.041133	0.653982
v_e	-0.034848	0.734132	-0.036499	0.734301	-0.04907	0.778102
u_k	0	0.732816	0	0.732816	0	0.732816
v_k	0	0.468766	0	0.468766	0	0.468766
e_u	-0.034119	0.575265	-0.034284	0.576482	-0.041133	0.607585
e_v	-0.034848	0.852512	-0.036499	0.853057	-0.04907	0.901227
$\|e\|$	0.752741	0.702456	0.749403	0.707757	0.75331	0.786112
$\|e_u\|$	0.432005	0.381391	0.430673	0.384735	0.434779	0.426394
$\|e_v\|$	0.56265	0.641409	0.55952	0.644953	0.561541	0.706596
r	1.265056	1.384341	1.257897	1.39099	1.258519	1.488815
$\angle$	0.986302	0.877607	0.985243	0.87738	0.986416	0.876944

Table 6.9.7: The averages and standard deviations of measures associated with the type 2B, 2B′, and 2B″ Min. A optical flow estimation. The measure r is unitless. The measure $\angle$ is in radians. All other measures are in pixels.

Type 2B, 2B′, and 2B″ Min. B Optical Flow Estimation

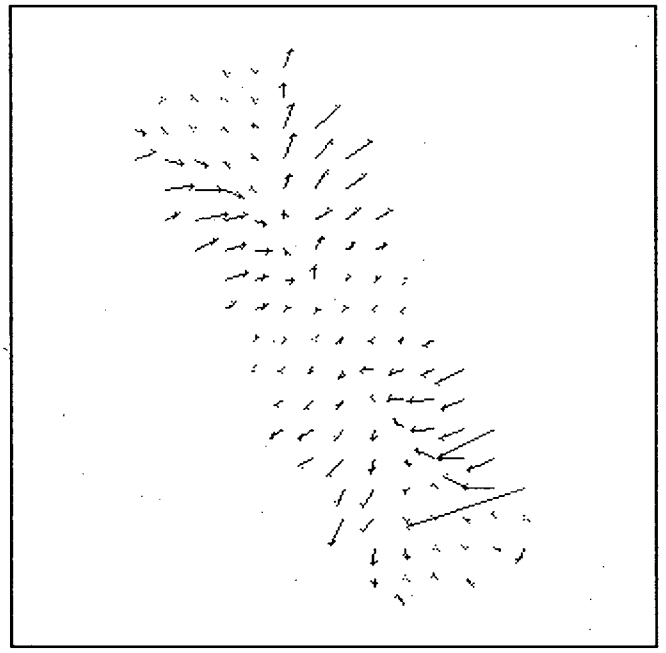

Figure 6.9.8: The type 2B Min. B optical flow estimation for the rotating surface with positive Gaussian curvature. Vectors are magnified 20 times and sampled every 20 pixels.

	2B Min. B		2B′ Min. B		2B″ Min. B	
Measure	Average	Standard Deviation	Average	Standard Deviation	Average	Standard Deviation
u_e	-0.017073	0.384558	-0.014975	0.341235	-0.008858	0.120254
v_e	-0.004904	0.254803	-0.001787	0.215919	0.003439	0.063951
u_k	0	0.732816	0	0.732816	0	0.732816
v_k	0	0.468766	0	0.468766	0	0.468766
e_u	-0.017073	0.616772	-0.014975	0.632305	-0.008858	0.726078
e_v	-0.004904	0.475876	-0.001787	0.463655	0.003439	0.459389
$\|e\|$	0.671855	0.394686	0.683304	0.384828	0.774848	0.371358
$\|e_u\|$	0.462847	0.408001	0.493397	0.395708	0.624157	0.371055
$\|e_v\|$	0.407402	0.245967	0.390987	0.249204	0.383592	0.252788
r	0.837169	0.177333	0.864187	0.149412	0.991242	0.041432
$\angle$	1.041031	0.368464	1.041566	0.368379	1.04158	0.368559

Table 6.9.8: The averages and standard deviations of measures associated with the type 2B, 2B′, and 2B″ Min. B optical flow estimation. The measure r is unitless. The measure $\angle$ is in radians. All other measures are in pixels.

Type 2B, 2B′, and 2B″ Min. C Optical Flow Estimation

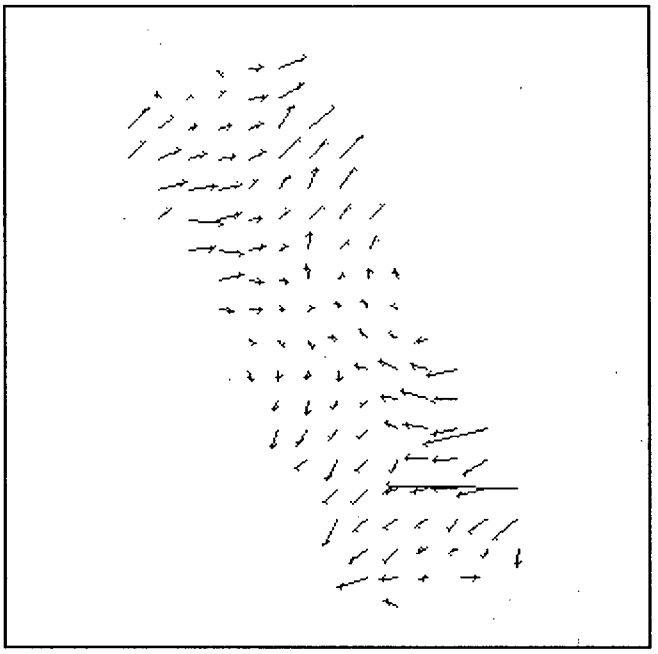

Figure 6.9.9: The type 2B Min. C optical flow estimation for the rotating surface with positive Gaussian curvature. Vectors are magnified 20 times and sampled every 20 pixels.

	2B Min. C		2B′ Min. C		2B″ Min. C	
Measure	**Average**	**Standard Deviation**	**Average**	**Standard Deviation**	**Average**	**Standard Deviation**
u_e	-0.026647	0.459427	-0.022188	0.439344	-0.024229	0.411696
v_e	-0.014404	0.307725	-0.013404	0.282412	-0.015622	0.24474
u_k	0	0.732816	0	0.732816	0	0.732816
v_k	0	0.468766	0	0.468766	0	0.468766
e_u	-0.026647	0.485939	-0.022188	0.485339	-0.024229	0.498795
e_v	-0.014404	0.458205	-0.013404	0.433852	-0.015622	0.411448
$\|e\|$	0.605692	0.283071	0.585675	0.285352	0.579586	0.288072
$\|e_u\|$	0.386608	0.295593	0.383176	0.298693	0.391427	0.310102
$\|e_v\|$	0.405271	0.214264	0.380002	0.209763	0.361834	0.196482
r	0.877475	0.418385	0.835206	0.386688	0.815678	0.358595
$\angle$	0.87495	0.693722	0.829868	0.698959	0.792386	0.683293

Table 6.9.9: The averages and standard deviations of measures associated with the type 2B, 2B′, and 2B″ Min. C optical flow estimation. The measure r is unitless. The measure $\angle$ is in radians. All other measures are in pixels.

Type 2B, 2B′, and 2B″ Min. D Optical Flow Estimation

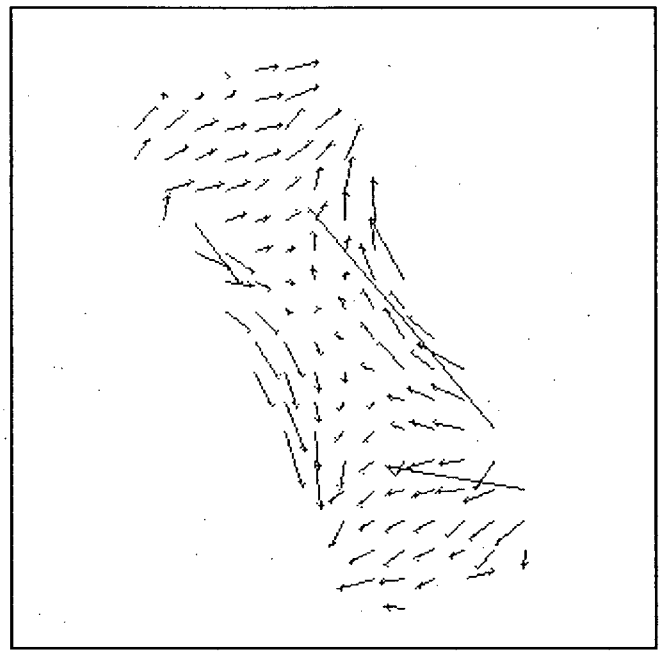

Figure 6.9.10: The type 2B Min. D optical flow estimation for the rotating surface with positive Gaussian curvature. Vectors are magnified 20 times and sampled every 20 pixels.

	2B Min. D		2B′ Min. D		2B″ Min. D	
Measure	**Average**	**Standard Deviation**	**Average**	**Standard Deviation**	**Average**	**Standard Deviation**
u_e	-0.034118	0.618236	-0.034283	0.619824	-0.041139	0.654038
v_e	-0.034846	0.734097	-0.036498	0.734338	-0.049079	0.778224
u_k	0	0.732816	0	0.732816	0	0.732816
v_k	0	0.468766	0	0.468766	0	0.468766
e_u	-0.034118	0.575259	-0.034283	0.576495	-0.041139	0.607644
e_v	-0.034846	0.852482	-0.036498	0.853088	-0.049079	0.901342
$\|e\|$	0.752741	0.702416	0.749403	0.707804	0.753325	0.786276
$\|e_u\|$	0.432004	0.381382	0.430673	0.384754	0.434787	0.426471
$\|e_v\|$	0.562649	0.641369	0.559519	0.644994	0.561553	0.706734
r	1.265052	1.384237	1.257895	1.391045	1.25853	1.48899
$\angle$	0.986302	0.877606	0.985242	0.877379	0.98642	0.876943

Table 6.9.10: The averages and standard deviations of measures associated with the type 2B, 2B′, and 2B″ Min. D optical flow estimation. The measure r is unitless. The measure $\angle$ is in radians. All other measures are in pixels

6.10 Translation of a Surface With Positive Gaussian Curvature

Known Motion Field

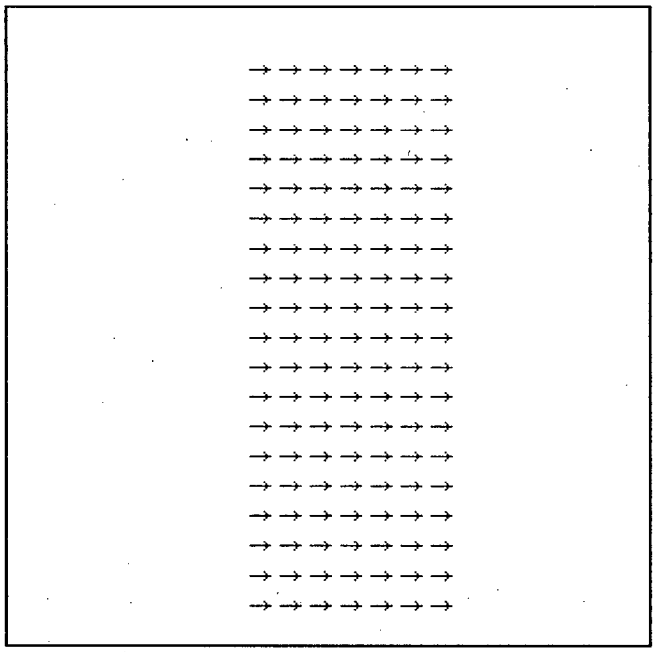

Figure 6.10.1: The known motion field for the translating surface with positive Gaussian curvature. Vectors are magnified 10 times and sampled every 20 pixels.

Measure	Average	Standard Deviation
u_k	1.000000	0.000000
v_k	0.000000	0.000000
$\|u_k\|$	1.000000	0.000000
$\|v_k\|$	0.000000	0.000000
$\|(u_k, v_k)\|$	1.000000	0.000000

Table 6.10.1: The averages and standard deviations of measures associated with the known motion field. All measures are in pixels.

Type 1 Optical Flow

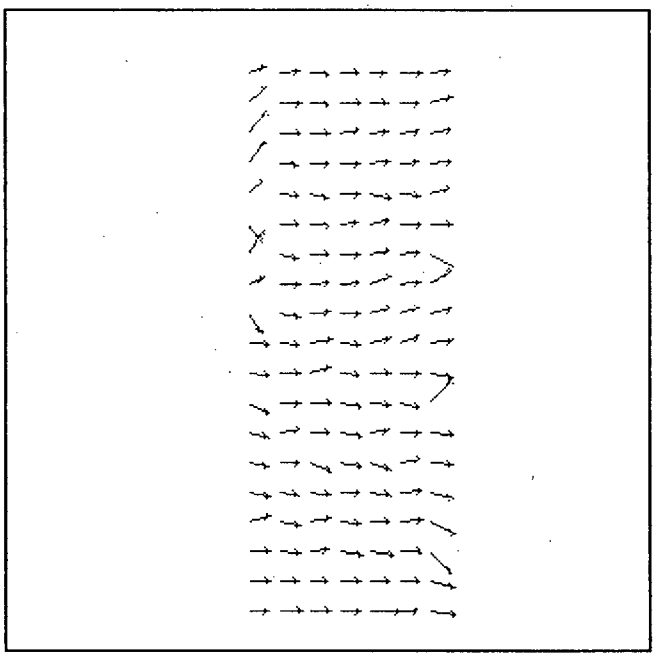

Figure 6.10.2: The type 1 optical flow estimation for the translating surface with positive Gaussian curvature. Vectors are magnified 10 times and sampled every 20 pixels.

Measure	Average	Standard Deviation
u_e	1.025517	0.227234
v_e	0.006833	1.366753
u_k	1	0
v_k	0	0
e_u	0.025517	0.227234
e_v	0.006833	1.366753
$\|e\|$	0.295394	1.353915
$\|e_u\|$	0.090913	0.209812
$\|e_v\|$	0.259299	1.341947
r	0.295394	1.353915
$\angle$	0.165197	0.241831

Table 6.10.2: The averages and standard deviations of measures associated with the type 1 optical flow estimation. The measure *r* is unitless. The measure $\angle$ is in radians. All other measures are in pixels.

Type 2A Min. A Optical Flow

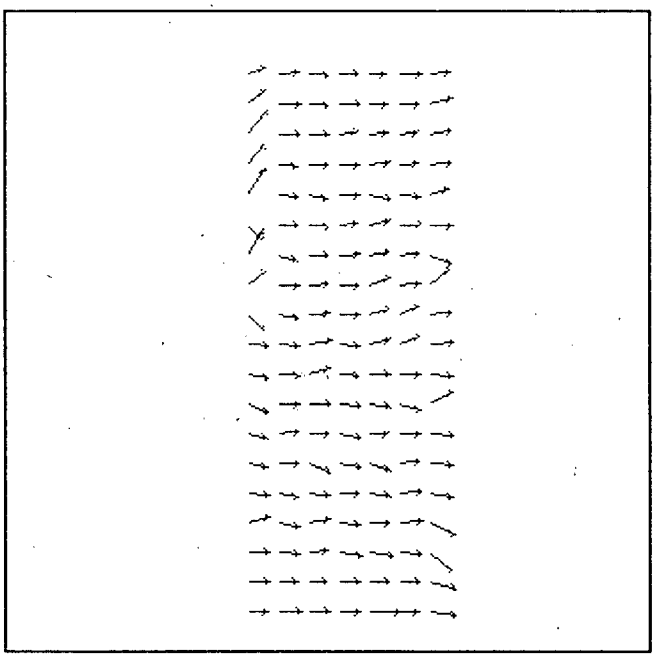

Figure 6.10.3: The type 2A Min. A optical flow estimation for the translating surface with positive Gaussian curvature. Vectors are magnified 10 times and sampled every 20 pixels.

Measure	Average	Standard Deviation
u_e	1.015957	0.225237
v_e	-0.013608	1.301582
u_k	1	0
v_k	0	0
e_u	0.015957	0.225237
e_v	-0.013608	1.301582
$\|e\|$	0.308788	1.284498
$\|e_u\|$	0.094621	0.20502
$\|e_v\|$	0.266682	1.27404
r	0.308788	1.284498
$\angle$	0.16787	0.245508

Table 6.10.3: The averages and standard deviations of measures associated with the type 2A Min. A optical flow estimation. The measure *r* is unitless. The measure $\angle$ is in radians. All other measures are in pixels.

Type 2A Min. B Optical Flow

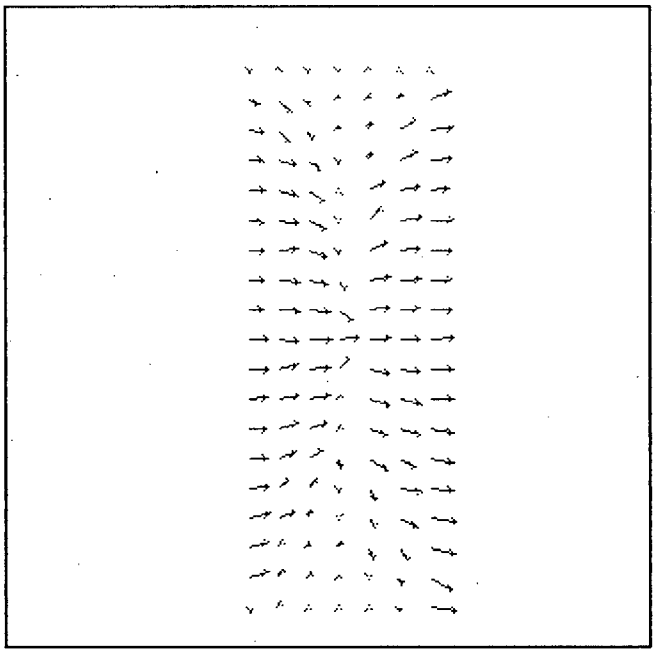

Figure 6.10.4: The type 2A Min. B optical flow estimation for the translating surface with positive Gaussian curvature. Vectors are magnified 10 times and sampled every 20 pixels.

Measure	Average	Standard Deviation
u_e	0.644317	0.458264
v_e	0.004278	0.295703
u_k	1	0
v_k	0	0
e_u	-0.355683	0.458264
e_v	0.004278	0.295703
$\|e\|$	0.525498	0.384477
$\|e_u\|$	0.415829	0.404476
$\|e_v\|$	0.228316	0.187959
r	0.525498	0.384477
$\angle$	0.607421	0.546064

Table 6.10.4: The averages and standard deviations of measures associated with the type 2A Min. B optical flow estimation. The measure r is unitless. The measure $\angle$ is in radians. All other measures are in pixels.

Type 2A Min. C Optical Flow

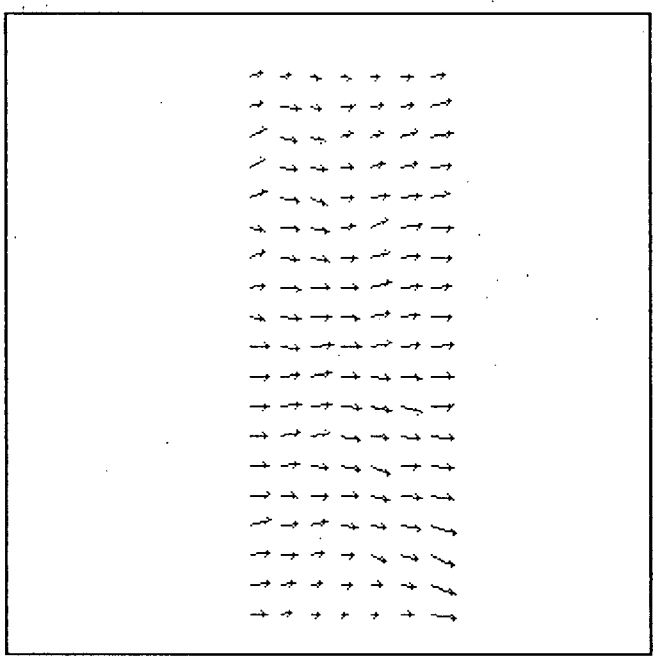

Figure 6.10.5: The type 2A Min. C optical flow estimation for the translating surface with positive Gaussian curvature. Vectors are magnified 10 times and sampled every 20 pixels.

Measure	Average	Standard Deviation
u_e	0.886484	0.269735
v_e	-0.003978	0.248934
u_k	1	0
v_k	0	0
e_u	-0.113516	0.269735
e_v	-0.003978	0.248934
$\|e\|$	0.25546	0.286993
$\|e_u\|$	0.177741	0.232487
$\|e_v\|$	0.136184	0.208416
r	0.25546	0.286993
$\angle$	0.143571	0.144375

Table 6.10.5: The averages and standard deviations of measures associated with the type 2A Min. C optical flow estimation. The measure *r* is unitless. The measure $\angle$ is in radians. All other measures are in pixels.

Type 2A Min. D Optical Flow

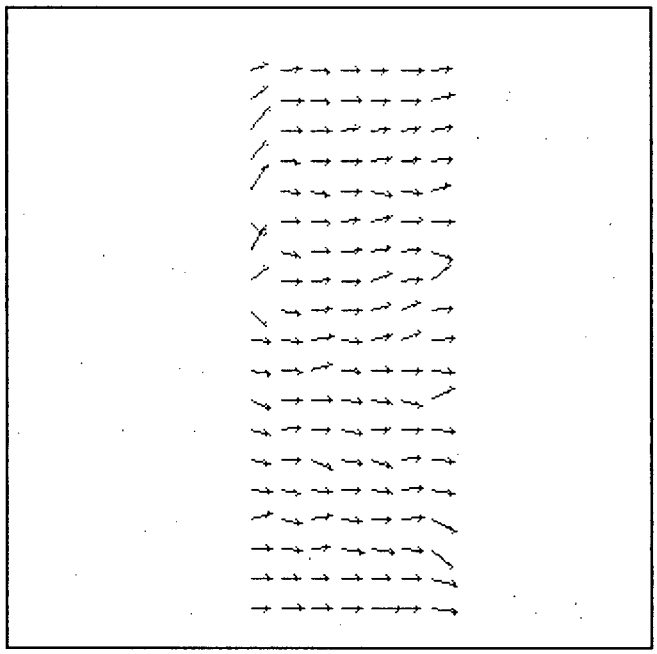

Figure 6.10.6: The type 2A Min. D optical flow estimation for the translating surface with positive Gaussian curvature. Vectors are magnified 10 times and sampled every 20 pixels.

Measure	Average	Standard Deviation
u_e	1.015957	0.22524
v_e	-0.013604	1.301629
u_k	1	0
v_k	0	0
e_u	0.015957	0.22524
e_v	-0.013604	1.301629
$\|e\|$	0.308792	1.284544
$\|e_u\|$	0.094621	0.205023
$\|e_v\|$	0.266685	1.274087
r	0.308792	1.284544
$\angle$	0.167869	0.245507

Table 6.10.6: The averages and standard deviations of measures associated with the type 2A Min. D optical flow estimation. The measure r is unitless. The measure $\angle$ is in radians. All other measures are in pixels.

Type 2B, 2B′, and 2B″ Min. A Optical Flow

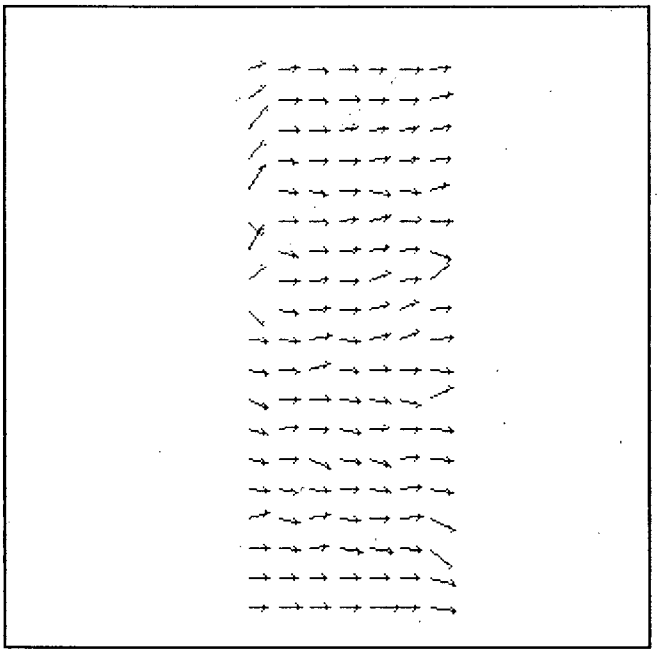

Figure 6.10.7: The type 2B Min. A optical flow estimation for the translating surface with positive Gaussian curvature. Vectors are magnified 10 times and sampled every 20 pixels.

	2B Min. A		2B′ Min. A		2B″ Min. A	
Measure	Average	Standard Deviation	Average	Standard Deviation	Average	Standard Deviation
u_e	1.024111	0.205278	1.024233	0.207827	1.025478	0.226717
v_e	-0.013479	1.301753	-0.01136	1.303557	0.006757	1.365383
u_k	1	0	1	0	1	0
v_k	0	0	0	0	0	0
e_u	0.024111	0.205278	0.024233	0.207827	0.025478	0.226717
e_v	-0.013479	1.301753	-0.01136	1.303557	0.006757	1.365383
$\|e\|$	0.301854	1.283099	0.298837	1.286025	0.295243	1.352477
$\|e_u\|$	0.087338	0.187329	0.087551	0.190036	0.090824	0.209286
$\|e_v\|$	0.267532	1.274035	0.264303	1.276531	0.259288	1.340554
r	0.301854	1.283099	0.298837	1.286025	0.295243	1.352477
$\angle$	0.167584	0.245748	0.166093	0.244278	0.165339	0.242044

Table 6.10.7: The averages and standard deviations of measures associated with the type 2B, 2B′, and 2B″ Min. A optical flow estimation. The measure r is unitless. The measure $\angle$ is in radians. All other measures are in pixels.

Type 2B, 2B′, and 2B″ Min. B Optical Flow

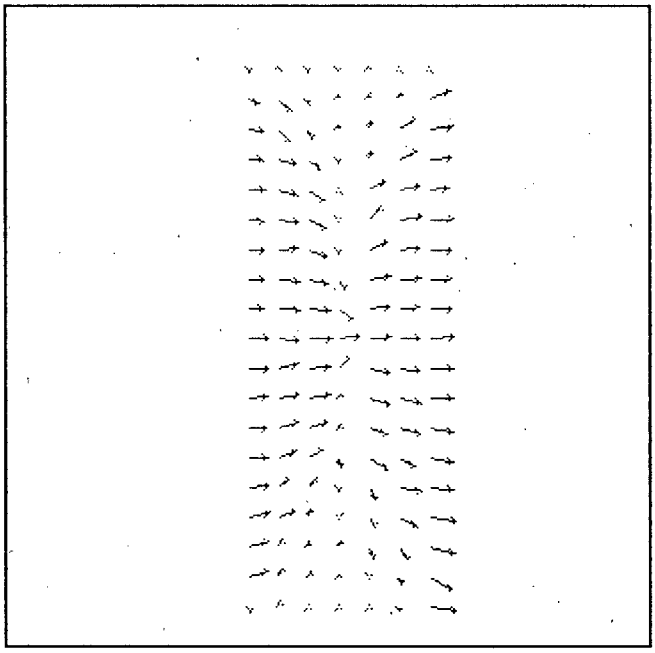

Figure 6.10.8: The type 2B Min. B optical flow estimation for the translating surface with positive Gaussian curvature. Vectors are magnified 10 times and sampled every 20 pixels.

	2B Min. B		2B′ Min. B		2B″ Min. B	
Measure	**Average**	**Standard Deviation**	**Average**	**Standard Deviation**	**Average**	**Standard Deviation**
u_e	0.644237	0.458205	0.464752	0.431849	0.02266	0.090479
v_e	0.004116	0.295361	0.003403	0.214856	0.001088	0.045915
u_k	1	0	1	0	1	0
v_k	0	0	0	0	0	0
e_u	-0.355763	0.458205	-0.535248	0.431849	-0.97734	0.090479
e_v	0.004116	0.295361	0.003403	0.214856	0.001088	0.045915
$\|e\|$	0.52528	0.384512	0.62606	0.356657	0.980031	0.070918
$\|e_u\|$	0.415866	0.404441	0.579204	0.370816	0.978921	0.071369
$\|e_v\|$	0.228009	0.18779	0.150215	0.153653	0.008067	0.045214
r	0.52528	0.384512	0.62606	0.356657	0.980031	0.070918
$\angle$	0.615197	0.555658	0.61643	0.55666	0.614235	0.555405

Table 6.10.8: The averages and standard deviations of measures associated with the type 2B, 2B′, and 2B″ Min. B optical flow estimation. The measure r is unitless. The measure $\angle$ is in radians. All other measures are in pixels.

Type 2B, 2B′, and 2B″ Min. C Optical Flow

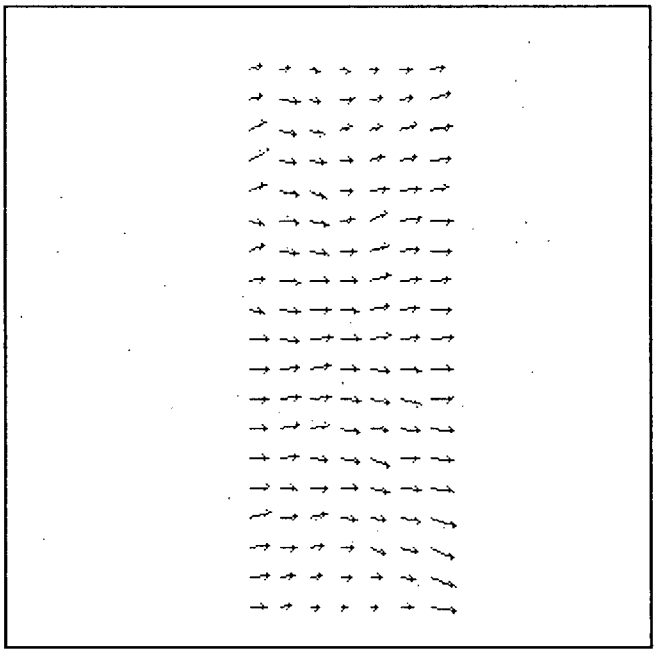

Figure 6.10.9: The type 2B Min. C optical flow estimation for the translating surface with positive Gaussian curvature. Vectors are magnified 10 times and sampled every 20 pixels.

	2B Min. C		2B′ Min. C		2B″ Min. C	
Measure	Average	Standard Deviation	Average	Standard Deviation	Average	Standard Deviation
u_e	0.889569	0.261477	0.855194	0.254277	0.808671	0.262887
v_e	-0.004228	0.249166	-0.008183	0.221797	-0.011086	0.160312
u_k	1	0	1	0	1	0
v_k	0	0	0	0	0	0
e_u	-0.110431	0.261477	-0.144806	0.254277	-0.191329	0.262887
e_v	-0.004228	0.249166	-0.008183	0.221797	-0.011086	0.160312
$\|e\|$	0.252315	0.281073	0.243787	0.274687	0.264394	0.248261
$\|e_u\|$	0.174575	0.223804	0.193088	0.219868	0.233625	0.22613
$\|e_v\|$	0.136806	0.208291	0.109119	0.19327	0.085334	0.136164
r	0.252315	0.281073	0.243787	0.274687	0.264394	0.248261
$\angle$	0.144089	0.145502	0.119124	0.135191	0.100342	0.107289

Table 6.10.9: The averages and standard deviations of measures associated with the type 2B, 2B′, and 2B″ Min. C optical flow estimation. The measure r is unitless. The measure $\angle$ is in radians. All other measures are in pixels.

Type 2B, 2B′, and 2B″ Min. D Optical Flow

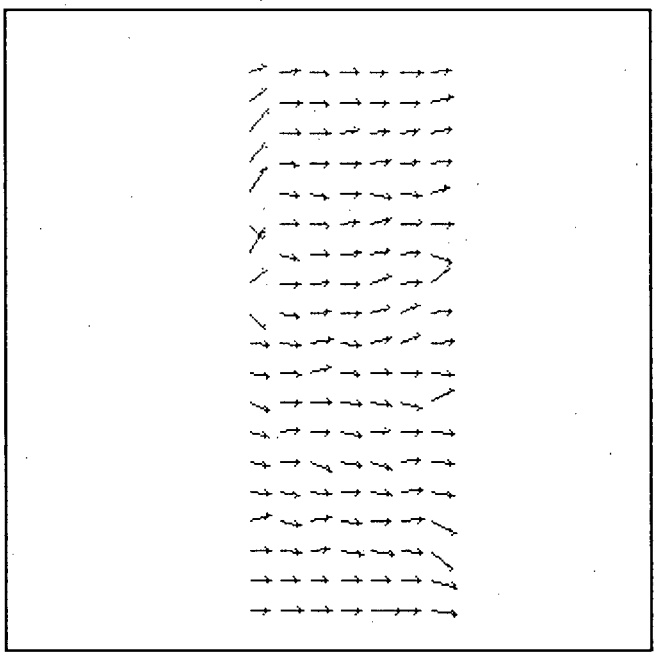

Figure 6.10.10: The type 2B Min. D optical flow estimation for the translating surface with positive Gaussian curvature. Vectors are magnified 10 times and sampled every 20 pixels.

	2B Min. D		2B′ Min. D		2B″ Min. D	
Measure	**Average**	**Standard Deviation**	**Average**	**Standard Deviation**	**Average**	**Standard Deviation**
u_e	1.024111	0.205281	1.024233	0.20783	1.025479	0.226738
v_e	-0.013475	1.301802	-0.011356	1.303614	0.006772	1.365593
u_k	1	0	1	0	1	0
v_k	0	0	0	0	0	0
e_u	0.024111	0.205281	0.024233	0.20783	0.025479	0.226738
e_v	-0.013475	1.301802	-0.011356	1.303614	0.006772	1.365593
$\|e\|$	0.301858	1.283148	0.298841	1.286083	0.29526	1.352689
$\|e_u\|$	0.087339	0.187333	0.087551	0.19004	0.090827	0.209307
$\|e_v\|$	0.267535	1.274085	0.264306	1.276589	0.259302	1.340765
r	0.301858	1.283148	0.298841	1.286083	0.29526	1.352689
$\angle$	0.167582	0.245747	0.166092	0.244277	0.165339	0.242045

Table 6.10.10: The averages and standard deviations of measures associated with the type 2B, 2B′, and 2B″ Min. D optical flow estimation. The measure r is unitless. The measure $\angle$ is in radians. All other measures are in pixels.

6.11 Rotation and Translation of a Surface with Positive Gaussian Curvature

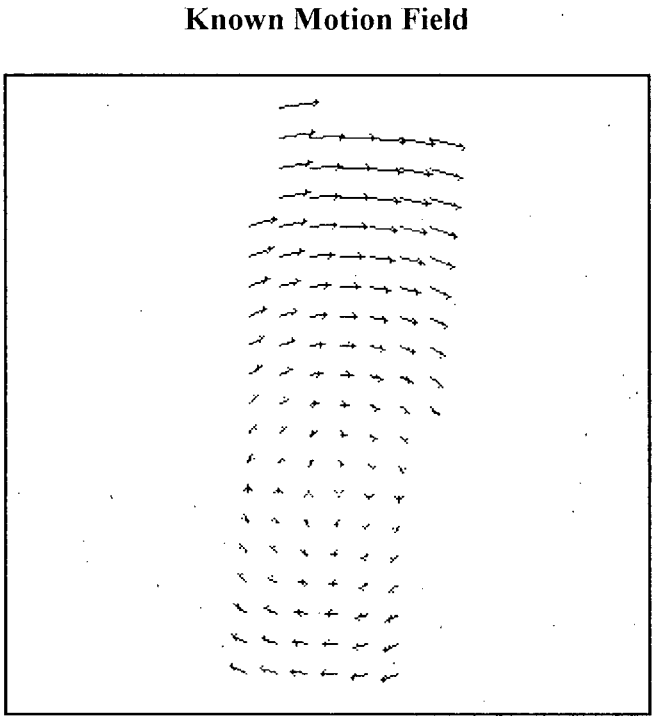

Figure 6.11.1: The known motion field for the rotating and translating surface with positive Gaussian curvature. Vectors are magnified 10 times and sampled every 20 pixels.

Measure	Average	Standard Deviation
u_k	0.5	0.828117
v_k	0	0.280359
$\|u_k\|$	0.80427	0.537506
$\|v_k\|$	0.241545	0.142319
$\|(u_k, v_k)\|$	0.873972	0.500532

Table 6.11.1: The averages and standard deviations of measures associated with the known motion field. All measures are in pixels.

Type 1 Optical Flow

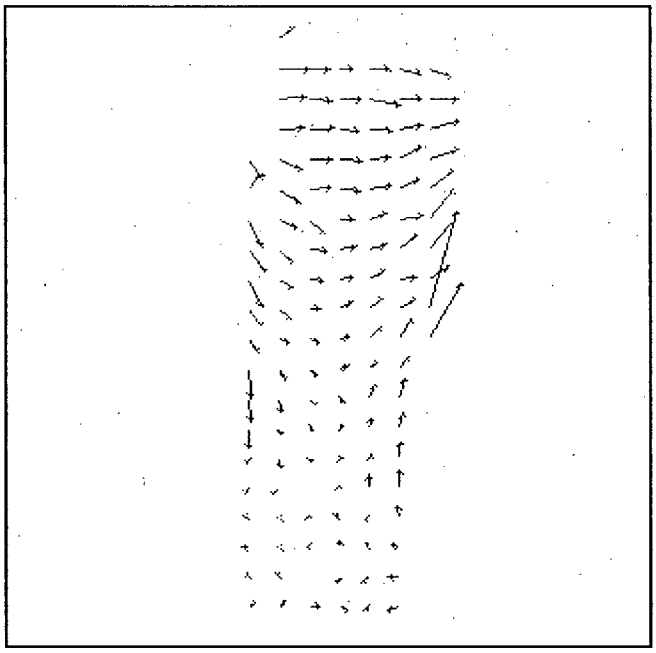

Figure 6.11.2: The type 1 optical flow estimation for the rotating and translating surface with positive Gaussian curvature. Vectors are magnified 10 times and sampled every 20 pixels.

Measure	Average	Standard Deviation
u_e	0.507621	0.566288
v_e	-0.049223	1.005767
u_k	0.5	0.828117
v_k	0	0.280359
e_u	0.007621	0.431403
e_v	-0.049223	1.137235
$\|e\|$	0.782229	0.932732
$\|e_u\|$	0.308546	0.301599
$\|e_v\|$	0.601414	0.966444
r	1.269681	1.813566
$\angle$	1.020951	0.900852

Table 6.11.2: The averages and standard deviations of measures associated with the type 1 optical flow estimation. The measure *r* is unitless. The measure $\angle$ is in radians. All other measures are in pixels.

Type 2A Min. A Optical Flow

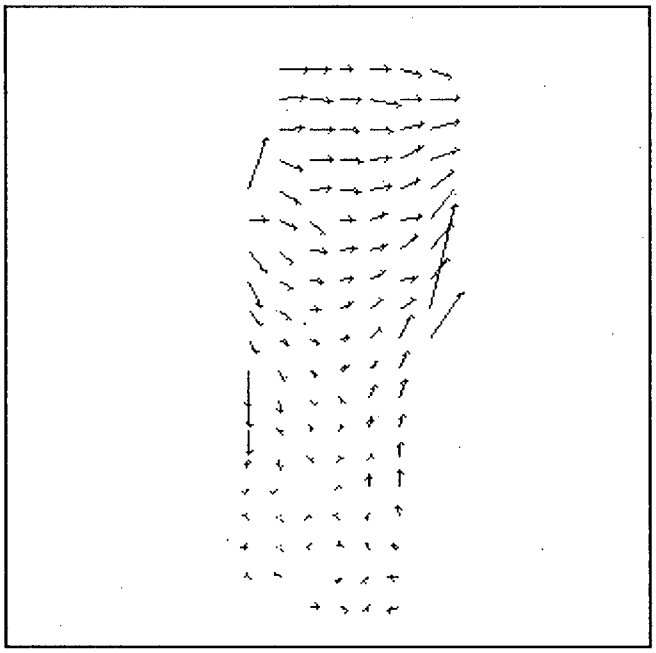

Figure 6.11.3: The type 2A Min. A optical flow estimation for the rotating and translating surface with positive Gaussian curvature. Vectors are magnified 10 times and sampled every 20 pixels.

Measure	Average	Standard Deviation
u_e	0.497357	0.560068
v_e	-0.056957	1.07724
u_k	0.5	0.828117
v_k	0	0.280359
e_u	-0.002643	0.445587
e_v	-0.056957	1.206419
$\|e\|$	0.806202	1.003624
$\|e_u\|$	0.312235	0.3179
$\|e_v\|$	0.622167	1.035174
r	1.310182	1.998251
$\angle$	1.029846	0.902167

Table 6.11.3: The averages and standard deviations of measures associated with the type 2A Min. A optical flow estimation. The measure r is unitless. The measure $\angle$ is in radians. All other measures are in pixels.

Type 2A Min. B Optical Flow

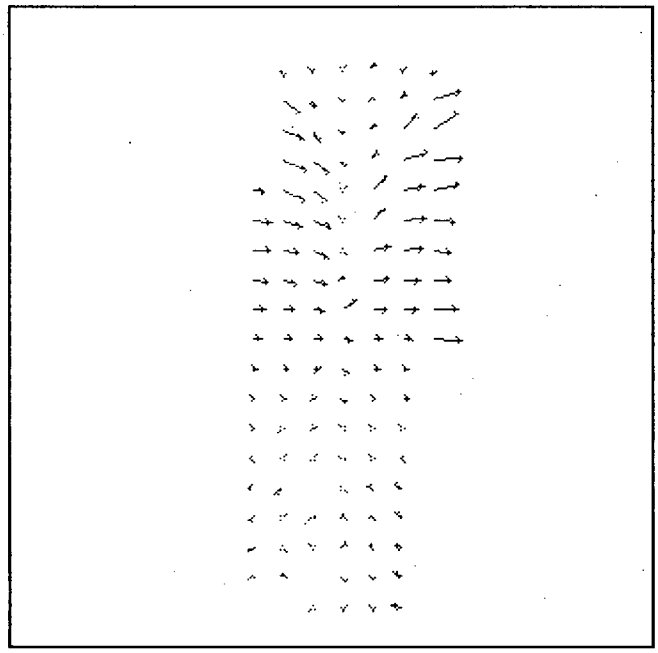

Figure 6.11.4: The type 2A Min. B optical flow estimation for the rotating and translating surface with positive Gaussian curvature. Vectors are magnified 10 times and sampled every 20 pixels.

Measure	Average	Standard Deviation
u_e	0.306493	0.471503
v_e	-0.001064	0.245655
u_k	0.5	0.828117
v_k	0	0.280359
e_u	-0.193507	0.701012
e_v	-0.001064	0.435231
$\|e\|$	0.68733	0.495835
$\|e_u\|$	0.479903	0.546397
$\|e_v\|$	0.360952	0.243179
r	0.795609	0.351071
$\angle$	0.972872	0.48828

Table 6.11.4: The averages and standard deviations of measures associated with the type 2A Min. B optical flow estimation. The measure *r* is unitless. The measure $\angle$ is in radians. All other measures are in pixels.

Type 2A Min. C Optical Flow

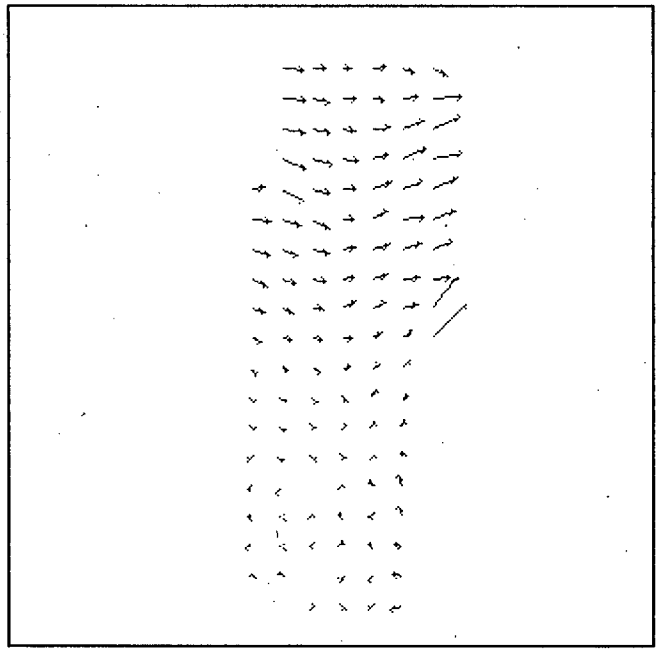

Figure 6.11.5: The type 2A Min. C optical flow estimation for the rotating and translating surface with positive Gaussian curvature. Vectors are magnified 10 times and sampled every 20 pixels.

Measure	Average	Standard Deviation
u_e	0.425582	0.500532
v_e	-0.030096	0.304835
u_k	0.5	0.828117
v_k	0	0.280359
e_u	-0.074418	0.524139
e_v	-0.030096	0.505238
$\|e\|$	0.635109	0.364764
$\|e_u\|$	0.364147	0.384256
$\|e_v\|$	0.397148	0.313749
r	0.906237	0.741561
$\angle$	0.913032	0.764985

Table 6.11.5: The averages and standard deviations of measures associated with the type 2A Min. C optical flow estimation. The measure *r* is unitless. The measure $\angle$ is in radians. All other measures are in pixels.

Type 2A Min. D Optical Flow

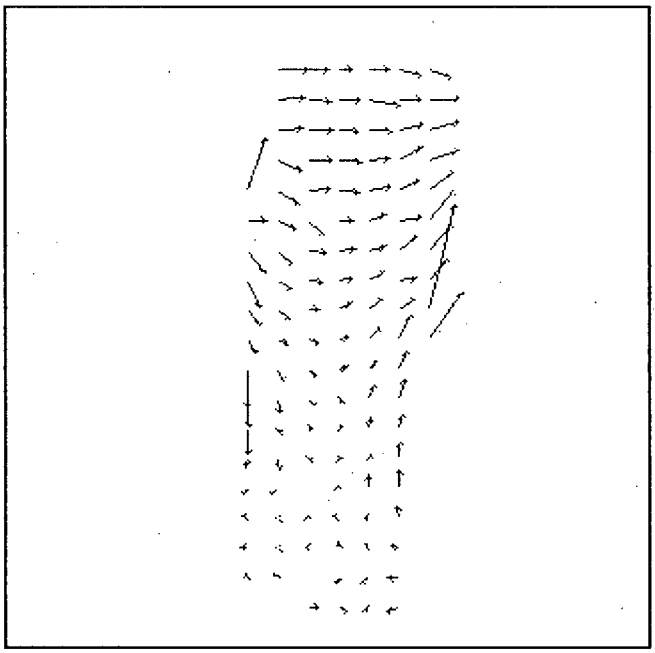

Figure 6.11.6: The type 2A Min. D optical flow estimation for the rotating and translating surface with positive Gaussian curvature. Vectors are magnified 10 times and sampled every 20 pixels.

Measure	Average	Standard Deviation
u_e	0.497355	0.560068
v_e	-0.056948	1.07723
u_k	0.5	0.828117
v_k	0	0.280359
e_u	-0.002645	0.445589
e_v	-0.056948	1.206409
$\|e\|$	0.806199	1.003614
$\|e_u\|$	0.312236	0.317901
$\|e_v\|$	0.622163	1.035164
r	1.310174	1.998207
$\angle$	1.029844	0.902165

Table 6.11.6: The averages and standard deviations of measures associated with the type 2A Min. D optical flow estimation. The measure *r* is unitless. The measure $\angle$ is in radians. All other measures are in pixels.

Type 2B, 2B′, and 2B″ Min. A Optical Flow

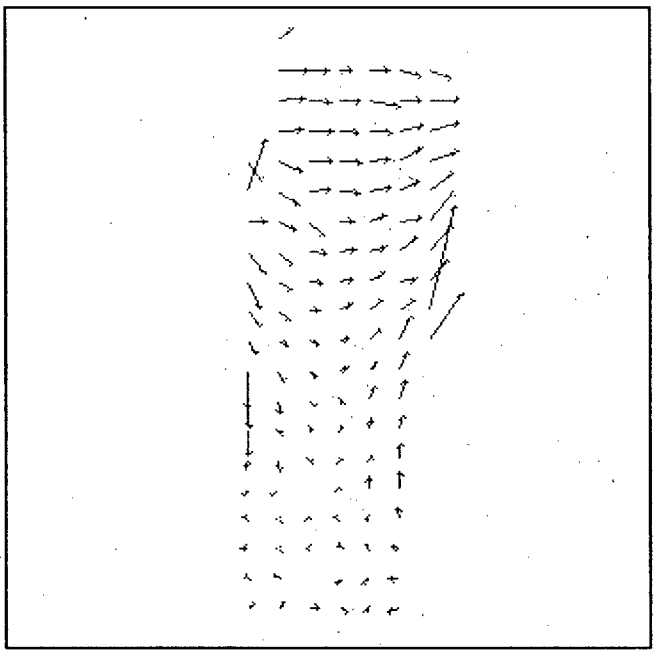

Figure 6.11.7: The type 2B Min. A optical flow estimation for the rotating and translating surface with positive Gaussian curvature. Vectors are magnified 10 times and sampled every 20 pixels.

	2B Min. A		2B′ Min. A		2B″ Min. A	
Measure	**Average**	**Standard Deviation**	**Average**	**Standard Deviation**	**Average**	**Standard Deviation**
u_e	0.505935	0.564189	0.506717	0.563791	0.507751	0.566453
v_e	-0.059675	1.079824	-0.05745	1.042139	-0.049459	1.005777
u_k	0.5	0.828117	0.5	0.828117	0.5	0.828117
v_k	0	0.280359	0	0.280359	0	0.280359
e_u	0.005935	0.426	0.006717	0.426607	0.007751	0.431269
e_v	-0.059675	1.208647	-0.05745	1.173326	-0.049459	1.137146
$\|e\|$	0.801466	1.001762	0.793565	0.965539	0.7823	0.932516
$\|e_u\|$	0.304359	0.298117	0.305072	0.298272	0.308466	0.301494
$\|e_v\|$	0.623707	1.036997	0.615187	1.000763	0.601594	0.96624
r	1.30895	1.999626	1.29059	1.898176	1.269828	1.813396
$\angle$	1.029662	0.903543	1.027422	0.902852	1.021109	0.90082

Table 6.11.7: The averages and standard deviations of measures associated with the type 2B, 2B′, and 2B″ Min. A optical flow estimation. The measure r is unitless. The measure $\angle$ is in radians. All other measures are in pixels.

Type 2B, 2B′, and 2B″ Min. B Optical Flow

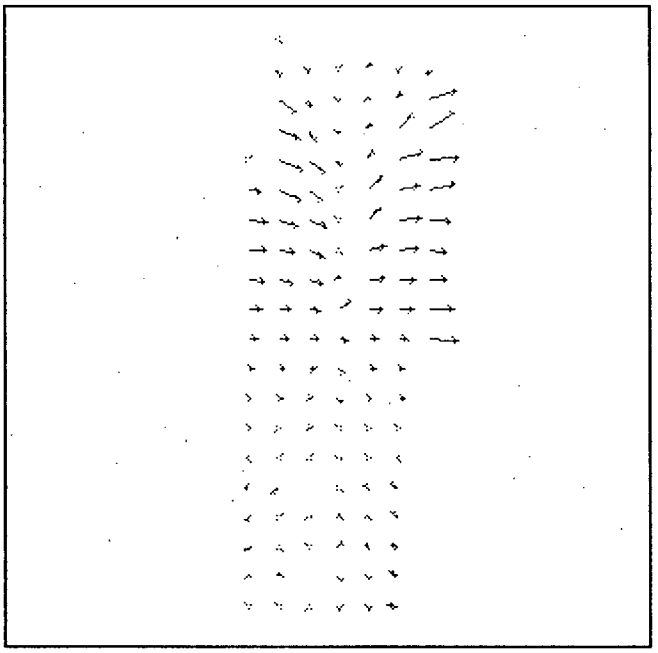

Figure 6.11.8: The type 2B Min. B optical flow estimation for the rotating and translating surface with positive Gaussian curvature. Vectors are magnified 10 times and sampled every 20 pixels.

	2B Min. B		2B′ Min. B		2B″ Min. B	
Measure	**Average**	**Standard Deviation**	**Average**	**Standard Deviation**	**Average**	**Standard Deviation**
u_e	0.306049	0.471849	0.215673	0.421748	0.004231	0.117099
v_e	-0.001117	0.245555	0.000042	0.19006	-0.001267	0.046651
u_k	0.5	0.828117	0.5	0.828117	0.5	0.828117
v_k	0	0.280359	0	0.280359	0	0.280359
e_u	-0.193951	0.700683	-0.284327	0.71691	-0.495769	0.813087
e_v	-0.001117	0.435192	0.000042	0.393499	-0.001267	0.283724
$\|e\|$	0.687094	0.495836	0.721574	0.478496	0.863075	0.492422
$\|e_u\|$	0.479642	0.546361	0.561	0.529218	0.790977	0.530319
$\|e_v\|$	0.360878	0.24322	0.320031	0.228949	0.241435	0.149023
r	0.795308	0.350908	0.841983	0.232489	0.991672	0.055754
$\angle$	0.981682	0.506227	0.982106	0.506385	0.981977	0.505957

Table 6.11.8: The averages and standard deviations of measures associated with the type 2B, 2B′, and 2B″ Min. B optical flow estimation. The measure r is unitless. The measure $\angle$ is in radians. All other measures are in pixels.

Type 2B, 2B′, and 2B″ Min. C Optical Flow

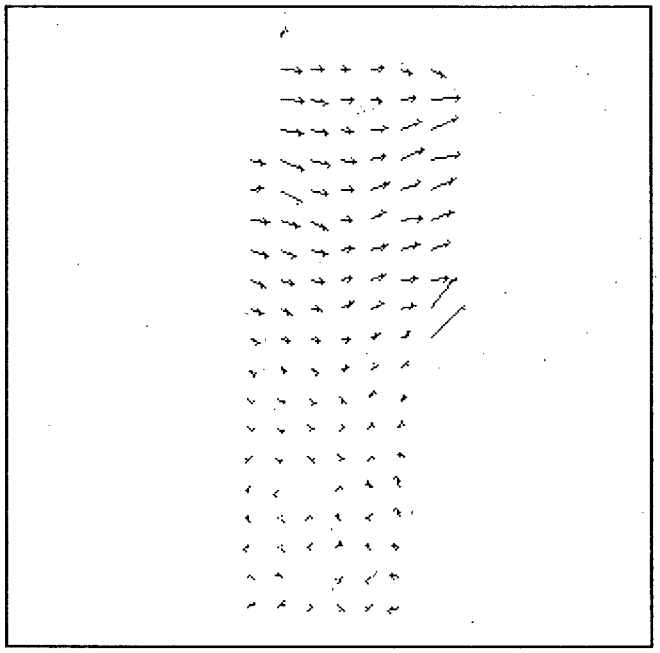

Figure 6.11.9: The type 2B Min. C optical flow estimation for the rotating and translating surface with positive Gaussian curvature. Vectors are magnified 10 times and sampled every 20 pixels.

	2B Min. C		2B′ Min. C		2B″ Min. C	
Measure	Average	Standard Deviation	Average	Standard Deviation	Average	Standard Deviation
u_e	0.43066	0.504944	0.41747	0.48343	0.397221	0.451114
v_e	-0.031968	0.306354	-0.025905	0.272953	-0.016183	0.215445
u_k	0.5	0.828117	0.5	0.828117	0.5	0.828117
v_k	0	0.280359	0	0.280359	0	0.280359
e_u	-0.06934	0.510124	-0.08253	0.519961	-0.102779	0.552031
e_v	-0.031968	0.505366	-0.025905	0.47472	-0.016183	0.424729
$\|e\|$	0.629224	0.354279	0.617952	0.348314	0.617508	0.338568
$\|e_u\|$	0.357135	0.370789	0.376969	0.367505	0.409595	0.384094
$\|e_v\|$	0.396422	0.315057	0.369417	0.29926	0.341282	0.253335
r	0.902814	0.742346	0.862428	0.64093	0.841073	0.594276
$\angle$	0.913482	0.765897	0.883429	0.75185	0.844306	0.724234

Table 6.11.9: The averages and standard deviations of measures associated with the type 2B, 2B′, and 2B″ Min. C optical flow estimation. The measure r is unitless. The measure $\angle$ is in radians. All other measures are in pixels.

Type 2B, 2B′, and 2B″ Min. D Optical Flow

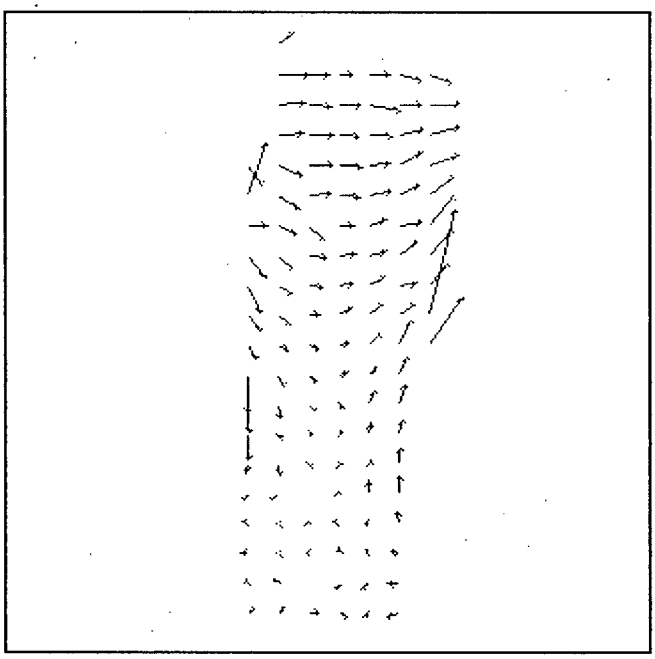

Figure 6.11.10: The type 2B Min. D optical flow estimation for the rotating and translating surface with positive Gaussian curvature. Vectors are magnified 10 times and sampled every 20 pixels.

	2B Min. D		2B′ Min. D		2B″ Min. D	
Measure	Average	Standard Deviation	Average	Standard Deviation	Average	Standard Deviation
u_e	0.505933	0.564188	0.506716	0.56379	0.507745	0.566452
v_e	-0.059666	1.079833	-0.057441	1.042132	-0.049438	1.005785
u_k	0.5	0.828117	0.5	0.828117	0.5	0.828117
v_k	0	0.280359	0	0.280359	0	0.280359
e_u	0.005933	0.426002	0.006716	0.426609	0.007745	0.431285
e_v	-0.059666	1.208653	-0.057441	1.173318	-0.049438	1.137147
$\|e\|$	0.801464	1.001772	0.793562	0.965532	0.782296	0.932527
$\|e_u\|$	0.30436	0.298118	0.305073	0.298273	0.308474	0.301508
$\|e_v\|$	0.623704	1.037006	0.615183	1.000755	0.601582	0.966247
r	1.308943	1.999653	1.290581	1.898132	1.269809	1.813351
$\angle$	1.029661	0.903541	1.027421	0.90285	1.021098	0.900816

Table 6.11.10: The averages and standard deviations of measures associated with the type 2B, 2B′, and 2B″ Min. D optical flow estimation. The measure r is unitless. The measure $\angle$ is in radians. All other measures are in pixels.

Chapter 7

7 Conclusions and Future Work

Although our approach is specialized for translations and rotations in the image plane, the problem of optical flow estimation still remains under-determined locally. We have attempted to select the optical flow estimate which best matches the known motion field by using a number of local regularization schemes. This was met with varying degrees of success.

For the curving sheet sequence results of section 6.4, all the optical flow estimation techniques found a solution which poorly matched the known motion field. This sequence yielded the largest $\bar{r}$ error measure for all optical flow estimation techniques implemented. All the $\bar{r}$ error measures were over 10^{11}. The underlying motion in this sequence was neither a translation nor a rotation. The motion was a curving deformation of the sheet. This violated the assumption that the underlying motion was a rotation, translation, or a combination of both.

Many translating motion fields were estimated very well by the optical flow estimation techniques implemented. For the translating calibration sphere results of section 6.3, the type 1 and the type 2B" Min. A optical flow estimation techniques do very well with the $\bar{r}$ error measures being less than 0.18. The type 1 technique assumes the classic optical flow constraint which is correct for this sequence. The type 2B" Min. A minimizes the rotational component of the solution which is appropriate for this sequence. For the translating curved sheet sequence results of section 6.5, the type 2B'

Min. A and the type 2A Min. C optical flow estimation techniques do very well with the $\bar{r}$ error measures being less than 0.109. The 2B' Min. A minimizes the rotational component of the solution which is appropriate for this sequence. However, the type 2A Min. C minimizes all the components of the solution.

In sections 6.6, 6.7 and 6.8, we experimented with sequences involving a surface with negative Gaussian curvature under rotation, translation, and combined motions. In these sequences the type 2B, 2B', and 2B" Min. C selects the optical flow estimate which comes closest to the known motion field. For this particular surface with negative Gaussian curvature, the stabilizing function which minimizes all the components of the solution is able to select the best optical flow estimate under conditions of rotation, translation, and combined motions.

In sections 6.9, 6.10 and 6.11, we experimented with sequences involving the surface with positive Gaussian curvature under rotation, translation, and combined motions. In the sequences involving rotation, all the optical flow estimation techniques selected an optical flow estimate which poorly matched the known motion field. This was the case even under different light source directions. This leads us to hypothesize that the sign of the Gaussian curvature of a surface plays an important role in how well our optical flow estimation techniques perform under rotational cases. Under rotation, our optical flow estimation techniques performed very well for the surface with negative Gaussian curvature, but performed poorly for the surface with positive Gaussian curvature. Further research is necessary to validate this hypothesis.

There were a number of general trends which were noticeable among the techniques implemented. In general, the type 2A and 2B methods yielded similar results,

under the same stabilizing functions. The only time they differ significantly is in the sequence involving a translating curved sheet. In this case the type 2A Min. A and 2A Min. D yield very bad results, whereas the type 2B estimation does not. So the assumption of exact measurements which is made in the regularization of type 2A, is not acceptable under all conditions. Also in the type 2A and 2B optical flow estimation techniques, the minimum intensity change and rotation stabilization yields a similar, if not the same result, as if just the minimum intensity change stabilization had been used. This is evident from all the test cases.

Also noticeable was the fact that the type 2B, 2B', or 2B" optical flow estimation techniques yield similar $\bar{r}$ values when the optical flow estimate is quite good. The three different λ values used have little effect in these cases. An example is in Table 6.6.9. When the type 2B optical flow estimate was not so good, the type 2B', and the type 2B" optical flow also yield bad optical estimates, but the $\bar{r}$ values can vary more significantly. An example is in Table 6.3.9.

Our approach to optical flow estimation is very local, in which only information at a given pixel is considered. This information includes images derivatives and surface gradients at that pixel. Because our approach solves a linear system, it has the potential to be very fast. There are many possible improvements to this approach which have yet to be investigated. The stabilizing function plays a very important role in determining the most appropriate optical flow estimation. In our implementations, the stabilizing function for a certain optical flow estimation technique was constant for all pixels in the image. However, customizing the stabilizing function for each pixel may yield better results. Knowledge or estimates of the general underlying motion gained from such

methods as feature tracking or previous optical flow iterations could be used to customize the stabilizing function to each pixel. Another area of further research is the use of global regularization, instead of the local regularization techniques which we investigated.

Bibliography

1. Elli Angelopoulou, "Gaussian Curvature from Photometric Scatter Plots", Proceeding of IEEE Workshop on Photometric Modeling for Computer Vision and Graphics (PMCVG, CVPR Workshop) pp. 12-19, 1999.
2. Elli Angelopoulou, Lawrence B. Wolff, "Photometric Computation of the Sign of Gaussian Curvature Using a Curve-Orientation Invariant", Proceedings of IEEE Conference on Computer Vision and Pattern Recognition (CVPR), pp. 432-437, 1997.
3. Elli Angelopoulou, Lawrence. B. Wolff, Sign of Gaussian Curvature from Curve Orientation in Photometric Space, IEEE Transactions On Pattern Analysis and Machine Intelligence, Vol. 20, No. 10, pp. 1056-66, October 1998.
4. J. L. Barron, D. J. Fleet, S. S. Beauchemin, "Performance of Optical Flow Techniques", IJCV, 12(1), pp. 43-77,1994.
5. Richard.L. Burden, J. Douglas Faires, "Numerical Analysis Sixth Edition", Brooks/Cole Publishing Company, 1997.
6. James D. Foley, Andries van Dam, Steven K. Feiner, John F. Hughes, "Computer Graphics Principles and Practice Second Edition in C", Addison-Wesley Publishing Company, Inc., 1996.
7. E.C. Hildreth, "The Measurement of Visual Motion", MIT Press, Cambridge, Mass., 1984.
8. B.K.P.Horn, "Robot Vision", The MIT Press 1986.
9. B.K.P. Horn, B.G. Schunck, "Determining Optical Flow", Artificial Intelligence(17), pp. 185-203, 1981.

10. R. A. Horn and C. R. Johnson, *Matrix Analysis*, Cambridge University Press, 1990.

11. David Hsu, "Multiple light source estimation of the 2-D motion field when reflectance properties are known", Bachelor's Thesis, Computer Science, UBC, April 1995.

12. Yuji Iwahori, R. J. Woodham, Ardeshir Bagheri, "Principal Components Analysis and Neural Network Implementation of Photometric Stereo", Proceedings of the IEEE Workshop on Physics-Based Modeling in Computer Vision (PBMCV), pp. 117-125, 1995.

13. W. Keith Nicholson, "Linear Algebra With Applications Third Edition", PWS Publishing Company, Boston, 1995.

14. Cristina Elena Siegerist, Master's Thesis, Computer Science, UBC, April 1996.

15. Cristina Elena Siegerist, "Parallel near-real-time implementation of multiple light source optical flow", VI-96, pp. 167-174, 1996.

16. R. J. Woodham, "Analysing Images of Curved Surfaces", Artificial Intelligence, pp. 117-140, 1981.

17. R. J. Woodham, "Gradient and Curvature from Photometric Stereo Including Local Confidence Estimation", J. Opt. Soc. Am. A, vol 11, pp. 3050-3068, 1994.

18. R. J. Woodham, "Multiple Light Optical Flow", Proceedings of the Third International Conference in Computer Vision, pp. 42-45, Osaka, Japan, 1990.